ELSEVIER

Physics Reports 371 (2002) 151–230

PHYSICS REPORTS

www.elsevier.com/locate/physrep

The potential for neutrino physics at muon colliders and dedicated high current muon storage rings

I. Bigi[a], T. Bolton[b], J. Formaggio[c], D.A. Harris[d], B. Kayser[e], B.J. King[f,*], K.S. McFarland[g], J. Morfin[d], A.A. Petrov[h], H. Schellman[i], R. Shrock[j], P.G. Spentzouris[d], M. Velasco[i], J. Yu[d]

[a] *Notre Dame University, South Bend, IN, USA*
[b] *Kansas State University, Manhattan, KS, USA*
[c] *Columbia University, New York, NY, USA*
[d] *Fermilab, Batavia, IL, USA*
[e] *National Science Foundation, Washington, DC, USA*
[f] *Brookhaven National Laboratory, P.O. Box 5000, Upton, NY, 11973–5000, USA*
[g] *University of Rochester, Rochester, NY, USA*
[h] *LNS, Cornell University, Ithaca, NY, USA*
[i] *Northwestern University, Evanston, IL, USA*
[j] *State University of New York, Stonybrook, NY, USA*

Received 1 October 2001
editor J.A. Bagger

Abstract

Conceptual design studies are underway for muon colliders and other high-current muon storage rings that have the potential to become the first true "neutrino factories". Muon decays in long straight sections of the storage rings would produce precisely characterized beams of electron and muon type neutrinos of unprecedented intensity. This article reviews the prospects for these facilities to greatly extend our capabilities for neutrino experiments, largely emphasizing the physics of neutrino interactions.

PACS: 13.15.+g

Keywords: Muon colliders; Muon storage rings; Neutrino factories

* Corresponding author.
E-mail address: king@lotus.phys.nwu.edu (B.J. King).

0370-1573/02/$ - see front matter
PII: S0370-1573(02)00011-X

Contents

1. Overview

1.1. Introduction

Muon colliders have been proposed to provide lepton–lepton collisions while circumventing the energy limitations on electron–positron storage rings caused by synchrotron radiation. The larger muon mass suppresses synchrotron radiation energy losses by a factor $m_e^4/m_\mu^4 \simeq 5 \times 10^{-10}$ relative to

those of a circulating electron beam of the same energy and, incidentally, also opens up promising possibilities for s-channel Higgs boson production [1].

Recent feasibility and design studies for future muon colliders [2,1] have begun to focus attention on the exciting physics possibilities for experiments using neutrino beams from the decays of the circulating high-energy muons. This report explores the potential for a "neutrino experiment at a muon collider", or νMC for short. A νMC program could operate either parasitically during a colliding beam experiment, or it could be installed as part of a program in neutrino physics at a dedicated muon storage ring.

Amongst the potential physics topics for νMCs, neutrino oscillations have garnered the most intense experimental and theoretical activity, and particular possibilities for long baseline oscillation experiments exploiting a muon storage ring are covered elsewhere [3,4]. In this report, we wish to also highlight the superb capabilities of neutrinos as probes of the strong and weak interaction dynamics of quarks and the parton structure of nucleons, as well as the power of a νMC in searches for evidence of new types of weak interactions.

The remainder of this section lays out the expected experimental parameters and capabilities of a νMC and provides concise overviews for the more detailed physics discussions that follow.

1.2. Experimental overview

1.2.1. High-current muon storage rings

Recent ideas for neutrino experiments at either muon colliders [5,6] or dedicated neutrino factories [7] represent reincarnations of earlier proposals for neutrino experiments at muon storage rings that date back at least to the 1960s. The essential advantages of modern νMCs derive from the very large muon currents that might be produced and stored using the technologies developed for muon colliders. Current design scenarios for muon colliders [2,1] and neutrino factories [10,4] envision of order 10^{21} positive and negative muons per year circulating and decaying in the storage ring.

Neutrinos from decays in the longest straight sections of the storage ring will emerge in intense collinear beams that are highly suitable for experiments. Beams from such production straight sections should provide many orders of magnitude higher event rates than considered in the early versions of muon storage rings and, indeed, should be considerably more intense than today's "conventional" neutrino beams produced from π/K decays. No need exists for a conventional beam's muon shielding berm, and detectors can be placed relatively close to the end of the production straight section. Coupled with the relativistic kinematics of muon decay, this permits the possibility of detectors only tens of centimeters across and allows for the use of high-precision vertex detectors as active neutrino targets.

Additional physics advantages over π/K decay neutrino beams will result from the unique and precisely understood flux composition of the νMC beams. Negative and positive muons decay according to

$$\begin{aligned} \mu^- &\to \nu_\mu + \bar{\nu}_e + e^- \,, \\ \mu^+ &\to \bar{\nu}_\mu + \nu_e + e^+ \,, \end{aligned} \tag{1}$$

producing pure 2-component neutrino beams [1] via perhaps the best understood of all weak decay processes. These beams will be designated as $\nu_\mu\bar{\nu}_e$ or $\bar{\nu}_\mu\nu_e$, respectively, in the rest of this report.

Experimental requirements for the two broad classes of neutrino physics at νMCs differ greatly, chiefly because the experiments would be conducted at very different baseline distances from beam production to the detector. Experiments for neutrino interaction physics will be conducted as close to the muon ring as possible ("short baseline") in order to maximize event rates and to subtend the neutrino beam with a target of small transverse cross section. On the other hand, the choice of baseline for neutrino oscillation studies will be dictated by the specific range of possible oscillation parameters under investigation, as discussed further in Section 7. Oscillation parameters of current interest motivate the use of very long baselines, even extending to the possibility of transcontinental experiments [7].

As an important caveat on the contents of this report, it should always be borne in mind that the ambitious technologies of these high-current muon storage rings still only exist at the feasibility or early design study stage and it is by no means guaranteed that realizable devices will appear anytime soon. Nevertheless, recent progress has been impressive, and the pace of R& D is accelerating. The reader is referred to the specialist literature for a more thorough overview of the technological challenges in building a muon collider [2,1] or neutrino factory [10,4].

1.2.2. Event rates

Event rates in all νMC experiments will be dominated by the charged current (CC) and neutral current (NC) deep inelastic scattering (DIS) of neutrinos or antineutrinos with nucleons ($N = p$ or n):

$$\begin{aligned} \nu_\ell + N &\to \ell^- + X \qquad (\nu_\ell\text{-CC}) , \\ \bar{\nu}_\ell + N &\to \ell^+ + X \qquad (\bar{\nu}_\ell\text{-CC}) , \\ \nu_\ell(\bar{\nu}_\ell) + N &\to \nu_\ell(\bar{\nu}_\ell) + X \qquad (\nu_\ell(\bar{\nu}_\ell)\text{-NC}) , \end{aligned} \tag{2}$$

where $\ell = e$ or μ and X represents a typically multi-particle hadronic final state. Neutrino–nucleon DIS cross sections scale with neutrino energy E_ν to a good approximation for neutrino energies above a few GeV, with numerical values of [12]

$$\sigma_{\nu N}(f\text{b}) \begin{pmatrix} \nu\text{-CC} \\ \nu\text{-NC} \\ \bar{\nu}\text{-CC} \\ \bar{\nu}\text{-NC} \end{pmatrix} \simeq \begin{pmatrix} 6.8 \\ 2.1 \\ 3.4 \\ 1.3 \end{pmatrix} \times E_\nu \ (\text{GeV}) . \tag{3}$$

At the many-GeV energies of νMCs, νN DIS is well described as the quasi-elastic scattering of neutrinos off one of the many quarks or antiquarks inside the nucleon through the exchange of

[1] We implicitly assume here the absence of a significant lepton family number violating decay of the type $\mu^- \to e^-\nu_e\bar{\nu}_\mu$ but caution that the current experimental limit on the branching fraction for this decay is only 1.5%. This limit will clearly be greatly improved upon from the consistency of the observed νMC spectra with predictions.

a virtual W or Z boson:

$$\nu_\ell(\bar{\nu}_\ell) + q \to \nu_\ell(\bar{\nu}_\ell) + q \qquad (\text{NC}) , \tag{4}$$

$$\nu_\ell + q_d(\bar{q}_u) \to \ell^- + q'_u(\bar{q}'_d) \qquad (\nu\text{-CC}) , \tag{5}$$

$$\bar{\nu}_\ell + q_u(\bar{q}_d) \to \ell^+ + q'_d(\bar{q}'_u) \qquad (\bar{\nu}\text{-CC}) . \tag{6}$$

All quarks q participate in the NC process. The CC interactions change quark flavor, with neutrino interactions producing u- and $\bar{d}$-type final state quarks, q'_u and $\bar{q}'_d$, from d- and $\bar{u}$-type targets, q_d and $\bar{q}_u$. Antineutrinos participate in the charge-conjugate processes. Much of the richness of neutrino interaction physics derives from the variety of processes contained in Eqs. (4)–(6).

1.2.3. Neutrino production spectra and event rates in detectors

Neutrino flux spectra at νMCs will be precisely predictable since the decay of muons is a well-understood purely electroweak process. Characteristics of the parent muon beam in the production straight section can be reliably calculated and modeled through a knowledge of the focusing magnet lattice and through beam monitoring. Calibration of the muon energies in the storage ring might reach the level of a few parts per million fractional uncertainty [11].

Due to the differing angular coverages, the neutrino spectrum seen by an oscillation detector at a long baseline will differ from that seen by detectors placed at short baselines to study interaction physics. Long-baseline detectors will sample the very forward-going neutrinos, at angles in the muon rest frame (θ') and laboratory frame (θ) close to $\theta' = \theta = 0$, while detectors close to the production straight section will instead accept a production solid angle bite that is comparable to the boosted forward hemisphere of the decaying neutrinos:

$$\theta' = \frac{\pi}{2} \;\Leftrightarrow\; \theta_\nu \simeq \sin\theta_\nu = 1/\gamma = \frac{m_\mu c^2}{E_\mu} \simeq \frac{10^{-4}}{E_\mu\,(\text{TeV})} . \tag{7}$$

Fig. 1 gives an illustrative example of the neutrino spectra at νMCs for detectors at both short and long baselines [10], and Table 1 gives beam and event rate parameters for several other νMC scenarios. Further explanation for the choices of storage ring parameters in Table 1 and a derivation for the following simple numerical expressions for event rates used to fill Table 2 are provided elsewhere [9].

For short-baseline detectors,

$$N^{\text{sb}}\,(\text{events yr}^{-1}\,\text{g}^{-1}\,\text{cm}^2) = 2.1 \times 10^{-15} \times E_\mu\,(\text{GeV}) \times N_\mu^{\text{ss}}\,(\text{yr}^{-1}) , \tag{8}$$

where N^{sb} is the number of neutrino interactions per year of running per g/cm^2 of a cylindrically symmetric target centered on the beam, E_μ is the muon beam energy and N_μ^{ss} is the number of forward-going muons (as opposed to muons circulating in the opposite direction in, e.g., a collider ring) decaying in the production straight section per year. Eq. (8) assumes the parent muon beam to have an angular divergence in the production straight section that is small compared to the $\delta\theta_\nu = 1/\gamma$ natural divergence of the neutrino beam. This will normally be the case [13] unless the choice of straight section is in the final focus region of a collider storage ring. Table 2 accounts simplistically for this exception (in this case for the illustrative parameter set at 500 GeV) by increasing the angular divergence of the neutrino beam by a simple scale factor. In this circumstance, the angular

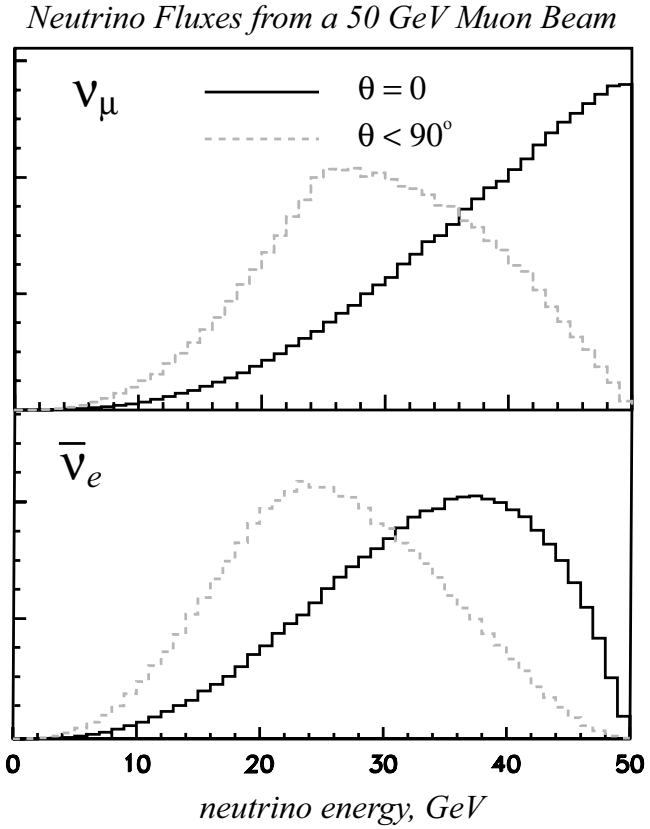

Fig. 1. Example neutrino event spectra for ν_μ and $\bar{\nu}_e$ from a 50 GeV negative muon beam from a neutrino factory [10]. Solid curves indicate the spectra for decays at zero degrees in the center of mass system. This is the spectrum expected for a detector located very far from the muon decay region. The dashed curves indicate the spectra for decays within the forward hemisphere in the center of mass frame. This is what would be expected for a detector close enough to the muon decay region to subtend an angle of $1/\gamma$.

coverage of the target would need to be increased by this same scale factor in order to retain the event rate predicted by the parameter N^{sb}.

In contrast to short-baseline detectors, the event rate in long-baseline detectors is not sensitive to the geometry of the detector since the entire detector will always be bathed uniformly by the forward-going neutrino flux. The number of interactions in the detector will vary in proportion to the target mass M and inversely as the square of the baseline length L. This leads to a definition, analogous to Eq. (8), for the event rate benchmark N^{lb}:

$$N^{\mathrm{lb}}(\text{events yr}^{-1}\,\text{kt}^{-1}\,(10^3\,\text{km})^2) = \frac{1.6\times 10^{-20}\times N_\mu^{\mathrm{ss}}\,(\text{yr}^{-1})\times (E_\mu\,(\text{GeV}))^3}{(\gamma\,\delta\theta)^2}\,, \tag{9}$$

where N^{lb} is the number of neutrino interactions per kiloton per year of running with a target centered on the beam at a 1000 km distance from the production point. The previously discussed angular divergence scaling factor, $\gamma\,\delta\theta$, has been explicitly included.

Table 1
Neutrino fluxes and event rates for representative example parameter sets for dedicated neutrino factories or muon colliders [9] spanning the energy range $E_\mu = 20$ GeV–5 TeV. The angular divergence scaling factor, $\gamma\,\delta\theta$, is the factor by which the divergence of the parent muon beam increases the neutrino beam's angular divergence beyond the characteristic size, $\delta\theta = 1/\gamma$, expected for a divergenceless muon beam

Description	ν-Factory	Higgs factory	Top factory
Muon energy E_μ	20 GeV	50 GeV	175 GeV
$\mu^\pm$/yr ($N_\mu/10^{20}$)	3.0	6.0	6.0
Flight time to beam dump ($t_D/\gamma\tau_\mu$)	No dump	No dump	No dump
Ring circumference C (m)	300	345	900
Straight section (SS) length l_{ss} (m)	90	40	110
Fractional SS length ($f_{ss} \equiv l_{ss}/C$)	0.30	0.12	0.12
μ^+/yr in SS ($N_\mu^{ss} \equiv f_{ss}N_\mu/10^{20}$)	0.90	0.72	0.72
ν from SS/yr ($/10^{20}$)	1.8	1.4	1.4
ν angular divergence ($/\gamma\,\delta\theta_\nu$)	1	1	1
ν angular divergence (mrad)	5.3	2.1	0.60
N^{sb} (events/yr/g/cm^2)	3.8×10^6	6.5×10^6	2.7×10^7
Target thickness (g/cm^2) for 10^{10} events	2600	1500	370
N^{lb} [events/yr/kt/(10^3 km)^2]	1.2×10^4	1.4×10^5	6.2×10^6

Description	Frontier	2nd Generation
Muon energy E_μ	500 GeV	5 TeV
$\mu^\pm$/yr ($N_\mu/10^{20}$)	3.2	3.6
Flight time to beam dump ($t_D/\gamma\tau_\mu$)	0.5	No dump
Ring circumference C (m)	2000	15 000
Straight section (SS) length l_{ss}(m)	150	450
Fractional SS length ($f_{ss} \equiv l_{ss}/C$)	0.12	0.03
μ^+/yr in SS ($N_\mu^{ss} \equiv f_{ss}N_\mu/10^{20}$)	0.38	0.11
ν from SS/yr ($/10^{20}$)	0.30	0.22
ν angular divergence ($/\gamma\,\delta\theta_\nu$)	10	1
ν angular divergence (mrad)	2.1	0.021
N^{sb} (events/yr/g/cm^2)	2.3×10^7	1.0×10^8
Target thickness (g/cm^2) for 10^{10} events	430	100
N^{lb} [events/yr/kt/(10^{3}km)^2]	5.0×10^5	2.2×10^{10}

The event rates given in Table 2 are truly impressive. Samples of thousands of events per kiloton might be recorded at oscillation experiments with baselines as long as thousands of kilometers. For neutrino interaction physics, samples as large as 10 billion events can be reasonably contemplated in compact targets close to the production straight section. Eq. (7) shows that the radial extent of such targets can be as small as 10–20 cm.

1.2.4. Detector design considerations for νMCs

Event rates for oscillation experiments will probably be less of an extrapolation from today's experiments than will be the case for interaction experiments due to the compensating rate decrease at the expected longer baselines. Correspondingly, the innovations in neutrino detector design required

Table 2
Specifications, integrated luminosities and event rates for the high-rate neutrino targets discussed in this report, assuming the 50 and 175 GeV muon storage ring parameters of Table 1. The target is assumed to be situated 100 m (350 m) downstream from the center of the 50 GeV (175 GeV) production straight section

Target purpose	General	Polarized	$\nu - e$
Material	Si CCD	Solid HD	Liquid CH_4
Mean density (g/cm^3)	0.5	0.267	0.717
Length (m)	2	0.5	20
Thickness (g/cm^2)	100	13.4	1430
Radius (cm)	20	20	20
Mass (kg)	126	16.8	1800
Integrated luminosity (fb^{-1})	6.0×10^6	8.1×10^5	8.6×10^7
DIS events/yr at 50 GeV	7.7×10^8	1.0×10^8	1.1×10^{10}
DIS events/yr at 175 GeV	2.7×10^9	3.6×10^8	3.8×10^{10}
ν_e events/yr at 50 GeV	2×10^5	NA	3×10^6
ν_e events/yr at 175 GeV	7×10^6	NA	1×10^7

to upgrade to the neutrino beams at νMCs are likely to be rather less substantial for oscillation experiments at long baselines than for interaction physics experiments.

Two significant changes expected for the design of oscillation detectors for νMCs are that (i) the 2-component beams provide strong motivation for a magnetic spectrometer to distinguish muon charge signs; and (ii) larger detector masses might be financially justified in order to fully exploit the large financial investment in the muon storage ring. Design considerations for detectors for oscillation νMCs are discussed in more detail in Section 7.

In contrast to oscillation experiments, the increase in neutrino yield for νMCs relative to beams from pion decays as well as the collimation of the neutrino beams will allow the use of compact, specialized targets surrounded by high-performance detectors. These detectors must operate at high rate in order to cope with the data sets implied in Table 1. Considerable thought must be given to triggering, data acquisition, event reconstruction and data handling considerations.

Fig. 2 provides an example [6,9] of the sort of high-rate general purpose neutrino detector that would be well matched to the intense neutrino beams at νMCs. The neutrino target is 1 m long stack of CCD tracking planes represented by the small horizontal cylinder at mid-height on the right-hand side of the detector in Fig. 2. Its 10 cm radial extent could correspond to, e.g., the 0.2 mrad divergence of the neutrino beam originating from a 500 GeV muon beam 500 m upstream of the target. The scale of the entire detector is illustrated by a human figure in the lower left corner, emphasizing the striking contrast in target size with the kiloton-scale coarse-sampling calorimetric targets often used for past and present high-rate neutrino experiments.

The CCD target in Fig. 2 contains 750 planes of 300 μm thick silicon CCDs, corresponding to a mass per unit area of approximately 50 g/cm^2; this translates to 2.5 radiation lengths or 0.5 interaction lengths. Scaling to different target lengths and radii should be straightforward without altering the basic design of the surrounding detector.

Besides providing the mass for neutrino interactions, the tracking target allows for precise reconstruction of the event topologies from charged tracks, including event-by-event vertex tagging and

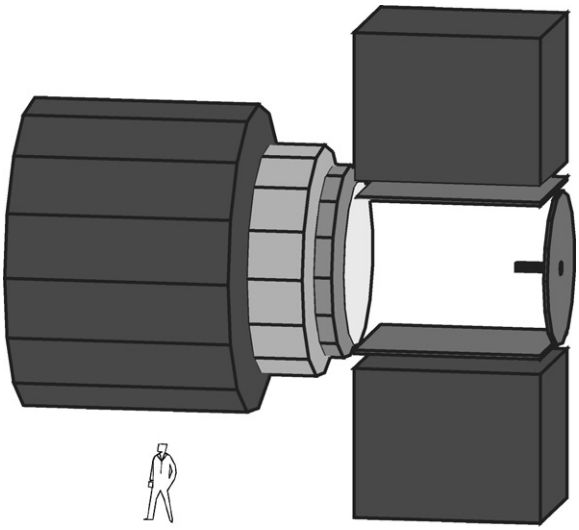

Fig. 2. Example of a general purpose neutrino detector [6]. Its scale is illustrated by a human figure in the lower left corner. The neutrino target is the small horizontal cylinder at mid-height on the right-hand side of the detector. Its radial extent corresponds roughly to the radial spread of the neutrino pencil beam, which is incident from the right-hand side. The illustration is partially schematic in that the geometries of the calorimeters and dipole magnet have been simplified for illustrative purposes.

reconstruction of those interactions containing heavy flavor final states. The fixed target geometry of νMC vertex detectors allows for much more frequent sampling than is possible in collider detectors: Fig. 3 gives a schematic comparison between the charm vertexing capabilities of the CCD detector of Fig. 2 and the current best vertexing detector in a collider experiment [14].

The CCD target is backed by a hermetic detector reminiscent of many collider detector designs. An enveloping time projection chamber (TPC) provides track-following, momentum measurements, and particle identification for essentially all charged tracks emanating from the interactions. Optionally, further particle identification might be available from a mirror that reflects Cherenkov light to an instrumented back-plane directly upstream from the target. The mirror is backed by electromagnetic and hadronic calorimeters and, lastly, by iron-core toroidal magnets for muon identification.

Other possible specialized high-rate neutrino target and detector possibilities include polarized solid protium–deuterium targets for spin physics (Section 2.6) and nuclear targets (Section 2.9) for studies of A dependence. A more massive tracking liquid target (Section 4) would be suitable for precision electroweak physics using neutrino–electron scattering. Table 2 provides a summary of some of the characteristics for examples of each of the three high-rate target types discussed in this section and also gives plausible but very approximate integrated luminosities and event sample sizes for the illustrative 50 and 175 GeV beam parameters in Table 1.

1.3. Physics overview

This overview motivates and introduces the more detailed discussions that follow on: deep inelastic scattering and quantum chromodynamics (Section 2), quark mixing (Section 3), precision electroweak

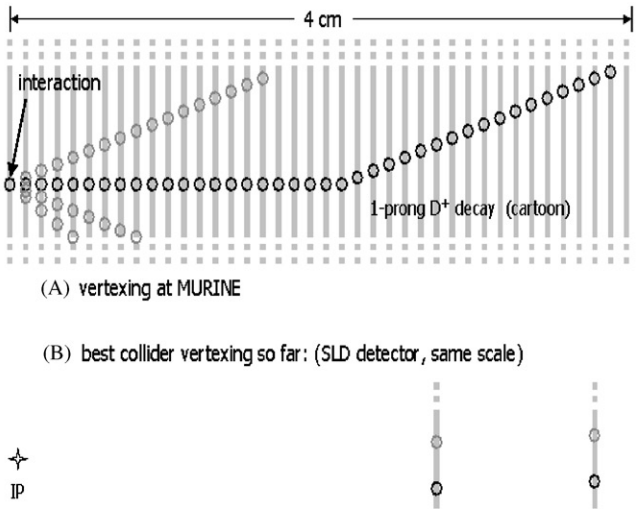

Fig. 3. Conceptual illustration of the vertex tagging superiority expected at νMCs over that with collider experiment geometries. (The figure is reproduced from [14], which used the terminology "MURINE", for MUon RIng Neutrino Experiment, instead of νMC.) Neutrino targets could have a vertex plane of CCD pixel detectors spaced at intervals of approximately 1 mm. For comparison, the VXD3 vertexing detector at the SLD experiment at SLAC, generally regarded as the best existing vertex detector in a collider experiment, has its two innermost CCD tracking planes at 2.8 and 3.8 cm from the interaction point (IP). A schematic of a one-prong D^+ decay has been drawn to illustrate the advantages of closely spaced vertex detectors. For clarity of illustration, the kink deflection angle has been drawn much larger than would be typical. The 2 cm distance to decay for the D^+ charmed meson corresponds to the average boosted lifetime for a 120 GeV D^+.

tests (Section 4), rare and exotic processes (Section 5), charm physics (Section 6) and neutrino oscillations (Section 7).

Before proceeding, we note that much of the interesting physics involves aspects of CC and NC charm and beauty production (and hence the motivation for active vertex detectors as targets). In addition to a CKM physics program that complements those from B and K factories and from precision W boson branching fraction measurements at colliders, b and c production at a νMC allows precisions tests of QCD near heavy flavor thresholds, permits sensitive probes for new physics such as flavor-changing neutral currents, and provides a novel, very high-statistics sample of charmed hadrons.

Figs. 4 and 5 show heavy quark production fractions and indicate that, given the expected multi-billion inclusive event samples, very high statistics can indeed be accumulated for both c and b final states at neutrino energies sufficiently above the relevant thresholds.

1.3.1. QCD and deep inelastic scattering

Historically, neutrino experiments have made major contributions to our understanding and verification of both the QCD theory of strong interactions and the constituent components of protons and neutrons. The extrapolation of present experimental statistics consisting of 10^6–10^7 events to the expected 10^9–10^{10} well-reconstructed DIS events at νMCs might well provide the best ever

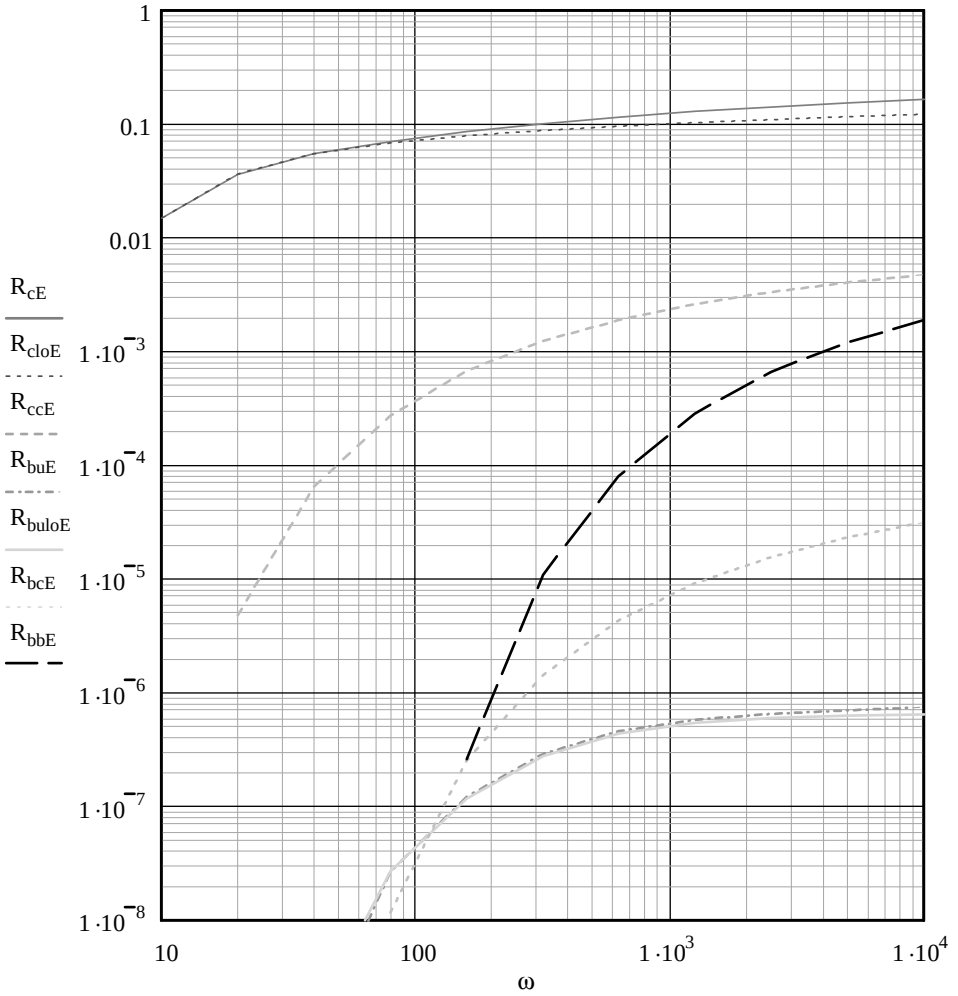

Fig. 4. Fractions of the total neutrino–nucleon cross section involving production of heavy flavors in the final state, for an isoscalar target and as a function of neutrino energy [8]. The plotted production fractions are for charged current charm production (R_{cE}, and R_{cloE} is the leading order approximation), neutral current production of a charm–anticharm pair (R_{ccE}), charged current B production from a u quark (R_{buE}, again with R_{buloE} as the leading order approximation), charged current B production from a c quark (R_{bcE}) and neutral current production of a $b\bar{b}$ pair (R_{bbE}).

experimental laboratory for studying QCD and the structure of the nucleon through a scattering process.

Both traditional and novel areas for potential study will be discussed in Section 2. They include: (1) one of the most precise and theoretically sound measurements of the strong coupling constant, α_s; (2) stringent consistency checks for the predictions of perturbative QCD; (3) detailed flavor and spin dependence nucleon structure functions using both CC and NC probes; (4) precise tests of QCD near the c and b quark heavy flavor transitions; and (5) the first systematic studies of QCD in nuclear environments probed by neutrino and antineutrino beams.

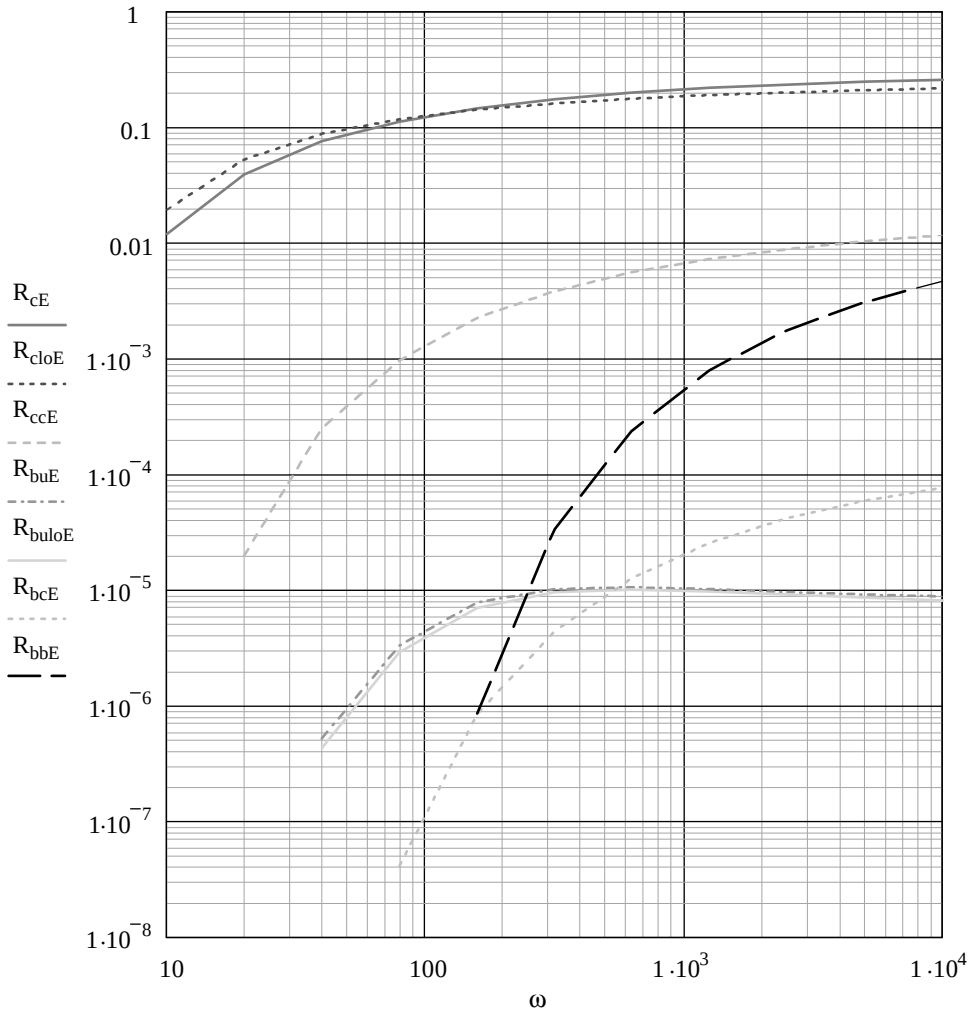

Fig. 5. Heavy quark fractional rates versus neutrino energies corresponding to Fig. 4, but for antineutrinos rather than neutrinos [8].

1.3.2. The CKM quark mixing matrix

Some of the most important high-rate measurements will involve the Cabibbo–Kobayashi–Maskawa (CKM) mixing matrix that characterizes CC weak interactions of quarks. This topic is discussed in detail in Section 3.

Neutrino–nucleon DIS offers unique and systematically independent measurements of CKM matrix elements since it uses a high Q^2 virtual W probe coupling directly to quarks rather than relying on the complex interplay of weak and strong interactions that is inherent in hadron decay. For sufficiently high energy and event rates, four of the nine CKM matrix element amplitudes—$|V_{cd}|$, $|V_{cs}|$, $|V_{ub}|$ and $|V_{cb}|$—are directly probed through c and b production.

The higher momentum transfers from the external W probe allow for a cleaner theoretical interpretation that requires only relatively small corrections from perturbative QCD. As a further theoretical

Table 3
Absolute squares of the elements in the first two rows of the Cabbibo–Kobayashi–Maskawa (CKM) quark mixing matrix, along with their uncertainties when no unitarity constraints are applied [15]. The second row of the entry for each element gives current percentage one-sigma uncertainties in the absolute squares and projections for the uncertainties after analyses from a νMC operating with neutrino energies well above the B production threshold

	d	s	b
u	0.948 $\pm 0.16\%$	0.048 $\pm 2.1\%$	1.45×10^{-5} $\pm 60\% \rightarrow O(3\%)$
c	0.050 $\pm 14\% \rightarrow O(1\%)$	1.08 $\pm 31\% \rightarrow O(3\%)$	1.6×10^{-3} $\pm 10.5\% \rightarrow O(3\%)$

advantage, the measurements are semi-inclusive—i.e., summing over all final states with single charm or beauty production—and thus do not suffer from uncertainties in hadronic branching ratios.

The fractional production rates shown in Figs. 4 and 5 for ν-CC c and $\bar{b}$ production at high energies are of order $|V_{cd}|^2$ and $|V_{ub}|^2$, respectively, where (V_{cd}, V_{ub}) are the $(d \rightarrow c, u \rightarrow b)$ Cabibbo–Kobayashi–Maskawa (CKM) matrix elements. Other significant contributions to heavy flavor production are proportional to $|V_{cs}|^2$ and $|V_{cb}|^2$, where (V_{cs}, V_{cb}) are the $(s \rightarrow c, c \rightarrow b)$ CKM elements.

The relatively clean theoretical interpretations and large samples of flavor-tagged events, particularly for charm production, should allow impressive measurements of the absolute squares for several of the elements in the CKM quark mixing matrix. Estimated precisions in determining the CKM matrix elements are summarized in Table 3.

Perhaps the most interesting potential measurement outlined in Section 3 is the determination of $|V_{ub}|$ to better than 5%, perhaps eventually reaching 1%. This is an order of magnitude better than the current uncertainty and might well be better than will be achieved in any other single measurement at, for example, a B factory. B production should also allow for an extraction of $|V_{cb}|$ at the few percent level that is systematically different, in both its experimental and theoretical aspects, from studies of decay processes and that is comparably accurate to the anticipated future measurements using decays.

The matrix element $|V_{cd}|$ is already best measured from CC charm production in today's neutrino experiments, based on event samples of several thousands of events. The present accuracy is mainly limited by statistics and uncertainties in charmed hadron production and decay characteristics. It is clear that the accuracy in $|V_{cd}|$ would be vastly improved from the analysis of hundreds of millions of vertex-tagged charm events in a high-performance detector.

1.3.3. Precision electroweak physics

Section 4 demonstrates that νMCs should be able to provide two types of precision measurements of the weak mixing angle $\sin^2\theta_W$: from the ratio of neutral current (NC) to charged current (CC) DIS events and also from neutrino–electron scattering.

Both types of determinations require a large extrapolation in event statistics and experimental technique from today's best neutrino results. They will allow vigorous consistency checks of the Standard Model and provide sensitivity to several potential possibilities for new physics.

With its huge statistics, the DIS measurement of $\sin^2\theta_W$ will eventually be systematically limited by theoretical hadronic uncertainties but it should anyway become several times more precise than today's best neutrino measurements, which are already equivalent to about a 100 MeV uncertainty on the W mass.

By contrast, no significant theoretical uncertainties enter into neutrino–electron scattering—a simple scattering process between two elementary point particles—and so the measurements will be limited only by statistics and experimental ingenuity. One can contemplate neutrino–electron scattering event samples as large as 10^8 events using a dedicated detector with parameters like those given in Table 2. This would correspond to impressive statistical uncertainties in $\sin^2\theta_W$ of order 10^{-4} and sensitivity to new contact interactions at energy scales up to approximately 25 TeV. The biggest experimental challenges may come from normalizing the neutrino beam flux. If the experimental uncertainties could be reduced to the extremely challenging level of the statistical uncertainties, then this process holds the potential for measurements of $\sin^2\theta_W$ that might potentially be as good as or better than the best current measurements from collider experiments.

1.3.4. Rare and exotic processes

A *ν*MC provides a facility for several unique searches for physics beyond the Standard Model and provides a venue for observing a number of very rare Standard Model processes, as outlined in Section 5. Examples of the former include flavor changing $u \to c$, $d \to b$ and $s \to b$ neutral currents and isosinglet electron- and muon-type neutral heavy leptons. A list of the latter includes $\bar{\nu}_e e^-$ annihilation and the scattering of virtual W and Z bosons from quasi-real photons in a nuclear Coulomb field; these serve as weak analogs of e^+e^- and $\gamma\gamma$ physics. Sensitivity to high-energy scales through mixing of W or Z with higher mass propagators is limited due to the characteristically weak dependence of the new propagator mass reach as the fourth root of experimental statistics.

1.3.5. Charm decays

A *ν*MC should function as an efficient factory for the study of charm decays, with a clean, well-reconstructed sample of several times 10^8 charmed hadrons produced in 10^{10} neutrino interactions. Section 6 points out several interesting physics motivations for charm studies at a *ν*MC. Measurements of charm decay branching ratios and lifetimes are useful both for QCD studies and for the theoretical calibration of the physics analyses on B hadrons. Charm decays also provide a clean laboratory to search for exotic physics contributions since the Standard Model predicts tiny branching fractions for rare decays, small CP asymmetries and slow $D^0 \to \overline{D^0}$ oscillations.

The charge of the final state lepton in CC-induced charm production from neutrinos tags charm quarks versus antiquarks with high efficiency and purity. This tag is of particular benefit to oscillation and CP studies, as is the expected precise vertexing reconstruction for the proper lifetime of decays. Section 6 shows it to be quite plausible that a *ν*MC could provide the first observations of both $D^0 - \bar{D}^0$ mixing and CP violation in the charm sector and additionally provide some context for their proper interpretation.

1.3.6. Neutrino oscillations

The potential for long-baseline oscillation experiments is the *ν*MC topic that is currently of most interest to the high-energy physics community. However, both the experimental and theoretical status

of neutrino oscillations are in such a state of flux that long-term predictions for νMCs can be stated only in general terms.

Long-baseline experiments at νMCs might well provide a definitive follow-up to the recent intriguing evidence for neutrino oscillations. There will presumably already have been some progress in the verification or refutation of today's oscillation signals by the time long-baseline νMCs come on-line. Even so, νMCs will still clearly be important for more probative follow-up studies to characterize the form and phenomenology of any observed oscillation signals. For example, νMCs might help to determine whether an observed oscillation signal is consistent with mixing between three neutrino families or whether a fourth, sterile neutrino is required, as is discussed in Section 7. In the former case, long-baseline νMCs can nail down the values of the mass-squared differences, search for CP violation and look for matter effects in oscillations in the Earth's interior. Clearly, the spectrum of possible studies would be richer still in the case of 4-neutrino mixing.

2. Deep inelastic scattering and QCD studies

Starting from SLAC electron scattering experiments in the late 1960s, proceeding through the CERN and Fermilab neutrino and muon experiments of the 1970s through 1990s, and continuing with HERA experiments still underway, deep inelastic scattering (DIS) has provided us with an increasingly accurate picture of the partonic structure of the nucleon. Moreover, DIS has served and still serves as one of the best test-beds for perturbative QCD.

A νMC could take the physics of DIS to a new level by: (1) providing the statistical power to extract all six structure functions for ν and $\bar{\nu}$ beams on proton and deuterium targets; (2) allowing for low-mass, high-acceptance spectrometers with vastly improved resolution over present calorimetric detectors; (3) creating naturally redundant measurements through simultaneous measurement of electron and muon final scattering final states; (4) generating the rate and small beam spot size required for the first polarized neutrino targets; (5) permitting use of active vertexing targets for systematic studies of heavy flavor production, and (6) facilitating the use of a large array of nuclear targets.

Examples of physics topics that would emerge include:

- *Definitive proton parton distribution functions* (*PDF*) *for* $x \geqslant 0.01$: The $x \geqslant 0.01$ behavior of parton densities at accessible νMC Q^2 controls the cross-section behavior of the highest energy scale physics of the Tevatron and LHC. Understanding subtle deviations caused by new physics requires precise control of PDF systematics. A νMC will have the statistical power and the systematic redundancy checks to generate a complete PDF set from a single experiment.
- *A test of QCD to next-to-next to leading order* (*NNLO*): Few experiments quantitatively test QCD beyond leading order in the coupling $\alpha_s(Q^2)$. It is frequently the case instead that leading order (LO) and next-to-leading order (NLO) provide equally good descriptions of the data; the NLO calculation is preferred mainly because it reduces theoretical systematic uncertainties in quantities such as $\alpha_s(Q^2)$. As an inclusive scattering process at space-like momentum transfer, DIS is perhaps the phenomenon for which QCD is most rigorously applicable. NLO cross sections are already fully calculated and NNLO computations for several processes exist as well. Testing the entire theory at NNLO seems feasible.

- *Precise measurements of α_s at moderate Q^2*: The running of the strong coupling constant is largely determined by excellent measurements of the τ lepton hadronic decay width at $s = m_\tau^2$ as well as a series of precise measurements at $s = M_Z^2$. Getting this running right is important; for example, one of the few experimental pieces of evidence for supersymmetry is its success in getting the strong, weak, and electromagnetic couplings to unify at one scale. Given this importance, further precise measurements of α_s at scales between m_τ^2 and m_Z^2 are valuable. A νMC provides at least two ways of achieving these: through scaling violations in non-singlet structure functions and through evaluations of the Gross–Lleweyllyn–Smith sum rule.
- *Studies of two-scale QCD via ν and $\bar{\nu}$ heavy flavor production*: A quark q is treated as a heavy object in DIS if $Q^2 < m_q^2$ whereas it is instead considered to be a parton when $\log(Q^2/m_q^2) \gg 1$. Deep inelastic scattering at a νMC allows study of the transition of q from heavy quark to parton by opening the possibility of measuring quark mass effects at a series of scales in CC and NC scattering. The possibility of using vertexing targets maintains the inclusive nature of measurements by avoiding the need for final state lepton tagging.
- *Neutrino spin physics*: Charged lepton scattering experiments from polarized targets show that u and d type quarks carry very little of the nucleon spin and have hinted at strong polarization effects in gluons and strange quarks. A νMC creates the first possibility of using polarized targets for neutrinos and brings all of their power for flavor and helicity selection to bear on nucleon spin physics.
- *Neutrino nuclear physics*: Thin nuclear targets at a νMC can rapidly acquire the statistics to make measurements of the A dependence of the F_2 structure function for neutrinos that complement those from charged lepton scattering. The first precise measurements of the A dependence of xF_3 will become available as well.

2.1. Background on measuring parton distribution functions and QCD with non-polarized targets

Invariance principles dictate the general form of νN ($N = p$ or n) nucleon scattering. For energies much greater than the final state lepton mass and to leading order in electroweak couplings:

$$\frac{\mathrm{d}^2\sigma^{\nu N(\bar{\nu}N)}_{\mathrm{CC/NC}}}{\mathrm{d}x\,\mathrm{d}y} = \frac{G_\mathrm{F}^2 M_N E_\nu}{\pi(1+Q^2/M_\mathrm{V}^2)^2}\left[\left(1-y-\frac{M_N x y}{2E_\nu}\right)F_{2,\mathrm{CC/NC}}^{\nu N(\bar{\nu}N)}(x,Q^2) + \left(\frac{y^2}{2}\right)2xF_{1,\mathrm{CC/NC}}^{\nu N(\bar{\nu}N)}(x,Q^2) \pm y(1-y/2)\,xF_{3,\mathrm{CC/NC}}^{\nu N(\bar{\nu}N)}(x,Q^2)\right], \tag{10}$$

with G_F the Fermi coupling constant, M_N the nucleon mass, E_ν the neutrino energy, y the inelasticity, x the Bjorken scaling variable and Q^2 the negative squared four-momentum transfer to the nucleon target. The plus (minus) sign in the final term is conventional for neutrino (antineutrino) scattering, and $M_\mathrm{V} = M_W$ (M_Z) for CC (NC) scattering. The structure functions $2xF_{1,\mathrm{CC/NC}}^{\nu N(\bar{\nu}N)}(x,Q^2)$, $F_{2,\mathrm{CC/NC}}^{\nu N(\bar{\nu}N)}(x,Q^2)$ and $xF_{3,\mathrm{CC/NC}}^{\nu N(\bar{\nu}N)}(x,Q^2)$ contain all the information about the internal structure of the target. The cross sections for electron–neutrinos and muon–neutrinos are nearly identical, up to electroweak radiative corrections.

The SF depend on the A and Z of the target nucleus, whether the beam is neutrino or antineutrino, and whether the scattering is CC or NC. They can be experimentally extracted in principle by measuring the differential cross sections in fixed x and Q^2 bins as a function of y and then exploiting the y dependences shown in Eq. (10) to fit for $2xF_1$, F_2 and xF_3. In practice, the reduced y coverage created by cuts on final state lepton energies and kinematic constraints limits this procedure, and various model-dependent alternatives have been assumed. For example, the SF $2xF_1$ has rarely been measured in neutrino scattering; instead, it has been related to F_2 through a model for the longitudinal structure function

$$R_{\mathrm{L}}(x,Q^2) \equiv \frac{F_2(x,Q^2)(1+4M^2x^2/Q^2)}{2xF_1(x,Q^2)} - 1 \ , \tag{11}$$

with $R_{\mathrm{L}}(x,Q^2)$ computed from QCD or taken from charged lepton scattering. Charged current interactions, with their observable lepton in the final state, can be much better reconstructed than NC interactions and so we will assume CC SF in the discussion that follows.

Neutrino–nucleon scattering is the only DIS process that can provide measurements of the parity-violating F_3 structure functions, apart from the much less precise measurements in a different kinematic regime from HERA. The parity-conserving $2xF_1$ and F_2 structure functions for neutrino–nucleon scattering probe different combinations of quarks to the analogous SFs defined for charged lepton DIS experiments.

A rough summary of the current knowledge of neutrino SF follows. A more complete review may be found in Ref. [12].

(1) Measurements at an accuracy of a few percent exist for n/p, $\nu/\bar{\nu}$ averaged CC SF

$$F_{2,\mathrm{CC}}(x,Q^2) = \frac{1}{4}\sum_{k=\nu,\bar{\nu}}\sum_{N=n,p} F^{kN}_{2,\mathrm{CC}}(x,Q^2) \ ,$$

$$xF_{3,\mathrm{CC}}(x,Q^2) = \frac{1}{4}\sum_{k=\nu,\bar{\nu}}\sum_{N=n,p} xF^{kN}_{3,\mathrm{CC}}(x,Q^2) \ , \tag{12}$$

using iron targets for $10^{-3} \lesssim x \lesssim 0.7$ and $Q^2 \lesssim 200\,\mathrm{GeV}^2$. The x and Q^2 ranges are highly correlated by the limited range of beam energies. These measurements assume a model for $R_{\mathrm{L}}(x,Q^2)$. Uncertainties on $F_{2,\mathrm{CC}}(x,Q^2)$ are dominated by systematic effects, while $xF_{3,\mathrm{CC}}(x,Q^2)$ errors still contain a significant statistical contribution.

(2) Measurements at the $\sim 10\%$ level exist for:
   (a) the n/p, $\nu/\bar{\nu}$ averaged $R_{\mathrm{L}}(x,Q^2)$ using an iron target;
   (b) the n/p averaged $xF^{\nu}_{3,\mathrm{CC}}(x,Q^2) - xF^{\bar{\nu}}_{3,\mathrm{CC}}(x,Q^2)$;
   (c) $F^{kp}_{2,\mathrm{CC}}(x,Q^2)$, $F^{k\mathrm{D}}_{2,\mathrm{CC}}(x,Q^2)$ and $xF^{kp}_{3,\mathrm{CC}}, xF^{k\mathrm{D}}_{3,\mathrm{CC}}$ for $k=\nu,\bar{\nu}$ and with $\mathrm{D}=$ deuterium.

(3) No SF-oriented neutrino experiments are currently in operation and no new experiments are planned other than a possible νMC program.

The SF goal for an νMC is simple: to measure, over as wide a range of x and Q^2 as possible, the six SF of Eq. (10), particularly for the proton and deuteron but also for other nuclear targets.

2.2. Measurement of quark parton distribution functions

Structure functions provide much of the information used to deduce PDFs. In turn, the PDFs are crucial for all predictions of event rates at the Tevatron and LHC. To avoid nuclear complications, νMC SF should be extracted with proton and deuterium targets.

To leading order (LO) in QCD, the SF can be expressed in terms of nucleon PDF as [2]

$$
\begin{aligned}
F_{2,\mathrm{CC}}^{\nu N}(x,Q^2) &= 2[d^N(x,Q^2) + s^N(x,Q^2) + \bar{u}^N(x,Q^2) + \bar{c}^N(x,Q^2)]\ ,\\
F_2^{\bar{\nu}N}(x,Q^2) &= 2[u^N(x,Q^2) + c^N(x,Q^2) + \bar{d}^N(x,Q^2) + \bar{s}^N(x,Q^2)]\ ,\\
xF_3^{\nu N}(x,Q^2) &= 2[d^N(x,Q^2) + s^N(x,Q^2) - \bar{u}^N(x,Q^2) - \bar{c}^N(x,Q^2)]\ ,\\
xF_3^{\bar{\nu}N}(x,Q^2) &= 2[u^N(x,Q^2) + c^N(x,Q^2) - \bar{d}^N(x,Q^2) - \bar{s}^N(x,Q^2)]
\end{aligned}
\tag{13}
$$

and x can be identified as the target's fractional 4-momentum carried by the struck quark. The Callan–Gross relation holds,

$$
2xF_1^{\nu N(\bar{\nu}N)}(x,Q^2) = F_2^{\nu N(\bar{\nu}N)}(x,Q^2)\ , \tag{14}
$$

implying that $F_2^{\nu N(\bar{\nu}N)}(x,Q^2)$ and $2xF_1^{\nu N(\bar{\nu}N)}(x,Q^2)$ provide redundant parton information.

Measurements of the eight independent observables of Eq. (13) (two SF for each beam on two targets) represents more information than is available from charged lepton scattering but is not enough to specify the 18 independent PDF for each target N (u, d, s, c, plus their antiquarks and the gluon for n and p). Further constraints emerge from isospin symmetry:

$$
\begin{aligned}
u^n(x,Q^2) &= d^p(x,Q^2) \equiv d(x,Q^2)\ ,\\
d^n(x,Q^2) &= u^p(x,Q^2) \equiv u(x,Q^2)\ ,\\
\bar{u}^n(x,Q^2) &= \bar{d}^p(x,Q^2) \equiv \bar{d}(x,Q^2)\ ,\\
\bar{d}^n(x,Q^2) &= \bar{u}^p(x,Q^2) \equiv \bar{u}(x,Q^2)\ ,\\
s^n(x,Q^2) &= s^p(x,Q^2) \equiv s(x,Q^2)\ ,\\
\bar{s}^n(x,Q^2) &= \bar{s}^p(x,Q^2) \equiv \bar{s}(x,Q^2)\ ,\\
c^n(x,Q^2) &= c^p(x,Q^2) \equiv c^p(x,Q^2)\ ,\\
\bar{c}^n(x,Q^2) &= \bar{c}^p(x,Q^2) \equiv \bar{c}(x,Q^2)\ ,\\
g^n(x,Q^2) &= g^p(x,Q^2) \equiv g(x,Q^2)\ .
\end{aligned}
\tag{15}
$$

The nine extra constraints of Eqs. (15) reduce the number of independent PDF to nine. More reduction occurs if one assumes

$$
\bar{s}(x,Q^2) = s(x,Q^2)\ , \tag{16}
$$

[2] We adopt the convention that the PDF are given as parton probability functions multiplied by x, i.e., $u(x,Q^2)$ is x times the probability of finding a u quark with momentum fraction x. This is close to what is actually measured in experiments and is also the form provided in compilations such as PDFLIB [16].

which is supported by measurements of dimuon production in νFe and $\bar{\nu}$Fe scattering [17,18]. Furthermore, at the Q^2 accessible to lower energy νMCs, one can consistently adopt a three-flavor QCD scheme, whence

$$c(x,Q^2) = \bar{c}(x,Q^2) = 0 \ ; \tag{17}$$

these relations are supported by measurements of NC charm production in ν_μFe and $\bar{\nu}_\mu$Fe scattering [19,20]. This finally leaves six independent PDF: $\bar{u}(x,Q^2)$, $\bar{d}(x,Q^2)$, $s(x,Q^2)$, $g(x,Q^2)$, and the *valence distributions*

$$\begin{aligned} u_{\mathrm{V}}(x,Q^2) &= u(x,Q^2) - \bar{u}(x,Q^2) \ , \\ d_{\mathrm{V}}(x,Q^2) &= d(x,Q^2) - \bar{d}(x,Q^2) \ . \end{aligned} \tag{18}$$

At LO, the four deuterium SF can be combined to yield the total quark and valence quark distributions

$$\begin{aligned} F_{2,\mathrm{CC}}^{\nu\mathrm{D}}(x,Q^2) &= F_{2,\mathrm{CC}}^{\bar{\nu}\mathrm{D}}(x,Q^2) \\ &= u(x,Q^2) + d(x,Q^2) + \bar{u}(x,Q^2) + \bar{d}(x,Q^2) + 2s(x,Q^2) \ , \\ \tfrac{1}{2}[xF_{3,\mathrm{CC}}^{\nu\mathrm{D}}(x,Q^2) + F_{3,\mathrm{CC}}^{\bar{\nu}\mathrm{D}}(x,Q^2)] &= u_{\mathrm{V}}(x,Q^2) + d_{\mathrm{V}}(x,Q^2) \ . \end{aligned} \tag{19}$$

The four individual proton SF then allow separation of the u and d quark contributions. Sensitivity to $s(x,Q^2)$ emerges from

$$xF_{3,\mathrm{CC}}^{\nu\mathrm{D}}(x,Q^2) - xF_{3,\mathrm{CC}}^{\bar{\nu}\mathrm{D}}(x,Q^2) = 4s(x,Q^2) \ , \tag{20}$$

and, in principle, from comparison to the charged lepton $F_{2,\mathrm{CC}}^{\ell\mathrm{D}}(x,Q^2)$,

$$\tfrac{5}{18}F_{2,\mathrm{CC}}^{\nu\mathrm{D}}(x,Q^2) - F_2^{\ell\mathrm{D}}(x,Q^2) = \tfrac{1}{3}s(x,Q^2) \ . \tag{21}$$

Practical implementation of Eqs. (20) and (21) has been stymied by difficulties in controlling systematic errors, and current measurements of $s(x,Q^2)$ all come from semi-inclusive $\nu_\mu N$ and $\bar{\nu}_\mu N$ charm production.

The gluon PDF does not enter directly at LO for CC SF. It affects the QCD evolution of F_2 and $2xF_1$, appears with next-to-leading order (NLO) cross-section terms, and enters directly into semi-inclusive double heavy quark production through the NC and CC processes

$$\nu_\ell N \to \nu_\ell c\bar{c}X \ , \tag{22}$$

$$\nu_\ell N \to \nu_\ell b\bar{b}X \ , \tag{23}$$

$$\nu_\ell N \to \ell^- c\bar{b}X \ , \tag{24}$$

as well as neutrino J/ψ and Υ production [21].

2.3. Tests of perturbative QCD

At a νMC, data will be of sufficient precision to probe QCD to NLO, and perhaps to NNLO.

In practice, the data will be in the form of differential cross sections in x and y at different neutrino energies. The general procedure for a QCD analysis of the data consists of: (1) defining a favorable kinematic region where pQCD is expected to apply to within small corrections; (2) choosing a parameterization of the six PDF $\vec{p}(x,Q_0^2;\{\lambda\})$, where $\vec{p}=(u_V,d_V,\bar{u},\bar{d},\bar{s},g)$, Q_0^2 is a reference Q^2 and $\{\lambda\}$ are a set of parameters describing the PDF; (3) using pQCD to fit the data over all Q^2 by varying $\{\lambda\}$.

The quality of such a fit to the data constitutes an immediate test of QCD. For example, QCD can be verified to NLO if NLO pQCD provides a better fit than LO. While contemporary practice dictates fitting with NLO pQCD, it is worth pointing out that neutrino *data* do not convincingly favor the higher order calculation over an LO interpretation. Assuming a good pQCD fit, one can then go on to extract the single parameter of QCD itself, which can be taken to be the strong coupling constant evaluated at the reference Q^2 of the experiment $\alpha_s(Q_0^2)$.

As a technical comment, the fit procedure is admittedly somewhat complex, and the need to treat PDF parameterizations and QCD together arises from kinematic acceptance issues. The Q^2 value will anyway be limited to $Q^2 \lesssim 2ME$ and cuts on final state lepton energies may further limit the available (x,Q^2,y) phase space, particularly at lower energy νMCs. More precisely, if $P_\ell^{\min}$ and $E_{had}^{\min}$ represent the minimum acceptable final state lepton and hadron energies, then for a given Q^2, one has

$$\begin{aligned} &Q^2/2M(E-P_\ell^{\min}) \lesssim x \lesssim \min[1,Q^2/2ME_{had}^{\min}]\,,\\ &E_{had}^{\min}/E \lesssim y \lesssim 1-P_\ell^{\min}/E\,. \end{aligned} \tag{25}$$

This implies that it is impossible to span all of x for a fixed Q^2 in order to extract the PDF of Eqs. (13). An interpolation scheme is needed to connect different regions of x and Q^2 space; fortunately, pQCD provides just that scheme through the DGLAP equations [22–25].

More important even than the high statistics and potentially improved systematics promised by νMCs are the richness of evolution tests created by the availability of 12 proton and deuterium SF, even with the limited phase space. Examples include:

(1) $\frac{1}{2}[xF_{3,\mathrm{CC}}^{\nu\mathrm{D}}(x,Q^2)+xF_{3,\mathrm{CC}}^{\bar{\nu}\mathrm{D}}(x,Q^2)]$: the "classic" non-singlet SF's evolution is independent of $g(x,Q^2)$ but suffers uncertainties from charm production.
(2) $\frac{1}{2}[F_{2,\mathrm{CC}}^{\nu\mathrm{D}}(x,Q^2)+F_{2,\mathrm{CC}}^{\bar{\nu}\mathrm{D}}(x,Q^2)]$: the most precisely measurable SF usefully constrains $g(x,Q^2)$ and cross-checks charged lepton scattering.
(3) $F_{2,\mathrm{CC}}^{\bar{\nu}\mathrm{D}}(x,Q^2)-F_{2,\mathrm{CC}}^{\bar{\nu}p}(x,Q^2)$: a new combination for a νMC; this difference is both independent of $g(x,Q^2)$ and charm production.

Sum-rule tests comprise some of the most accurately calculated observables in QCD. For example, the Gross Llewellyn Smith (GLS) sum rule [26,28] yields

$$\begin{aligned} S_{\mathrm{GLS}}(Q^2) &\equiv \int_0^1 \frac{\mathrm{d}x}{x}[xF_{3,\mathrm{CC}}^{\nu\mathrm{D}}(x,Q^2)+xF_{3,\mathrm{CC}}^{\nu\mathrm{D}}(x,Q^2)]\,\mathrm{d}x\\ &= 3\left[1-\frac{\alpha_s}{\pi}-a(N_f)\left(\frac{\alpha_s}{\pi}\right)^2-b(N_f)\left(\frac{\alpha_s}{\pi}\right)^3+O\left(\frac{\alpha_s^4}{\pi^4}\right)+O'\left(\frac{M^2}{Q^2}\right)\right]\,, \end{aligned} \tag{26}$$

with $a(N_f)$ and $b(N_f)$ being known functions of Q^2 and the specified number of active flavors N_f used in the pQCD analysis. Corrections from order $(\alpha_s/\pi)^4$ pQCD [27] and order M^2/Q^2 higher twist effects have been calculated [29,30]. A νMC would, for the first time, provide sufficient statistics on appropriate targets for testing QCD through a precise evaluation of the Adler sum [31]

$$S_{\mathrm{A}}(Q^2) = 2\int_0^1 \frac{\mathrm{d}x}{x}\,[F_{2,\mathrm{CC}}^{\nu\mathrm{D}}(x,Q^2) - F_{2,\mathrm{CC}}^{\nu p}(x,Q^2)]\,\mathrm{d}x\ ,$$

using the assumed relation $2F_{2,\mathrm{CC}}^{\nu\mathrm{D}}(x,Q^2) = F_{2,\mathrm{CC}}^{\nu p}(x,Q^2) + F_{2,\mathrm{CC}}^{\nu n}(x,Q^2)$.

Structure function analyses in neutrino scattering are a complex business that requires a painstaking attention to systematic error sources. The current best QCD measurements—the evolution [32] of xF_3 and the GLS sum rule [33]—are limited by energy calibration uncertainties in the former and flux-related errors in the latter. Calibration uncertainties will be reduced at νMCs through use of lower mass particle spectrometers that allow better resolution and the possibility of calibration checks using K_S^0 and J/ψ decays. The ability to simultaneously measure $\bar{\nu}_e$ and ν_μ scattering provides built in cross-checks, and the electrons from the $\bar{\nu}_e$ CC scattering can be measured both magnetically and calorimetrically to cross-calibrate the spectrometer and calorimeter. Flux errors will be diminished considerably by the simplicity of the neutrino source compared to π/K decay beams, which permits much more reliable monitoring. High rates will also allow direct flux measurement in the $\nu_\mu\bar{\nu}_e$ mode through use of the electroweak reactions $\nu_\mu e^- \to \mu^-\nu_e$ and $\bar{\nu}_e e^- \to \mu^-\bar{\nu}_\mu$.

2.4. Heavy quark production

The simple language of the quark parton model must be modified for νN DIS events with a charm or beauty quark in the final state in order to take into account the non-negligible quark mass. This presents both a challenge and an opportunity to test the QCD formalism for making these corrections.

Perhaps, the simplest and most widely used correction scheme is the essentially kinematic "slow rescaling" model of Georgi and Politzer [34], which amounts to a redefinition of the scaling variable x through

$$x \to \xi = x\left(1 + \frac{m_Q^2}{Q^2}\right)\ , \tag{27}$$

where m_Q is a heavy quark mass. One of the shortcomings of this prescription is that it fails to address ambiguities in the PDF that arise when one attempts a self-consistent pQCD treatment of heavy quark production.

Neutral current charm production illustrates this ambiguity. On the one hand, this can be treated as a "flavor-creation" process, $Z + g \to c\bar{c}$, which occurs at order α_s^1 in the pQCD expansion. In this case, the appropriate scheme for calculation of QCD radiative corrections involves only three light flavors (the so-called three-flavor scheme), and all of the effects associated with the charm quark are accounted for perturbatively in the hard scattering. On the other hand, the charm quark can be considered to be "light" at high energies when $Q^2 \gg m_c^2$, so the mass of the charm quark is much smaller than the relevant physical scale. In this case, one can view the charm quark as a parton with a corresponding parton distribution function (the so-called four-flavor scheme). In particular, the lowest order Wilson coefficient for charm production in this situation is a "flavor-excitation"

process, $Z + c \to c$, which is of order α_s^0. These two viewpoints must be reconciled in a consistent manner in order to avoid double counting.

The corresponding calculational problem for pQCD is the presence of a heavy quark mass scale that can be comparable to the Q^2 of the interaction. In the absence of this complication, the factorization theorem of QCD separates the high scale set by the value of transferred momentum, $\mu_{\rm H}^2 \sim Q^2$, from the low scale of hadronic physics, $\mu_{\rm L}^2 \sim \Lambda_{\rm QCD}^2$, and operator product expansion techniques can be used to sum the large logarithms of the form $\log(\mu_{\rm h}^2/\mu_{\rm l}^2)$ that multiply the expansion parameter, α_s.

A practical recipe for incorporating heavy quark masses in the pQCD summations is provided by the ACOT [35] prescription, which treats the number of active flavors, N_f, as a scale-dependent quantity. In particular, it suggests the use of a three-flavor evolution for $\mu < m_c$ and a four-flavor evolution above m_c, with continuity at the break point. In this prescription, the parton distribution functions are labeled by the number of active flavors and the heavy quark parton distribution functions, $f_{Q/N}(\xi, \mu)$, vanish for $\mu_{\rm H} \leqslant m_Q$ and satisfy the usual $\bar{MS}$ QCD evolution equation (with massless kernel functions) for $\mu_{\rm h} > m_Q$.

Charm and beauty production at νMCs will include large numbers of events with Q^2 above, below and around the effective m_Q^2 scale and should provide the most stringent tests from any experimental process of the pQCD formalism for heavy quark production. At that point, the experimental precision will likely require a more careful quantum field theoretical treatment of heavy quark masses.

Available rates at a νMC (Figs. 4 and 5) provide access to five different values for m_Q: m_c (from $\nu_\ell N \to \ell^- cX$) $2m_c$ (from $\nu_\ell N \to \nu_\ell c\bar{c}X$), m_b (from $\nu_\ell N \to \ell^- \bar{b}X$), $m_b + m_c$ (from $\nu_\ell N \to \ell^- c\bar{b}X$) and $2m_b$ (from $\nu_\ell N \to \nu_\ell b\bar{b}X$). To the degree a consistent pair of values for m_b and m_c emerges, one would have established theoretical control over these production processes. Those mass values could also be compared to what QCD sum rules, heavy quark expansions and lattice QCD yield. They can also be used to calibrate models for heavy quark production that enter into other νMC analyses, such as the pQCD tests described above and the precision $\sin^2\theta_W$ measurements in inclusive NC scattering that are discussed in Section 4.

Other than the ubiquitous high rates, the main experimental asset for a νMC in these studies will be the opportunity to use vertexing targets. This should allow for lifetime tagging of heavy flavors that minimizes systematic effects due to fragmentation and decay uncertainties.

2.5. Parton distribution functions at large Bjorken x

The unique level of quark-by-quark characterization of nucleon structure expected at νMCs will provide an invaluable reference source for many diverse analyses in collider and fixed target physics including, of course, other precision analyses at νMCs. Precise measurements as $x \to 1$ are particularly relevant to the modeling of rates for interesting physics processes and backgrounds at hadron colliders because uncertainties at high x and at the typical Q^2 values for νMCs will evolve to uncertainties at much lower x as Q^2 increases to collider values. Uncertainties at high x in current nucleon PDF derive from two sources: the ratio $d(x, Q^2)/u(x, Q^2)$ as $x \to 1$ and the role of higher twist corrections.

Analyses on present leptoproduction data sets that used hydrogen and deuterium targets have been unable to precisely pin down the high-x behavior of $d(x)/u(x)$. For example, QCD fits [36]

to the high-x NMC data and the CDF W-decay asymmetry improve with the inclusion of a simple x-dependent correction for a $d(x)/u(x)$ ratio that asymptotically approaches 0.2 rather than zero for $x \to 1$. On the other hand, the recent CTEQ5 global QCD analysis [37] found that including this correction had little effect on the quality of their fits.

Besides the statistical and experimental uncertainties in the data sets, a complication with high x analyses is the need to model nuclear binding effects in deuterium. This issue can be avoided at a νMC, where a high-statistics exposure to an H_2 target alone could directly measure the $d(x)/u(x)$ ratio in protons as $x \to 1$ from the ratio of $\nu_\ell p$ to $\bar{\nu}_\ell p$ cross sections. Such a measurement would require only a small correction for the residual sea quark contributions at high x.

Measurement of quark PDFs at high x is closely related to the question of the leading power corrections in the QCD perturbative expansion that are known as "higher twist effects". The nth-order higher twist effects are proportional to $1/Q^{2n}$ and reflect the fact that quarks have transverse momentum within the nucleon and that the probe becomes larger as Q^2 decreases, thus increasing the probability of multi-quark participation in an interaction. As was the case with the u/d ratio, different analyses of higher twist corrections in current data leave unresolved issues that would benefit from new experimental information.

An analysis by Milsztajn [38] that combined electroproduction data from SLAC with BCDMS muo-production data found that the relative size of the twist-4 contribution rapidly increased above $x = 0.4$ and was equal in magnitude to the leading $1/\log Q^2$ term for $x > 0.75$. The only measurements of this higher-twist term in neutrino experiments have been two low-statistics bubble chamber experiments: in Gargamelle [39] with freon and in BEBC with NeH_2. Both bubble chamber analyses are complicated by nuclear corrections at high x. However, both found a twist-4 contribution that is smaller in magnitude and, most significantly, of opposite sign to that of the charged leptoproduction analysis.

In contrast, a CTEQ global QCD analysis that combines neutrino and charged lepton production analyses up to $x = 0.75$, finds that *no* higher-twist term is required for values of Q^2 down to $0.7\,\mathrm{GeV}^2$. However, this analysis uses a cut on the invariant mass of the hadronic system, $W > 4\,\mathrm{GeV}$, that could exclude the bulk of any twist-4 contribution. Most recently, the Yang–Bodek analysis mentioned above [36] reanalyzed electroproduction data looking for a higher twist contribution. They find that by incorporating an NLO QCD analysis, as opposed to the LO analysis used by Milsztajn, the higher-twist contribution becomes much smaller. However, they have also included the $d/u \to 0.2$ model in their extraction of higher-twist, which will reduce the size of any extracted higher-twist term.

From a more theoretical viewpoint, a recent CTEQ paper by Guo and Qiu [40] has predicted the leading x dependence to the higher-twist term in $F_2(x, Q^2)$ in the region of large x and found that the higher-twist contribution is *different* for u and d quarks. Were this to be true, then the $d(x)/u(x)$ analysis and the leading power correction analysis would be directly intertwined. Interestingly enough, this prediction only depends on two non-perturbative parameters and is therefore highly constrained. It could be tested at both CEBAF and a νMC.

2.6. Examining the spin structure of the nucleon

A unique new feature of νMCs would be the availability of sufficiently intense beams to allow, for the first time, measurements of neutrino scattering off nucleons in polarized targets. This would

provide access to the polarized nucleon structure functions for neutrino–nucleon scattering and could answer several currently unresolved questions about the spin structure of the nucleon.

Polarized structure functions (PSFs) can be represented approximately by the quark–parton model in terms of the differences between the parton densities of quarks and gluons polarized parallel to the nuclear spin and those that are polarized anti-parallel:

$$\delta q(x,Q^2) = q^{\uparrow\uparrow}(x,Q^2) - q^{\uparrow\downarrow}(x,Q^2)\ , \tag{28}$$

$$\delta\bar{q}(x,Q^2) = \bar{q}^{\uparrow\uparrow}(x,Q^2) - \bar{q}^{\uparrow\downarrow}(x,Q^2), \qquad \delta g(x,Q^2) = g^{\uparrow\uparrow}(x,Q^2) - g^{\uparrow\downarrow}(x,Q^2)\ . \tag{29}$$

In the naive (LO) quark–parton model, the polarized structure functions g_1 and g_3 have quark spin content corresponding to the quark content of the parity-conserving and parity-violating unpolarized structure functions F_1 and F_3, respectively:

$$g_1^{\nu N}(x,Q^2) = \delta d^N(x,Q^2) + \delta s^N(x,Q^2) + \delta\bar{u}^N(x,Q^2) + \delta\bar{c}^N(x,Q^2)\ , \tag{30}$$

$$g_1^{\bar{\nu}N}(x,Q^2) = \delta u^N(x,Q^2) + \delta c^N(x,Q^2) + \delta\bar{d}^N(x,Q^2) + \delta\bar{s}^N(x,Q^2) \tag{31}$$

and

$$2xg_3^{\nu p}(x,Q^2) = -[\delta d(x,Q^2) + \delta s(x,Q^2) - \delta\bar{u}(x,Q^2) - \delta\bar{c}(x,Q^2)]\ , \tag{32}$$

$$2xg_3^{\bar{\nu}p}(x,Q^2) = -[\delta u(x,Q^2) + \delta c(x,Q^2) - \delta\bar{d}(x,Q^2) - \delta\bar{s}(x,Q^2)]\ . \tag{33}$$

The other parity-conserving PSF, g_2, has no simple interpretation in the LO quark–parton model, as is also the case with the parity-violating g_4. The remaining PSF, g_5, is related to g_3 via $g_5 = 2xg_3$ in the naive quark–parton model.

The levels of the different polarized quark PDFs can be regarded as quantifying the extent to which a parton of flavor q "remembers" the polarization of its nucleon parent in interactions at a given Q^2. The nucleon spin, $(\frac{1}{2})$, can be decomposed as

$$\tfrac{1}{2} = \tfrac{1}{2}(\Delta\Sigma(Q^2) + \Delta g(Q^2) + L_q(Q^2) + L_g(Q^2))\ , \tag{34}$$

where $\Delta\Sigma = \Delta u + \Delta d + \Delta s + \cdots$ and Δg are the integrated net quark and gluon helicities along the nucleon spin direction, e.g.,

$$\Delta u(Q^2) \equiv \int_0^1 \delta u(x,Q^2)\,\mathrm{d}x\ ,$$

$$\Delta g(Q^2) \equiv \int_0^1 \delta g(x,Q^2)\,\mathrm{d}x\ . \tag{35}$$

The L_q and L_g represent the relative orbital angular momenta of the quarks and gluons, respectively.

To date, the only charged lepton polarized DIS data come from non-collider experiments, running at energies where photon exchange dominates. Thus, only the parity-conserving polarized structure functions $g_1^{\ell N}$ and $g_2^{\ell N}$ have been studied so far. The results are surprising. From the measured

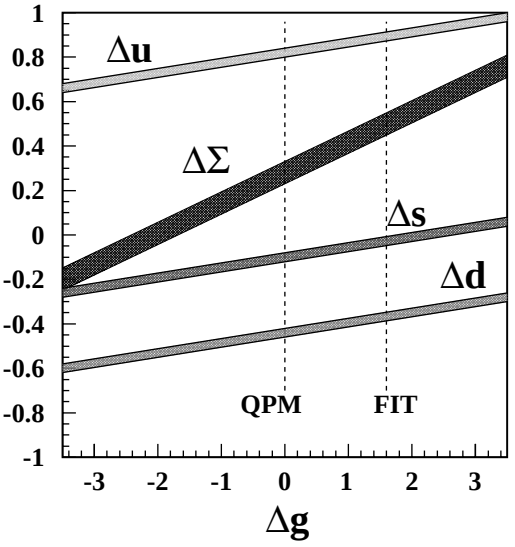

Fig. 6. Model-dependent decomposition of nucleon spin into contributions from quarks and gluons. The two vertical dotted lines show the naive QPM expectation and the results from an NLO fit to most of the available data on g_1^l.

first moment of $g_1^{\ell N}$ structure function, it can be concluded that only 30% of the nucleon spin is carried by quarks if one assumes $\Delta g = 0$, i.e., $\Delta\Sigma = 0.3$. An additional conclusion in this simple parton model interpretation is that the strange sea is anti-aligned with the nucleon spin, $\Delta s = -0.1$. In the more realistic QCD-enhanced parton model, the QCD evolution of the quark distributions brings in contributions from gluon radiation ($q \to qg$) and pair-production ($g \to q\bar{q}$) that induce a non-zero gluon spin distribution. This latter conclusion is supported by pQCD analyses of the Q^2 evolution of the available data on $g_1^{\ell N}$, as is illustrated in Fig. 6.

Although the decomposition of Fig. 6 is highly model dependent, the ability of neutrinos to select specific quark flavors should allow a polarized DIS experiment at a muon storage ring to greatly constrain such models.

2.7. Experimental setup and measurement technique

An ideal polarized target would have a mass of at least 10 kg, high polarizability, a large fraction f of polarizable material and the capability for polarizing both protons and neutrons. The solid HD compound material "ICE" appears to be a promising new technology [41]. Both the H and the D can be polarized, either in separate experimental runs or together. The expected polarization and dilution are $P_{\rm H} = 80\%$ and $f_{\rm H} = \frac{1}{3}$ for hydrogen, and $P_{\rm D} = 50\%$ and $f_{\rm D} = \frac{2}{3}$ for deuterium. A 7 kg (density $\rho_{\rm t} = 0.11\ {\rm g/cm^3}$) polarized target with the qualities mentioned above can be built out of an ICE target that is 20 cm in radius and 50 cm deep, perhaps mounted upstream from a general purpose neutrino detector like that in Fig. 2. Raw event rates in such a polarized target could be of order 10^8 events/yr, as shown in Table 2. A previous study for νMCs [42] has shown that a 200 kg target of polarized butanol with 10% polarization could measure the strange sea polarization

to about 3% in a 1 yr run in a beam downstream of a 250 GeV muon collider with a 10 m straight section.

Measurement of g_1 requires both ν and $\bar{\nu}$ beams and follows from the double cross-section difference:

$$A_{g_1} = \{\sigma^{\nu N}_{\uparrow\uparrow} - \sigma^{\nu N}_{\uparrow\downarrow}\} - \{\sigma^{\bar{\nu}N}_{\uparrow\uparrow} - \sigma^{\bar{\nu}N}_{\uparrow\downarrow}\} \,, \tag{36}$$

where $\sigma^{\nu N}_{\uparrow\uparrow}$ denotes, for example, the neutrino scattering off a target N with its spin polarized *parallel* to the neutrino helicity. This difference should be measured as a function of x and y to test for effects of unwanted PSF such as g_2. For g_3 one evaluates the similar quantity

$$A_{g_3} = \{\sigma^{\nu N}_{\uparrow\uparrow} - \sigma^{\nu N}_{\uparrow\downarrow}\} + \{\sigma^{\bar{\nu}N}_{\uparrow\uparrow} - \sigma^{\bar{\nu}N}_{\uparrow\downarrow}\} \,. \tag{37}$$

Cross-checks can be made with the target transversely polarized, where the suppression factors for the unwanted PSF are different.

2.8. Applications of polarized parton distribution data from νMCs

Measured values for g_1 from any nucleon target at a νMC would allow verification of the predicted decomposition:

$$\int_0^1 \mathrm{d}x(g_1^{\nu N} + g_1^{\bar{\nu}N}) = \Delta\Sigma - C\Delta g \,, \tag{38}$$

where the factor C is model dependent and a common choice is $C = N_f\alpha_s/2\pi$, and one has knowledge of $\Delta\Sigma$ from other data. In contrast to polarized charged lepton scattering, this determination can be done without relying on low-energy input from beta decay data augmented by SU(3) symmetry.

For another application, one notes that g_3, g_4 and g_5 probe only non-singlet combinations of parton densities so that they do not get a contribution from the gluon density. Then, for scattering off an isoscalar target:

$$xg_3^{\nu N} - xg_3^{\bar{\nu}N} = \delta c + \delta\bar{c} - \delta s - \delta\bar{s} \,. \tag{39}$$

(This is the polarized target analog of Eq. (20).) Assuming that $\delta c \ll \delta s$, this provides a measure of the level of polarization of the strange quark sea. Like xF_3, the non-singlet PSF, g_3, g_4 and g_5, have QCD evolutions containing no contribution from gluons at lowest order. Comparison of the non-singlet functions with the singlet SF g_1 and F_2 should therefore provide an indirect means for measuring the gluon contribution Δg.

As was the case for unpolarized targets, final state quark flavor tagging should provide additional semi-inclusive structure functions to augment the information on quark content from inclusive polarized structure functions. Probably, the most important example will be studies of the strange spin contribution via charm production. Figs. 4 and 5 show that approximately 5% of the events from a 50 GeV muon storage ring will have charm in the final state, with 20% of these decaying semi-leptonically. An experiment with 20 million neutrino interactions thus will have 2×10^5 semi-leptonic charm events before kinematic cuts, which should be sufficient for a precise measurement of δs and $\delta\bar{s}$.

2.9. Studying nuclear effects with neutrinos

Nuclear effects in DIS have been studied extensively using muon and electron beams but have only been glanced at for neutrinos in low-statistics bubble chamber experiments. Neutrino experiments with high statistics have formerly only been possible using heavy nuclear targets such as iron calorimeters and, for these targets, nuclear effects in νN interactions have typically been considered as problems to overcome rather than as a source of physics insights. This section reviews the physics of nuclear QCD that is relevant to neutrino interactions and shows that νMCs could instead provide experimental conditions where a great deal of interesting knowledge could be added to this field by using a variety of heavy nuclear targets as well as H_2 and D_2.

Nuclear studies at a νMC could use a general purpose detector such as that in Fig. 2 if it could be designed with interchangeable targets. Alternatively, a detector dedicated to nuclear studies could be used, perhaps with a geometry similar to that of the Fermilab E-665 Tevatron muon experiment [43]. For example, it could consist of a liquid H_2 or D_2 target followed by a rotating support of targets with different A interspersed with tracking chambers, and then by an appropriate calorimeter/muon spectrometer. A νMC should be easily capable of supplying the event sample sizes required to examine the predicted nuclear effects. For example, one can consider a 1-yr exposure of each target to the beam in the 50 GeV νMC scenario of Table 1. Then 10^7 events would be acquired in targets subtending out to the $1/\gamma_\mu$ characteristic angular size of the neutrino beam and that had lengths of 18 cm for D_2, 1.4 cm for graphite and only 0.16 cm for tungsten.

Different types of nuclear effects arise on passing through four distinct regions in Bjorken x:

(1) "shadowing" for $x < 0.1$,
(2) "anti-shadowing" for $0.1 < x < 0.2$,
(3) the "EMC Effect" for $0.2 < x < 0.7$ and
(4) "Fermi motion " for $x > 0.7$.

These regions will now be discussed in turn.

2.9.1. Low x: PCAC and nuclear shadowing

In the shadowing region, $x < 0.1$, there are several effects where a neutrino probe could provide different insights to charged lepton probes. Considering first the limit as $Q^2 \to 0$, the vector current is conserved and goes to zero but the axial-vector part of the weak current is only partially conserved (PCAC) and $F_2(x, Q^2)$ approaches a non-zero constant value as $Q^2 \to 0$. According to the Adler theorem [31], $\sigma_{\nu N}$ can be related to $\sigma_{\pi N}$ at $Q^2 = 0$. A νMC should be able to address the question of what effect a nuclear environment has on the Adler theorem.

The region of vector meson dominance (VMD) is reached in nuclear scattering of charged leptons ($\ell^{\pm}A$ scattering) in the low-x shadowing regime as Q^2 increases from 0 but remains below of order 10 GeV^2. The physics concept of VMD is the dissociation of a virtual photon into a q–$\bar{q}$ pair, one of which interacts strongly with the "surface" nucleons of the target nucleus. Thus the interior nucleons are shadowed by the surface nucleons. Neutrino scattering should involve not only a VMD effect (though now with dissociation of a virtual W rather than a photon) but also additional contributions from axial-vector mesons such as the A_1. Further, there should be additional non-perturbative effects that appear as nuclear shadowing (mainly in large nuclei) and which involve gluon recombination from nucleons neighboring the struck nucleon that shift the parton distributions toward higher values

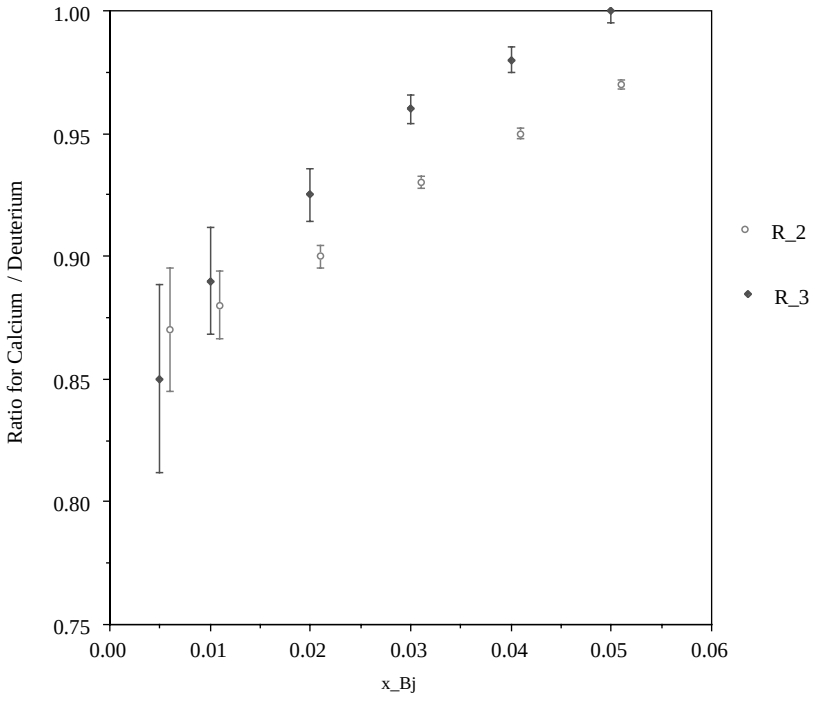

Fig. 7. Simulated predictions for the ratios of both the F_2 and xF_3 structure functions between calcium and deuterium, plotted as a function of Bjorken x and assuming the theoretical model of Kulagin [45] and data samples from a νMC. The sizes of the error bars correspond approximately to 1-yr exposures for both targets at the 50 GeV νMC of Table 1.

of x. Boros et al. [44] predict that the resulting shadowing effects in $\nu_\ell A$ scattering will be roughly $\frac{1}{2}$ that measured in $\ell^{\pm}A$ scattering. A more quantitative analysis by Kulagin [45] uses a non-perturbative parton model to predict that shadowing in $\nu_\ell A$ scattering to be either equal to or slightly above that in $\ell^{\pm}A$ scattering at $Q^2 = 5\,\mathrm{GeV}^2$. It also attempts to determine the quark flavor dependence of shadowing effects by separately predicting shadowing for $F_{2\mathrm{NC}}^{\nu A}(x,Q^2)$, $F_{2\mathrm{NC}}^{\nu A}(x,Q^2)$ and $xF_{3\mathrm{CC}}^{\nu A}(x,Q^2)$.

The predictions of Kulagin should be testable at a νMC, as is indicated by Fig. 7. This shows a simulation for a νMC data sample of the predicted measured ratios of the values for $F_2(x)$ and $F_3(x)$ on a calcium target divided by those on a deuterium target:

$$R_{2A}(x) \equiv F_2(x,Q^2)[\mathrm{Ca}]/F_2(x,Q^2)[\mathrm{D}_2]\ , \tag{40}$$

$$R_{3A}(x) \equiv F_3(x,Q^2)[\mathrm{Ca}]/F_3(x,Q^2)[\mathrm{D}_2]\ , \tag{41}$$

where the ratios are an event-weighted average over the experimental Q^2 range. As can be seen, the predicted difference between the shadowing on sea and valence quarks is clearly visible down to $x = 0.02$–0.03.

2.9.2. Mid-x: anti-shadowing and the EMC effect

Drell–Yan experiments have also measured nuclear effects and their results are quite similar to DIS experiments in the shadowing region. However, in the anti-shadowing region where R_{2A} makes

a brief but statistically significant excursion above 1.0 in DIS, Drell–Yan experiments see no effect. This could be an indication of differences in nuclear effects between valence and sea quarks.

Eskola et al. [46] have quantified this difference using a model which predicts that the differences between nuclear effects in $xF_{3\mathrm{CC}}^{\nu A}(x,Q^2)$ and $F_{2\mathrm{CC}}^{\nu A}(x,Q^2)$ should persist through the anti-shadowing region as well. Taking the work of Kulagin and Eskola together implies that nuclear effects in $xF_{3\mathrm{CC}}^{\nu A}(x,Q^2)$ should be quite dramatic, with more shadowing than $F_{2\mathrm{CC}}^{\nu A}(x,Q^2)$ at lower x followed by R_{3A} rising fairly rapidly to yield significant anti-shadowing around $x=0.1$. The 50 GeV νMC experiment assumed for Fig. 7 should be able to measure anti-shadowing effects and the difference between shadowing effects in $F_2(x,Q^2)$ and $xF_3(x,Q^2)$ at a statistical level of about 6 standard deviations.

2.9.3. High x: multi-quark cluster effects

Analyses from DIS experiments of $F_2(x,Q^2)$ in the "Fermi-motion" region, $x>0.7$, have required few-nucleon correlation models and multi-quark cluster models to fit the data. These models boost the momentum of some of the quarks, producing a high-x tail in $F_2(x,Q^2)$ that is predicted to behave as e^{-ax}. However, fits to μCa [47] and νFe [49] have obtained two different values for the fitted constant a: $a_{\mu\mathrm{Ca}}=16.5\pm0.5$ and $a_{\nu\mathrm{Fe}}=8.3\pm0.7$, respectively. This was considered surprising because of the expectation that any few nucleon correlation or multi-quark effects would have already saturated by carbon. A high-statistics data sample from a νMC, with precise kinematic reconstruction of the Bjorken x values for each event, could go a long way toward resolving the dependence of the value of a on the nucleus and on the lepton probe.

3. Studies of the CKM quark mixing matrix

3.1. Introduction

The CKM quark mixing matrix comprises a set of fundamental parameters of the Standard Model that reflect the dynamics shaping the generation of particle masses. Furthermore, it provides essential input for predictions on various CP asymmetries in B decays which should be sharpened as much as possible in order to increase their sensitivity to the presence of new physics processes.

It is likely that νMCs could make a very substantial contribution to measurements of quark mixing, with systematically unique measurements of four of the nine moduli in the CKM matrix that should be comparable to or better than the best future measurements at other experiments. The relevant moduli are $|V_{cd}|$, $|V_{cs}|$, $|V_{ub}|$ and $|V_{cb}|$, to be extracted from charm production off d and s quarks, and from beauty production off u and c quarks, respectively. If muon colliders ever reach the 100 TeV energy center-of-mass range, then their νMCs could further provide a unique opportunity for precise direct measurements of the CKM elements involving the top quark [14].

This section is organized as follows. Section 3.1.1 gives a summary of the current experimental status and future expectations for before the advent of νMCs. Section 3.1.2 then gives a general overview of the method for extracting CKM information at νMCs. Sections 3.2 and 3.3 then give more specific details on νMC experimental analyses involving the production of charm and bottom quarks, respectively. A further analysis that may have potential for a measurement of CKM parameters—diffractive charmed vector meson production—is briefly addressed in Section 3.4.

Finally, Section 3.5 summarizes all of these expected improvements from νMCs to our knowledge of the CKM matrix.

3.1.1. Current experimental knowledge of the relevant CKM matrix elements, and future expectations

Table 3 presented the current [15] experimental values and uncertainties for the absolute squares of the interesting CKM matrix elements for νMCs: V_{cd}, V_{cs}, V_{ub} and V_{cb}. The first two of these can be more tightly constrained by adding the assumption of three family unitarity, so improved measurements of these elements can be considered as testing these unitarity conditions.

The values for $|V_{cd}|$ and $|V_{cs}|$ have been extracted from charm production in deep inelastic scattering supplemented by information gathered in semileptonic D decays, while $|V_{cb}|$ and $|V_{ub}|$ have been obtained from semileptonic B decays.

In the next few years, *exclusive* semileptonic charm decays like $D \to \ell \nu K/K^*/\pi/\rho$ will be measured more precisely. However, it is not clear at present whether theoretical technologies like QCD simulations on the lattice will improve sufficiently to fully utilize such data for extracting more accurate values of $|V_{cs}|$ and $|V_{cd}|$.

At present $|V_{cb}|$ is measured with about a 5% *theoretical* uncertainty and a 5% or better *experimental* uncertainty. (For comparisons with the uncertainties quoted in Table 3 recall that the fractional uncertainty in the *square* of the modulus is twice that of the modulus itself.) The two most reliable determinations are from the semileptonic B width and the form factor for $B \to \ell \nu D^*$ at zero recoil. One can reasonably expect the theoretical uncertainty in these processes to go down to about 2% [50].

The situation is considerably less satisfactory for $|V_{ub}|$. Most of the analyses employed so far contain a large dependence on theoretical models, the accuracy of which is hard to evaluate. One can hope that studies of both exclusive and inclusive semileptonic B decays done at the B factories will yield values for $|V_{ub}|$ with a *theoretical* accuracy of no more than 10% by 2005. However, this is not guaranteed.

It is highly desirable to improve on this situation by obtaining more precise and reliable values for these CKM parameters. The main reason is that they are theoretically expected to be a consequence of the generation of quark masses which in turn reflects dynamics operating at presumably ultra-high-energy scales. It turns out that qualitatively quite distinct "textures" for the Yukawa couplings assumed to apply at GUT scales lead to CKM parameters that, due to differing renormalization effects, are numerically relatively similar at electroweak scales. Secondly, various CP asymmetries in B decays will be measured presumably to better than 5% over the next ten years; their predicted values depend crucially on the size of V_{ub} and V_{cb} (and V_{td}). To exploit the discovery potential for new physics to the fullest one wants to match up experimental and theoretical accuracy.

To be more specific:

- One wants at least to confirm the values for $|V_{cs}|$ and $|V_{cb}|$ by a *systematically* different method.
- One would like to determine a precise value for $|V_{cd}|$ *without* imposing 3-family unitarity.
- It is an important goal to extract the value of $|V_{ub}|$ with considerably less than 10% uncertainty.

It appears that νMCs are up to these tasks and possibly more. Indeed, if a future νMC in the 100 TeV energy range were ever to be realized, then even top quark production could be studied

and this would uniquely allow the extraction [14] of V_{td} and V_{ts} in a relatively straightforward way!

3.1.2. Extracting CKM matrix elements in νMCs*: an overview*

The experimental quantities used for all the quark mixing measurements in νMCs are the production cross sections and kinematic distributions of heavy flavor final states from CC interactions. These are related back to the quark couplings through a parameterization of the initial state quark distributions and a model of the production processes that includes threshold suppressions due to the quark masses. Measurements of CKM matrix elements at νMCs will be analogous to, but vastly superior to, current neutrino measurements of $|V_{cd}|^2$ that use dimuon events for final state tagging of charm quarks, which are reviewed elsewhere [12]. This improvement is due to the overall higher rate of interactions, the ability to tag charm *inclusively* by vertexing and the capability of fully reconstructing the event kinematics for charm decays to hadrons.

In principle, the struck quark can be converted into any of the three final state quarks that differ by one unit of charge. In practice, production of the heavy top quark is kinematically forbidden except from neutrinos at energies above about 16 TeV, and the production of other quark flavors is influenced by their mass. After correcting for this kinematic suppression, the Standard Model predicts the probability for the interaction to be proportional to the absolute square of the appropriate element in the CKM matrix. The most relevant theoretical uncertainty lies in the treatment of the production thresholds. Measuring these cross sections at different energies and separately for CC and NC reactions should help in understanding the threshold behavior.

3.2. Analyses involving charm production: the extraction of V_{cd} *and* V_{cs}

The extraction of $|V_{cd}|$ will be the cleanest of the four CKM measurements at νMCs discussed here and this is the one CKM element whose modulus is already best determined in neutrino–nucleon scattering. It is measured from charm production off valence d quarks in isoscalar targets, and this valence quark distribution can be accurately determined from nucleon structure function measurements.

Figs. 4 and 5 show that charm production occurs in $\sim 7\%$ of the CC interactions from 100 GeV neutrinos, and will occur at slightly lower/higher rates for lower/higher energies according to the changing level of mass threshold suppression. This implies that realistic charmed event sample sizes might reach the 10^8 level.

The feature of the $|V_{cd}|$ analysis that makes it systematically rather clean is that charm production from valence quarks occurs for neutrinos but not for antineutrinos. Valence quarks have a harder x distribution than sea contributions from both s and (at a lower level) d quarks. It is also helpful that the s and d seas seen by neutrinos are also closely equal to their antiquark counterparts that are probed by antineutrinos, as would be verified in structure function analyses of the νMC data set (Section 2). This allows use of the $\bar{\nu}$ sample as an effective background subtraction for the sea contributions to the charm production by neutrinos.

To illustrate, one can measure scattering from an isoscalar target D with $\nu/\bar{\nu}$ beams and extract the ratio

$$r_c(x,y,E) = \frac{\mathrm{d}\sigma^{\nu\mathrm{D}}_{\mu cX}/\mathrm{d}x\,\mathrm{d}y - \mathrm{d}\sigma^{\bar{\nu}\mathrm{D}}_{\mu cX}/\mathrm{d}x\,\mathrm{d}y}{\mathrm{d}\sigma^{\nu\mathrm{D}}_{\mu X}/\mathrm{d}x\,\mathrm{d}y - \mathrm{d}\sigma^{\bar{\nu}\mathrm{D}}_{\mu X}/\mathrm{d}x\,\mathrm{d}y}\,, \tag{42}$$

where $\mathrm{d}\sigma_{\mu cX}^{\nu\mathrm{D}(\bar{\nu}\mathrm{D})}/\mathrm{d}x\,\mathrm{d}y$ represent the charm production cross sections and $\mathrm{d}\sigma_{\mu cX}^{\nu\mathrm{D}(\bar{\nu}\mathrm{D})}/\mathrm{d}x\mathrm{d}y$ denote the total inclusive CC cross sections. To leading order in QCD, this ratio can be computed from

$$\frac{1}{r_c^{\mathrm{LO}}(x,y,E)} = \frac{(q(x,Q^2)-\bar{q}(x,Q^2))(|V_{ud}|^2-(1-y)^2)}{|V_{cd}|^2(q(\xi,Q^2)-\bar{q}(\xi,Q^2))(1-y+xy/\xi)} + 1\ , \tag{43}$$

where $q(x,Q^2)=(u(x,Q^2)+d(x,Q^2))/2$, $\xi = x(1+m_c^2/Q^2)$ and m_c is the charm quark mass. Note that $r_c^{\mathrm{LO}}(x,y,E)$ depends only on the precisely measured $|V_{ud}|^2$, the well understood valence quark distribution, $q(\xi,Q^2)-\bar{q}(\xi,Q^2)$, the charm mass, and $|V_{cd}|^2$. Because the valence distribution peaks at relatively high x, threshold effects associated with m_c are minimized. Next-to-leading-order calculations are more complicated but leave these features intact.

As in analyses of today's neutrino experiments, the d and s contributions to the charm event sample will in practice be separated from one another in a fit involving the measured x distributions of the events and with the charm quark mass as a fitted parameter. With such huge statistics, the statistical uncertainty in the measurement will be only at the 10^{-4} level, so the measurement will be dominated by systematic uncertainties. Major contributions to the uncertainty are likely to be:

- Estimation of the charm tagging efficiency. This error is minimized by the clean, high-efficiency charm tagging that is possible with high-performance vertexing and a negligible B hadron background [9].
- The charm production model. It is a very attractive feature that the measurement is effectively of the ratio of charm production to the total production in each kinematical bin. Therefore, one is sensitive only to the kinematical suppression of charm states and not to the initial parton distribution functions. Mass threshold corrections that are applied according to theoretical models can be checked and calibrated from the trends in the data itself over the range of kinematical bins. Therefore, this uncertainty should initially decrease with increasing sample size.
- Estimation of the extent to which the sea is symmetric in quarks versus antiquarks. This uncertainty is lessened because the signal is largely at higher x than the background. If helpful, a cut in x value could be applied to the fit to further reduce this uncertainty.

With experimental handles on the major systematic uncertainties, it may be guessed that the irreducible *theoretical* uncertainty on $|V_{cd}|^2$ due to violations of quark–hadron duality might be at the percent level.

A measurement of $|V_{cs}|^2$ presents more challenges because this matrix element always appears in combination with the strange quark PDF $s(x,Q^2)$, which is difficult, but not impossible, to measure separately. Perhaps the best scheme [3] involves a simultaneous analysis of inclusive charged current scattering and semi-inclusive charm production [51] on deuterium targets. The inclusive CC cross section is of the form

$$\frac{\mathrm{d}\sigma_{\mu X}^{\nu\mathrm{D}(\bar{\nu}\mathrm{D})}}{\mathrm{d}x\,\mathrm{d}y} = \frac{\mathrm{d}\sigma_{\mu cX}^{\nu\mathrm{D}(\bar{\nu}\mathrm{D})}}{\mathrm{d}x\,\mathrm{d}y} + \frac{\mathrm{d}\sigma_{\mu\bar{c}X}^{\nu\mathrm{D}(\bar{\nu}\mathrm{D})}}{\mathrm{d}x\,\mathrm{d}y}\ , \tag{44}$$

[3] Methods to extract $s(x,Q^2)$ discussed in Section 2 assume a known CKM matrix.

where $\mathrm{d}\sigma_{\mu\not{c}X}/\mathrm{d}x\,\mathrm{d}y$ represents the part of the cross section with no charm in the final state (b production is neglected). To leading order

$$\frac{\pi}{2G_{\mathrm{F}}^2 ME}\frac{\mathrm{d}\sigma^{\nu\mathrm{D}}_{\mu cX}}{\mathrm{d}x\,\mathrm{d}y} = [|V_{cs}|^2 s(\xi,Q^2) + |V_{cd}|^2 q(\xi,Q^2)]\left(1-\frac{m_c^2}{2ME\xi}\right)\,, \tag{45}$$

$$\frac{\pi}{2G_{\mathrm{F}}^2 ME}\frac{\mathrm{d}\sigma^{\bar{\nu}\mathrm{D}}_{\mu cX}}{\mathrm{d}x\,\mathrm{d}y} = [|V_{cs}|^2 \bar{s}(\xi,Q^2) + |V_{cd}|^2 \bar{q}(\xi,Q^2)]\left(1-\frac{m_c^2}{2ME\xi}\right)\,, \tag{46}$$

$$\frac{\pi}{2G_{\mathrm{F}}^2 ME}\frac{\mathrm{d}\sigma^{\nu\mathrm{D}}_{\mu\not{c}X}}{\mathrm{d}x\,\mathrm{d}y} = |V_{ud}|^2 q(x,Q^2) + |V_{us}|^2 s(x,Q^2) + \bar{q}(x,Q^2)(1-y)^2\,, \tag{47}$$

$$\frac{\pi}{2G_{\mathrm{F}}^2 ME}\frac{\mathrm{d}\sigma^{\bar{\nu}\mathrm{D}}_{\mu\not{c}X}}{\mathrm{d}x\mathrm{d}y} = |V_{ud}|^2 \bar{q}(x,Q^2) + |V_{us}|^2 \bar{s}(x,Q^2) + q(x,Q^2)(1-y)^2. \tag{48}$$

Measuring $\mathrm{d}\sigma^{\nu(\bar{\nu})}_{\mu X}/\mathrm{d}x\,\mathrm{d}y$ and $\mathrm{d}\sigma^{\nu(\bar{\nu})}_{\mu cX}/\mathrm{d}x\,\mathrm{d}y$ gives $\mathrm{d}\sigma^{\nu(\bar{\nu})}_{\mu\not{c}X}/\mathrm{d}x\,\mathrm{d}y$. The y dependencies of the non-charm cross sections allow measurement of $q(x,Q^2)$ and $\bar{q}(x,Q^2)$. Assuming that $|V_{ud}|^2$ and $|V_{us}|^2$ contribute negligible error, and that $s(x,Q^2)=\bar{s}(x,Q^2)$, one then extracts $s(x,Q^2)$ from the Cabibbo suppressed $s\to u$ pieces of $\mathrm{d}\sigma^{\nu(\bar{\nu})}_{\mu\not{c}X}/\mathrm{d}x\,\mathrm{d}y$, and then $|V_{cs}|^2$ (and $|V_{cd}|^2$) from $\mathrm{d}\sigma^{\nu(\bar{\nu})}_{\mu cX}/\mathrm{d}x\,\mathrm{d}y$.

This procedure will require very high statistics and extreme care with theoretical and experimental systematic errors as it turns on the $|V_{us}|^2 s(x,Q^2)$ term in the cross section, which contributes only $\sim 0.15\%$ of the total cross section. Inclusive and charm cross-sections must be cross-normalized to high accuracy, and expressions (45)–(48) must be generalized to include higher-order QCD and possible non-perturbative effects.

Additionally, it may also be possible to measure the total strange quark content of the nucleon in NC "leading particle tagging" with a $\phi(1020)$ final state [9], although no experience with this method yet exists in neutrino physics.

In the end, it will likely be difficult to compete with the indirect constraint on $|V_{cs}|^2$ from precise measurements of the hadronic width of the W, Γ^h_{W}, at LEP2, the Tevatron and the LHC. This observable is, to leading order,

$$\Gamma^h_{\mathrm{W}} = \frac{1}{3}\,\Gamma^{\mathrm{tot}}_{\mathrm{W}} \sum_{Q=u,c}\sum_{q=d,s,b} |V_{Qq}|^2\,, \tag{49}$$

where $\Gamma^{\mathrm{tot}}_{\mathrm{W}}$ is the total hadronic width. Because $|V_{ub}|^2$ is small and all other terms in the sum can be measured precisely elsewhere, a strong $|V_{cs}|^2$ constraint emerges.

3.3. Analyses involving bottom production: the extraction of V_{ub} and V_{cb}

Measurements of V_{ub} and V_{cb} from the two transitions with a b quark in the final state—$u\to b$ and $c\to b$, respectively—require analyses that are conceptually similar to those for charm discussed in the preceding subsection. Figs. 4 and 5 show the statistics for CC b quark production to be

of order 10^4 events for a total sample of 10^{10} inclusive events, depending on the energy of the muon storage ring and the consequent threshold suppression due to the b quark mass. Besides the threshold suppression, the main reasons why the B production levels are so low for the two processes are that, in one case, the production from u quarks is suppressed by $|V_{ub}|^2 \sim \mathcal{O}(10^{-5})$, while production from charm quarks is inhibited by $|V_{cb}|^2 \simeq 1.6 \times 10^{-3}$ and by the extra mass of the $\bar{b}c$ final state.

Given the nearly optimal vertexing geometry possible at a νMC, separating out much of the fractionally small b hadron event sample [9] from the charm background should be feasible. Assuming that the B tagging efficiency and purity are well known, then the b production analysis should be a relatively straightforward copy of that for charm, involving a simultaneous fit to the u and c contributions to B production from neutrino and antineutrino scattering.

In analogy to charm production, the resolving power of the fit arises because antineutrino (but not neutrino) interactions give a high-x contribution from u valence quarks, while $c \to b$ transitions will be equal for ν and $\bar{\nu}$ and typically at lower x. It is again easy to see the effect at LO in QCD, as follows.

Define, in analogy to Eq. (42),

$$r_b(x,y,E) = \frac{\mathrm{d}\sigma^{\nu\mathrm{D}}_{\mu bX}/\mathrm{d}x\,\mathrm{d}y - \mathrm{d}\sigma^{\bar{\nu}\mathrm{D}}_{\mu bX}/\mathrm{d}x\,\mathrm{d}y}{\mathrm{d}\sigma^{\nu\mathrm{D}}_{\mu X}/\mathrm{d}x\,\mathrm{d}y - \mathrm{d}\sigma^{\bar{\nu}\mathrm{D}}_{\mu X}/\mathrm{d}x\,\mathrm{d}y}\ , \tag{50a}$$

where now $\mathrm{d}\sigma^{\nu D(\bar{\nu}D)}_{\mu bX}/\mathrm{d}x\,\mathrm{d}y$ represents the beauty production cross sections. QCD then predicts

$$\frac{1}{r_b^{\mathrm{LO}}(x,y,E)} = -\frac{(q(x,Q^2)-\bar{q}(x,Q^2))(|V_{ud}|^2-(1-y)^2)}{|V_{ub}|^2(q(\xi',Q^2)-\bar{q}(\xi',Q^2))(1-y)(1-xy/\xi')} + 1\ , \tag{51}$$

with $\xi' = x(1+m_b^2/Q^2)$ and m_b the b quark mass. As was the case with charm, $r_b^{\mathrm{LO}}(x,y,E)$ depends only on the high-x valence quarks, which helps to reduce the more substantial suppression associated with the higher value of m_b.

Reasonably accurate estimates of the measurement precisions would require both a more detailed study and a knowledge of the expected event sample size. The precision of the $|V_{ub}|^2$ measurement may approach the statistical limit of around 1% for a total neutrino event sample of order 10^{10} events.

The $c \to b$ transition can (unlike $s \to c$) be identified experimentally by the presence of soft c quark observed in association with the $\bar{b}$ quark in ν scattering. At νMC energies, it is reasonable to assume that $\bar{b}c$ production will be dominated by W–gluon fusion, and a good knowledge of the gluon PDF at high x will be required. This may well limit the $|V_{cb}|^2$ measurement accuracy to the few percent level.

It is widely expected that $|V_{cb}|$ will be known from B decays in other experiments to a few percent or better by 2005 [50]. Given this, an alternative and maybe more useful analysis strategy for a νMC might be to combine the V_{cb} analysis data at the νMC with the value of V_{cb} as extracted from semileptonic B decays in other experiments, with the purpose of analyzing the mass suppression in beauty production close to threshold, or in constraining the gluon PDF. This information could then be used as input to the extraction of V_{ub} as sketched above.

3.4. V_{cd}/V_{cs} via diffractive charmed vector meson production

It is possible to diffractively produce charmed vector mesons via W–boson–pomeron scattering [52,53]:

$$\nu_\mu A \to \mu^- (W^+ \mathscr{P}) A \to \mu^- D_S^{*+} A \,, \tag{52}$$

$$\nu_\mu A \to \mu^- (W^+ \mathscr{P}) A \to \mu^- D^{*+} A \,. \tag{53}$$

The D_S^{*+} cross section is of order 0.01 fb/nucleus, while that for D^{*+} should be smaller by a factor of $|V_{cd}/V_{cs}|^2$. For 10^{10} CC events, one expects of order 1.5×10^6 D_S^* events and 7500 D^* events. If the $W - D_S^*$ and $W - D^*$ dynamical couplings are identical, the relative rate can measure the ratio of the CKM matrix elements.

The experimental signature is fairly unique: a two- or three-prong muon–meson vertex with a D^+/D^0 or D_S^+ secondary. The cross section will peak at low momentum transfer and there should be no evidence for nuclear breakup.

The chief theoretical uncertainty likely has to do with evaluating SU(3)-breaking effects in the W–vector meson couplings and this may limit the potential for CKM studies from this process. Again, an alternative perspective can be taken: to use the information available on $|V_{cd}/V_{cs}|^2$ to analyze the SU(3) pattern of diffractive D^* versus D_s^* production.

3.5. Improved knowledge of the CKM matrix from νMCs

The Particle Data Group [15] assigns the following uncertainties to the four CKM parameters that were the main focus of our discussion:

$$|\Delta V_{cd}|_{\text{now}} = 7\%\ [3\%] \,, \tag{54}$$

$$|\Delta V_{cs}|_{\text{now}} = 15\%\ [2\%] \,, \tag{55}$$

$$|\Delta V_{ub}|_{\text{now}} = 30\% \,, \tag{56}$$

$$|\Delta V_{cb}|_{\text{now}} = 8\% \,, \tag{57}$$

where the numbers for V_{cd} and V_{cs} quoted in square brackets hold after 3-family unitarity has been imposed.

The future before a νMC could contribute can be sketched as follows:

- Some improvements can be expected over the next several years in *direct* extractions of V_{cd} and V_{cs} (i.e., those that do not impose 3-family unitarity constraints). However, it is very unlikely that they could come close to the 2–3% level.
- A combination of more detailed data on semileptonic B decays and further refinement of heavy quark expansions will yield very significant improvements in V_{cb} and V_{ub}; not unreasonable expectations are

$$|\Delta V_{cb}|_{\text{pre-}\nu\text{MC}} \simeq 3\%, \qquad |\Delta V_{ub}|_{\text{pre-}\nu\text{MC}} \simeq 10\text{–}15\% \,. \tag{58}$$

Our discussion suggests that potential *v*MC analyses could have an essential impact on central aspects of the Standard Model by meeting the goals stated in the beginning of this section:

- provide a *systematically* different determination of $|V_{cs}|$ and $|V_{cb}|$ that is as good as can be achieved in charm and beauty decay studies:

$$|\Delta V_{cs}|_{vMC} \sim \mathcal{O}(\text{few}\%), \qquad |\Delta V_{cb}|_{vMC} \sim \mathcal{O}(\text{few}\%)\ ; \tag{59}$$

- yield a value for $|V_{cd}|$ through *direct* observation that is about as good as otherwise achieved *only* through imposing 3-family unitarity

$$|\Delta V_{cd}|_{vMC} \sim \mathcal{O}(1\%)\ ; \tag{60}$$

- lower the theoretical uncertainty in $|V_{ub}|$ considerably:

$$|\Delta V_{ub}|_{vMC} \sim \mathcal{O}(1\%)\ . \tag{61}$$

  This would enable us to predict various CP asymmetries in B decays with order 1% accuracy, thus calibrating the experimental results expected from next-generation experiments like LHC-B and BTeV and allowing us to exhaust the discovery potential for new physics in B decays;
- improve dramatically our numerical information on the CKM parameters involving top quarks if a very high-energy *v*MC could be built.

4. Precision electroweak studies

4.1. Introduction

Neutrino scattering is a natural place to study the structure of the weak interaction. Historically, it has played an important role in establishing both the basic structure of the weak interaction, particularly with the discovery of neutral currents [54], and in providing the first precision tests of electroweak unification [55]. It is reasonable, as the high-intensity neutrino beams at future *v*MCs offer the promise of a new level of statistics in high-energy neutrino interactions, that one considers a new generation of experiments to probe the weak interaction.

At the same time, given the ambitious collider physics programs of LEP I, SLD, LEP II and the Tevatron, which will have been completed at the time of a *v*MC, and given the physics program of the LHC that will be ongoing, the goals of such experiments must be correctly focused.

4.1.1. Knowledge at the time of *v*MCs

Between today and the advent of a *v*MC, it is safe to assume that little improvement will have been achieved in the amazingly precise measurements of Z^0 decay and production parameters [56]. However, it is very likely that LEP II and the Tevatron Run II will have produced a measurement of M_W to a $20\ \text{MeV}/c^2$ precision [58,59] and that the mass of the top quark will be known with a precision of $1\ \text{GeV}/c^2$ [59].

Furthermore, LEP-II has found experimental hints of a possible Higgs boson at a mass around $115\ \text{GeV}/c^2$ which, although far from being a sure bet, might possibly be confirmed at either the Tevatron or the LHC. Alternatively, one of these hadron colliders might instead discover the Higgs

at a higher mass or else something completely different. Of course, the odds of such a discovery are much higher if a Higgs exists close to the value hinted at by the LEP-II events, as present electroweak fits also seem to suggest [56].

An observation of a Standard Model Higgs, along with a precise prediction of its mass driven by the W and top quark mass measurements, will make an elegant *pièce de resistance* of the electroweak physics program at the energy frontier for the period between 1990 and 2010.

During this time, there may also be improvements in low-energy tests of the electroweak Standard Model. Atomic parity violation experiments may be able to yet again improve significantly in their ability to provide precision tests of weak interactions if experiments utilizing trapped unstable Francium become possible [60]. Also, SLAC E-158 [61], a proposed polarized Moller scattering experiment, may be able to probe $\sin^2\theta_W$ at a precision of 0.0008 at $Q^2 \sim 10^{-2}\ \mathrm{GeV}^2$.

4.1.2. Goals of fixed-target electroweak physics programs

The primary goals of a low-energy test of a high-energy theory remain largely the same as they have been in the past. Unification of the interactions of the on-shell weak bosons with their low-energy manifestations in weak interactions at high precision remains an appealing and elegant test of the model.

The low-energy experiments also allow access to some aspects of the theory that cannot be readily observed at high energies. For example, a demonstration of the running of the weak coupling strength now only awaits precise low-energy data [62], given the high precision at the scale of the weak boson masses. Another powerful use for low-energy data is the sensitivity to interference between new physics and tree-level processes. For example, if Z' bosons are discovered at the energy frontier, then observation of the interference between the Standard Model Z and the Z' at low energy may be one of the most powerful tests constraining models that relate the two interactions.

4.1.3. Electroweak processes with neutrinos

To provide a precision test of the Standard Model, a process must be reasonably common and precisely calculable. The two useful neutrino interaction processes for these sorts of studies are measurements of $\sin^2\theta_W$ through neutrino–nucleon DIS (neutrino–quark scattering), and neutrino–electron elastic and quasi-elastic scattering. The former, of course, wins on large cross section, but the latter wins on simplicity of target and therefore minimal theoretical uncertainties. The possibilities for using these processes are described below.

Electroweak processes not considered here include neutrino tridents—i.e., three lepton final states resulting from internal conversion of a virtual photon—which are effectively a test of boson–boson scattering. While these processes are interesting, they do not provide a stable basis on which to form a precision probe of the model because of large theoretical uncertainties in the cross section. See Section 5 for further discussion of this and other processes.

4.2. Elastic and quasi-elastic neutrino–electron scattering

Perhaps the most promising reaction for measuring $\sin^2\theta_W$ at a νMC is ν–e scattering. Neutrino–electron scattering possesses one significant advantage over DIS for precision electroweak studies, namely that the target is point-like and its structure does not introduce uncertainties in extracting the parameters of the fundamental interaction from the observed cross sections.

Table 4
The coupling coefficients, g_L and g_R, in Eq. (68) for the neutrino–electron scattering processes of Eqs. (62), (64), (65) and (66), respectively. The numerical values in the final column correspond to the combination of couplings that appears in the tree-level total cross section for $\sin^2\theta_W = 0.23$

Reaction	g_L	g_R	$g_L^2 + \frac{1}{3}g_R^2$
$\nu_\mu e^- \to \nu_\mu e^-$	$-\frac{1}{2} + \sin^2\theta_W$	$\sin^2\theta_W$	0.091
$\bar{\nu}_\mu e^- \to \bar{\nu}_\mu e^-$	$\sin^2\theta_W$	$-\frac{1}{2} + \sin^2\theta_W$	0.077
$\nu_e e^- \to \nu_e e^-$	$\frac{1}{2} + \sin^2\theta_W$	$\sin^2\theta_W$	0.551
$\bar{\nu}_e e^- \to \bar{\nu}_e e^-$	$\sin^2\theta_W$	$\frac{1}{2} + \sin^2\theta_W$	0.231

4.2.1. Survey of neutrino–electron scattering processes

Several ν–e scattering reactions will occur in the muon and electron neutrino and antineutrino beams at a νMC:

$$\nu_\mu e^- \to \nu_\mu e^- \,, \tag{62}$$

$$\nu_\mu e^- \to \nu_e \mu^- \,, \tag{63}$$

$$\bar{\nu}_\mu e^- \to \bar{\nu}_\mu e^- \,, \tag{64}$$

$$\nu_e e^- \to \nu_e e^- \,, \tag{65}$$

$$\bar{\nu}_e e^- \to \bar{\nu}_e e^- \,, \tag{66}$$

$$\bar{\nu}_e e^- \to \bar{\nu}_\mu \mu^-, \bar{\nu}_\tau \tau^-, \bar{u}d \ldots \,. \tag{67}$$

Reactions (62) and (64) are purely neutral-current processes mediated by the exchange of a Z^0. Reaction (65) has both charged current ($W^\pm$ exchange) and neutral current components, and reaction (66) has neutral current t-channel and charged-current s-channel components. Reactions (63) and (67) can result in the production of a single muon and therefore have a significant muon mass threshold in the cross section. Fig. 8 shows the Feynman diagrams for these processes.

Because of the small ratio of the electron to proton mass, the cross section for neutrino–electron scattering is much smaller than that for neutrino–nucleon DIS. The leading order differential cross section for neutrino–electron elastic scattering with respect to $y = E_e/E_\nu$ is given by

$$\frac{\mathrm{d}\sigma}{\mathrm{d}y}(\nu e^- \to \nu e^-) = \frac{G_F^2 s}{\pi}[g_L^2 + g_R^2(1-y)^2] \,, \tag{68}$$

where the center-of-momentum energy, s, is well approximated by $s \simeq 2m_e E_\nu$ when $E_\nu \gg m_e$, where terms of $\mathcal{O}(m_e/E_\nu)$ are neglected and where g_L and g_R are process dependent because of their exchange in the neutral current process under $\nu \leftrightarrow \bar{\nu}$ and because of the addition of the charged current process for electron–neutrino-induced reactions. The values of g_L and g_R are given in Table 4. Numerical values for the cross sections after integrating over y are

$$\sigma(\nu e^- \to \nu e^-) = 1.6 \times 10^{-41} \times E_\nu\,(\mathrm{GeV}) \times [g_L^2 + \tfrac{1}{3} g_R^2] \,, \tag{69}$$

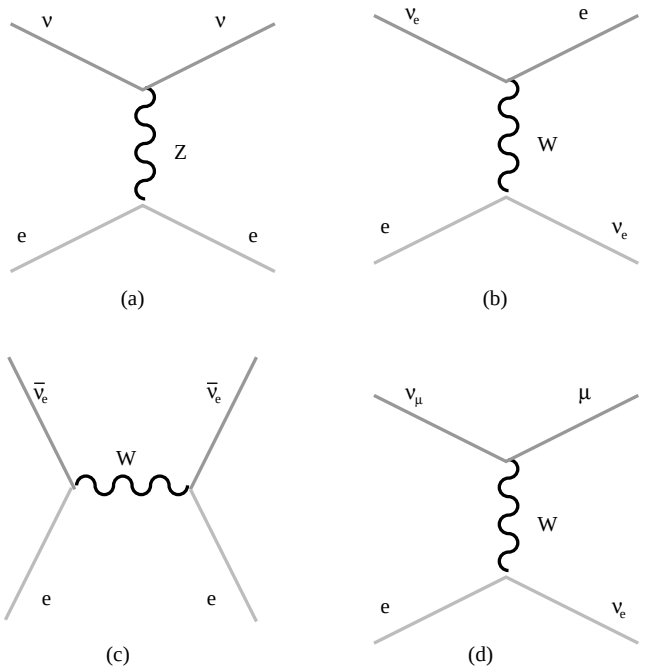

Fig. 8. Feynman diagrams contributing to the ν–e scattering processes of Eqs. (62)–(66): (a) NC ν–e elastic scattering (for Eqs. (62) and (64)–(66) (b) CC $\nu_e e$ scattering (for Eq. (65)), (c) CC $\bar{\nu}_e e$ annihilation (for Eq. (66)) and (d) inverse muon decay (for Eq. (64)).

where the values for the final term are given in the final column of Table 4. Radiative corrections for this process have been calculated to 1-loop [63], and theoretical techniques exist to extend this calculation to higher orders.

The differential cross section for inverse muon decay, Eq. (63), is

$$\frac{\mathrm{d}\sigma}{\mathrm{d}y}(\nu_\mu e^- \to \nu_e \mu^-) = \frac{G_F^2(s - m_\mu^2)}{4\pi} , \tag{70}$$

and the differential cross section for $\bar{\nu}_e e^- \to \bar{\nu}_\mu \mu^-$ is

$$\frac{\mathrm{d}\sigma}{\mathrm{d}y}(\bar{\nu}_e e^- \to \bar{\nu}_\mu \mu^-) = \frac{G_F^2(s - m_\mu^2)}{4\pi} \left[\frac{s}{s - m_\mu^2} y(1 - y) - \frac{m_\mu^2}{s} \right] . \tag{71}$$

4.2.2. Current measurements of $\sin^2\theta_W$ *from neutrino–electron scattering*

The best measurement of neutrino–electron scattering to date was performed in the CHARM II experiment in the CERN Sp$\bar{p}$S neutrino beam. The beam was predominantly ν_μ and $\bar{\nu}_\mu$, with an event sample of 2000 events in each of the ν_μ and $\bar{\nu}_\mu$ beams. This led to a measurement of the weak mixing angle of [64]

$$\sin^2\theta_W = 0.2324 \pm 0.0058(\mathrm{stat}) \pm 0.0059(\mathrm{syst}) . \tag{72}$$

Not surprisingly, systematic errors primarily result from normalization and background uncertainties.

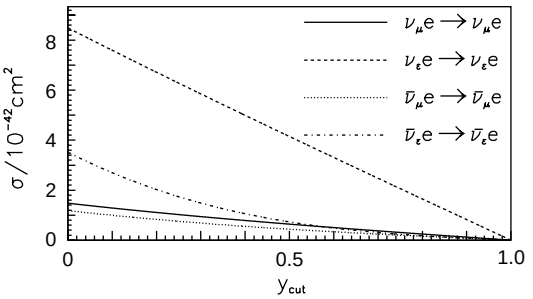

Fig. 9. Integral cross section for neutrino–electron scattering processes above any chosen cut on the inelasticity variable, $y > y_{\mathrm{cut}}$, and assuming $E_\nu = 30$ GeV.

4.2.3. Overview of the measurement technique at a νMC

The signature for ν–e scattering is a single electron with very low transverse momentum with respect to the neutrino beam direction, $p_t \lesssim \sqrt{m_e E_\nu}$. Therefore, the measured quantity to be converted to a cross section is the number of observed events consisting of a forward-going electron track with no hadronic activity and with an energy above some defined threshold value, E_{cut}.

In order to convert the event count to a cross section, the detector efficiency must be determined, backgrounds must be estimated and subtracted, and the integrated neutrino flux must measured and/or calculated.

In the discussion that follows, it will be seen that the physics sensitivity, backgrounds and flux normalization procedures will all differ markedly between the $\nu_\mu \bar{\nu}_e$ and $\bar{\nu}_\mu \nu_e$ beams. Experimental runs with the latter beam will have a greater statistical sensitivity to $\sin^2\theta_W$ but the $\nu_\mu \bar{\nu}_e$ beam will provide two experimental advantages: (1) the possibility of flux normalization using the muons produced from inverse muon decay and by $\bar{\nu}_e$–e^- annihilation processes; and (2) the background from quasi-elastic electron neutrino scattering off nucleons produces positrons rather than electrons, which can potentially be distinguished from the signal electrons by determining their charge sign.

4.2.4. Statistical sensitivity

The number of signal interactions is related to the cross section for the process, $\sigma(E_\nu)$, and to the neutrino flux through the fiducial volume of the target, $\Phi(E_\nu)$, through

$$N_{\nu\text{-}e} \propto \int \theta(yE_\nu - E_{\mathrm{cut}})\sigma(E_\nu)\Phi(E_\nu)\,\mathrm{d}E_\nu\,, \tag{73}$$

where the theta function is zero (one) for an argument less than (greater than) zero and the proportionality factor is determined by the mass depth of the target.

Fig. 9 shows the integral cross section for the reactions above an elasticity cut, $y > y_{\mathrm{cut}}$, and Fig. 10 shows the change in the cross section above $y > y_{\mathrm{cut}}$ as a function of $\sin^2\theta_W$. (A value of y_{cut} relatively close to zero should likely be attainable by using a dedicated detector for this analysis.)

The statistical sensitivity to $\sin^2\theta_W$ in any given channel is proportional to $\sqrt{\sigma}/(\mathrm{d}\sigma/\mathrm{d}\sin^2\theta_W)$, and is shown in Fig. 11. In a neutrino beam produced by muon decays, the observed rate of visible electrons will include scattering of both neutrinos and antineutrinos.

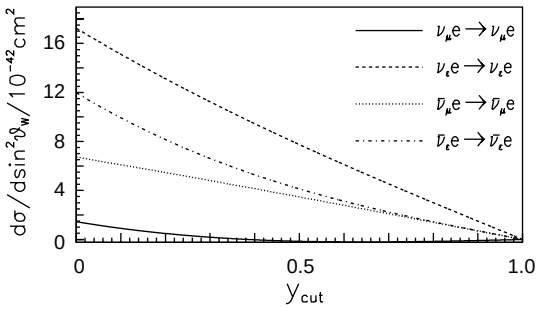

Fig. 10. Change in the integral cross section with respect to $\sin^2\theta_W$ for neutrino–electron scattering processes above $y > y_{\text{cut}}$, assuming $E_\nu = 30$ GeV.

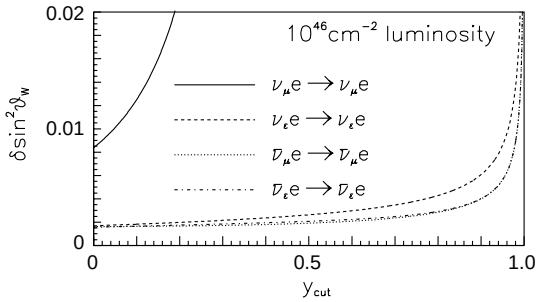

Fig. 11. Statistical uncertainty in $\sin^2\theta_W$ for any chosen value of y_{cut}, from neutrino–electron scattering in beams of either ν_μ, ν_e, $\bar{\nu}_\mu$ or $\bar{\nu}_e$. An integrated luminosity of 10^{46} cm^{-2} at a beam energy of $E_\nu = 30$ GeV has been assumed. The values can be scaled to other neutrino energies by noting that the measurement's statistical uncertainty, for a given integrated neutrino flux through a specified detector, is proportional to the inverse square root of the average energy.

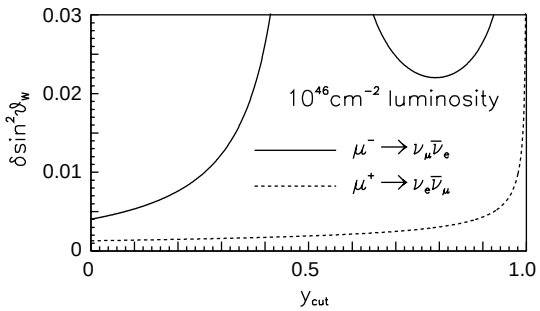

Fig. 12. Same as Fig. 11 except that the event statistics has been summed over the experimentally indistinguishable contributions from the two neutrino components in the μ^+-induced $\bar{\nu}_\mu \nu_e$ beams and the μ^--induced $\nu_\mu \bar{\nu}_e$ beams produced from muon storage rings.

Note that an undesirable feature of the μ^- beam for measuring $\sin^2\theta_W$ is that the dependences of the integral cross sections on $\sin^2\theta_W$ for ν_μ and $\bar{\nu}_e$ have opposite signs. The resulting sensitivity in integral cross sections for beams from $\mu^\pm$ decay is shown in Fig. 12, using the adequate approximation that the muon and electron type neutrino fluxes are assumed equal.

As an aside, for a neutrino beam from a polarized muon beam, the exact sensitivity for this sort of summed measurement would depend on beam polarization, particularly for the μ^- beam. Due to potential uncertainties in measuring the level of any muon beam polarization, better measurements of $\sin^2\theta_W$ may well be obtained from muon beams where the polarization is identically zero or can at least be shown to average to zero over the course of a fill.

4.2.5. Detector design and background rejection

The best types of detectors for detecting the signal of low-p_t single electrons are likely to be based around kiloton-scale active targets with inherent tracking capabilities and a high-rate capability. In order to minimize the level of confusion between the signal process and background events with $\gamma \to e^-e^+$, the target should be composed of only low-Z elements in order to maximize the radiation length, and should contain very little dead material. The incorporation of a magnetic field to identify the lepton charge would further be helpful so as to reduce backgrounds from $\bar{\nu}_e$ charged current interactions, and a lepton charge measurement would also provide a cross-check of sign-symmetric detector backgrounds, such as $\gamma \to e^+e^-$.

For a detector with all these capabilities, rare low-p_t backgrounds such as coherent single π^0 production, which were a significant problem in the high-mass CHARM II neutrino detector [64], should not be difficult to identify and/or subtract on a statistical basis.

In order to also remove quasi-elastic $\nu_e N$ scattering backgrounds, which cannot be separated by electron charge sign identification in the $\bar{\nu}_\mu \nu_e$ beam, the detector will need to be capable of resolving the different p_t distributions: ν_e quasi-elastic scattering off nucleons has a characteristic p_t scale of $\sqrt{m_N E_\nu}$, i.e., larger by a factor of $\sqrt{m_N/m_e} \simeq 43$ than the signal process. In this case, signal and background suppression can be achieved by fitting the observed single electron p_t distribution, which therefore must be measured with a p_t resolution much better than $\sqrt{m_N E_\nu}$. To give a numerical example, the quasi-elastic cross section off nucleons at $E_\nu = 30$ GeV on an isoscalar target is approximately 5 times greater than the inverse muon decay cross section and, in this case, a p_t cut at 100 MeV would leave a well-measured background of about 10% under the inverse muon decay peak.

These demanding and specialized requirements suggest using a dedicated detector rather than, e.g., the general purpose detector of Fig. 2. A natural choice is a time projection chamber (TPC) filled with a one or other of several candidate low-Z liquids.

A TPC using the lowest-Z element, liquid hydrogen, may unfortunately be ruled out because of insufficient electron mobility, although the possibilities for liquid-hydrogen TPCs are again attracting some attention [65]. Liquid helium also suffers from poor mobility and potentially difficult operation because it lacks the ability to self-quench; however, it deserves further consideration because it has a radiation length of 7.55 m, allowing very well-resolved events.

Fig. 13 gives an example of a Monte-Carlo-generated event in liquid helium. The interaction occurs at mid-height at the right-hand side of the figure and, in this typical case, the primary electron track travels easily sufficient distance to establish its initial vertex, direction, sign and the absence of extra tracks emerging from the vertex. Since the event is contained, the primary electron's energy could also be cross-checked calimetrically.

Liquid methane appears to be another good candidate for the TPC medium as its favorable electron transport properties have led to it being suggested for TPC detectors of up to several kilotons [66]. It is liquid at atmospheric pressure between -182.5°C and -161.5°C and has a density of 0.717 g/cm^3

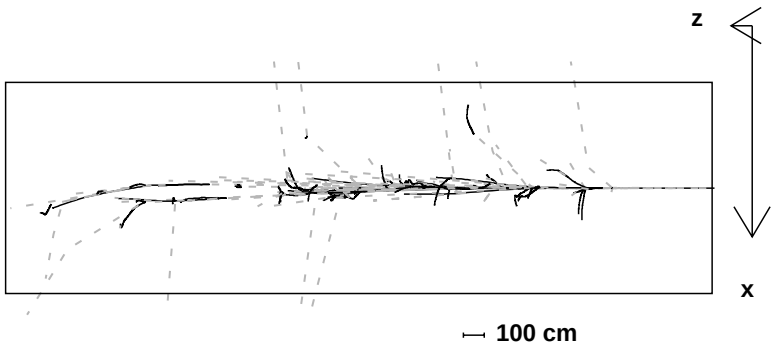

Fig. 13. Monte-Carlo-generated simulation of a high-energy neutrino–electron scattering interaction in liquid helium. The distorted scale is indicated by the 10:1 ratio in the relative lengths of the x- and z-axis. The solid lines are electrons and positrons and the dashed lines are photons that would not be seen in the detector. The view is perpendicular to both the beam direction and to a 0.1 T magnetic field. See text for further details.

and a radiation length of 65 cm. Heavier alkanes that are liquid at room temperature, such as octane, would be superior for safety and convenience if their electron transport properties were found to be acceptable.

Even if most DIS events are trivial to distinguish from the signal events, the detector must still be able to cope with the high interaction rate from the dominant background of DIS neutrino–nucleon interactions, which has a cross section three orders of magnitude larger than the signal processes. This problem is made even worse for the long drift times typical of the TPC geometry because the interactions from up to hundreds of turns (depending on experimental details) may pile up in the TPC readout. This suggests the need for additional fast readout of the events, which could plausibly come from, e.g., planes of scintillating fibers within the TPC volume.

Clearly, any such detector for the neutrino–electron scattering analysis must satisfy very stringent experimental requirements and its design and construction will be major projects.

4.2.6. Flux normalization for neutrino–electron elastic scattering

Normalization of the cross section is also a significant issue since this probe of weak couplings is only as good as the normalization of the beam flux.

Normalization to the muon beam flux itself is a possibility which would work for both $\nu_\mu\bar{\nu}_e$ and $\bar{\nu}_\mu\nu_e$ beams. Theoretical predictions of the decay process would likely not limit this normalization technique. Instead, the ultimate accuracy should depend on uncertainties in the measured number of muons in the ring and on the beam beam dynamics, such as spot sizes, orbits, divergences and polarization if this does not average to zero. It would require a detailed analysis for a precisely specified muon ring design to determine whether or not muon beam measurements and modeling could predict νMC neutrino fluxes at the 10^{-4} level required to be useful for this analysis.

For the $\nu_\mu\bar{\nu}_e$ beam, an alternative candidate for normalization is single muon production in neutrino–electron scattering through the processes of Eqs. (63) and (67). Like the signal, the absolute cross sections for these normalization processes are also extremely accurately predictable but with the crucial difference that they do not depend on $\sin^2\theta_W$.

It is conceivable that this absolute normalization in the $\nu_\mu\bar{\nu}_e$ beam could then also be transferred to the $\bar{\nu}_\mu\nu_e$ beam by using the ratio of quasi-elastic events to provide a relative normalization between the two beam types.

4.2.7. Sensitivity to new physics processes

For a μ^- beam, the cross-section calculations above show that if the very challenging experimental systematic uncertainties can be satisfactorily addressed, then sensitivities of approximately $\delta\sin^2\theta_W \sim 0.0007$ would be reached for an integrated luminosity of 10^{46} cm^{-2} and a mean neutrino beam energy of 30 GeV, which corresponds to approximately 1.5×10^9 DIS charged current events (cf. Table 2).

The μ^+ beam's statistical sensitivity would be about a factor of three better, with the caveat that beam flux normalization and experimental backgrounds are both even more challenging. With an integrated luminosity of 10^{46} cm^{-2}, expected event sample sizes would be approximately 1.5×10^6 for a μ^- beam and 3×10^6 for a μ^+ beam. Normalization and background uncertainties must therefore be kept at the few times 10^{-4} level in order to achieve this precision.

Such a measurement could be used to probe for hints of physics beyond the Standard Model by, for example, interpreting it in terms of a sensitivity to a high mass contact interaction with a Lagrangian of the form

$$\mathscr{L} = \sum_{H\in\{\mathrm{L,R}\}} \frac{\pm4\pi}{\Lambda^{\pm}_{H_eH_\nu}} (\Lambda^{\pm}_{H_eH_\nu})\bar{e}_{H_e}\gamma^\mu e_{H_e}\bar{\nu}_{H_\nu}\gamma_\mu\nu_{H_\nu}\ , \tag{74}$$

where the H indices represent helicity states of the electron and neutrino. The statistics given above would probe contact interactions at mass scales $\Lambda\sim10$ TeV, again assuming that statistical uncertainties dominate.

4.3. $\sin^2\theta_W$ from deep inelastic scattering

Existing measurements of $\sin^2\theta_W$ in neutrino–nucleon DIS experiments, using the neutrino beams that have been available from π/K decays, have already provided an excellent testing ground for the Standard Model. Nucleons, however, make for a most unappealing and difficult target, and it is necessary to consider ratios of observable processes in order to make sense of the results.

4.3.1. Previous measurements

The CCFR ν experiment extracted $\sin^2\theta_W$ [67,68] through a measurement of the ratio of the cross sections for NC and CC interactions, as expressed in the Llewellyn–Smith formula [69]:

$$R^{\nu(\bar{\nu})} = \frac{\sigma^{\nu(\bar{\nu})}_{\mathrm{NC}}}{\sigma^{\nu(\bar{\nu})}_{\mathrm{CC}}} = \rho^2\left(\frac{1}{2} - \sin^2\theta_W + \frac{5}{9}\sin^4\theta_W\left(1+\frac{\sigma^{\bar{\nu}(\nu)}_{\mathrm{CC}}}{\sigma^{\nu(\bar{\nu})}_{\mathrm{CC}}}\right)\right)\ , \tag{75}$$

where the value of the parameter ρ depends on the nature of the Higgs sector and has the value $\rho=1$ in the Standard Model. This method, although it removed much of the uncertainty due to QCD effects in the target, does leave some rather large uncertainties associated with heavy quark production from the quark sea of the nucleon target.

The successor experiment, NuTeV (FNAL-E815), has improved upon the CCFR measurement by using separate neutrino and antineutrino beams. Separation of neutrino and antineutrino neutral

current events allows the utilization of the Paschos–Wolfenstein relationship [70]:

$$R^- = \frac{\sigma^{\nu}_{\mathrm{NC}} - \sigma^{\bar{\nu}}_{\mathrm{NC}}}{\sigma^{\nu}_{\mathrm{CC}} - \sigma^{\bar{\nu}}_{\mathrm{CC}}} = \frac{R^{\nu} - rR^{\bar{\nu}}}{1-r} = \rho^2 \left(\frac{1}{2} - \sin^2\theta_W\right) , \tag{76}$$

where

$$r = \frac{\sigma(\bar{\nu}, CC)}{\sigma(\nu, CC)} \simeq 0.5 . \tag{77}$$

R^- is, by construction, sensitive only to scattering from valence quarks in the proton, and this considerably reduces the theoretical uncertainties associated with the target. NuTeV's result [71]

$$\sin^2\theta_W = 0.2277 \pm 0.0013(\mathrm{stat}) \pm 0.0009(\mathrm{syst}) \tag{78}$$

is three standard deviations above the Standard Model prediction. There were two dominant systematic uncertainties in the CCFR experiment: (1) ν_e flux and (2) CC charm production. These two major systematic uncertainties in CCFR were reduced in the NuTeV experiment by utilizing sign-selected neutrino beams, leaving event statistics as the largest uncertainty.

These past neutrino-fixed target experiments used dense calorimetric neutrino targets in order to increase the interaction rate, and such targets did not allow one to distinguish between electron–neutrino-induced charged current interactions (CC) and neutral current (NC) interactions. Such experimental setups would be fatal for νMC analyses with 2-component $\nu_\mu\bar{\nu}_e$ and $\bar{\nu}_\mu\nu_e$ beams, as will be discussed further; a high-performance tracking target such as that in Fig. 2 is instead indicated.

4.3.2. The experimental extraction of $\sin^2\theta_W$

As in previous neutrino experiments, the measured quantity used to determine $\sin^2\theta_W$ at νMCs will be a ratio of NC-to-CC DIS events. However, the NuTeV-style ratio of Eq. (76), R^-, will not be accessible in the 2-component beams at νMCs because NC events from neutrinos and those from antineutrinos will not be distinguishable on an event-by-event basis. Instead, the experimentally accessible NC-to-CC event ratios for both the $\nu_\mu\bar{\nu}_e$ and $\bar{\nu}_\mu\nu_e$ beams essentially correspond to linear combinations of the Llewellyn–Smith ratios for neutrinos and antineutrinos that were given in Eq. (75).

The relevant ratios for νMCs will be

$$R_{\mu^-} = \frac{\sigma(\nu_\mu, \mathrm{NC}) + \sigma(\bar{\nu}_e, \mathrm{NC})}{\sigma(\nu_\mu, \mathrm{CC}) + \sigma(\bar{\nu}_e, \mathrm{CC})} = \frac{R_\nu + grR_{\bar{\nu}}}{1+gr} \tag{79}$$

for the $\nu_\mu\bar{\nu}_e$ beam, and

$$R_{\mu^+} = \frac{\sigma(\bar{\nu}_\mu, \mathrm{NC}) + \sigma(\nu_e, \mathrm{NC})}{\sigma(\bar{\nu}_\mu, \mathrm{CC}) + \sigma(\nu_e, \mathrm{CC})} = \frac{R_\nu + g^{-1}rR_{\bar{\nu}}}{1+g^{-1}r} \tag{80}$$

for the $\bar{\nu}_\mu\nu_e$ beam, with r previously defined in Eq. (77) and g the energy-weighted flux ratio between $\bar{\nu}_e$ and ν_μ in a $\nu_\mu\bar{\nu}_e$ beam or—equivalently for a non-polarized beam—between ν_e and $\bar{\nu}_\mu$ in a $\bar{\nu}_\mu\nu_e$ beam:

$$g \equiv \frac{\langle x\rangle^e}{\langle x\rangle^\mu} = \frac{\int \Phi(E_{\bar{\nu}_e})E_{\bar{\nu}_e}\,\mathrm{d}E_{\bar{\nu}_e}}{\int \Phi(E_{\nu_\mu})E_{\nu_\mu}\,\mathrm{d}E_{\nu_\mu}} = \frac{\int \Phi(E_{\nu_e})E_{\nu_e}\,\mathrm{d}E_{\nu_e}}{\int \Phi(E_{\bar{\nu}_\mu})E_{\bar{\nu}_\mu}\,\mathrm{d}E_{\bar{\nu}_\mu}} . \tag{81}$$

Eqs. (79) and (80) have made use of lepton universality, which implies that $\nu_e N$ scattering cross sections become equal to those for $\nu_\mu N$ at energy scales well above the electron and muon masses. The second of the two equations differs from the first only in the replacement of g by g^{-1}.

An analytic calculation [9] gives the value $g=\frac{6}{7}$ for the neutrino beam produced from an idealized pencil beam of unpolarized muons. It follows that the numerical values of the measurements from the $\nu_\mu\bar{\nu}_e$ and $\bar{\nu}_\mu\nu_e$ beams will be nearly identical:

$$R_{\mu^-} \simeq 0.330, \qquad R_{\mu^+} \simeq 0.332\ , \tag{82}$$

where we have used the predictions from Eq. (75) of $R^{\nu}=0.317$ and $R^{\bar{\nu}}=0.359$ for $\sin^2\theta_W=0.225$. Of more experimental relevance, the statistical sensitivities to $\sin^2\theta_W$ are also nearly identical, as is indicated by the logarithmic derivatives:

$$\frac{1}{R_{\mu^-}}\frac{\mathrm{d}R_{\mu^-}}{\mathrm{d}\sin^2\theta_W}=-1.55, \quad \frac{1}{R_{\mu^+}}\frac{\mathrm{d}R_{\mu^+}}{\mathrm{d}\sin^2\theta_W}=-1.47\ .$$

The numerical similarities between the complementary variables R_{μ^-} and R_{μ^+}, from $\nu_\mu\bar{\nu}_e$ and $\bar{\nu}_\mu\nu_e$ beams respectively, mean that the two measurements can be regarded as nearly identical from a physics standpoint but with slightly different experimental systematics due to the approximate interchange of electron and muon energy spectra in the CC final states.

Because of the different kinematics for neutrino versus antineutrino interactions, the CC event sample from the $\nu_\mu\bar{\nu}_e$ beam will contain a softer spectrum of primary muons than electrons and vice versa for the $\bar{\nu}_\mu\nu_e$ beam. The comparison of two theoretically similar measurements with different experimental challenges will be a valuable cross-check on the analyses. In this respect, it is helpful that muon storage rings are likely [9] to have the capability to reverse the polarity of the ring to choose between $\nu_\mu\bar{\nu}_e$ and $\bar{\nu}_\mu\nu_e$ beams at any given time.

4.3.3. Detector requirements

Any νN DIS measurements of $\sin^2\theta_W$ at a νMC would be expected to be a large experimental extrapolation from today's measurements. The most demanding requirement on the detector for this analysis will be the ability to efficiently distinguish CC events, with their primary electrons or muons, from the purely hadronic events produced in NC interactions.

The large component of electron (anti)neutrinos in both the $\bar{\nu}_\mu\nu_e$ and $\nu_\mu\bar{\nu}_e$ beams at νMCs rules out use of traditional calorimetric neutrino target/detectors since these cannot easily distinguish ν_e-induced CC interactions from NC interactions.

In contrast, a CCD-based tracking target and general purpose detector such as that of Fig. 2 appears to be well suited to the requirements for this analysis because of its expected good performance [9] in identifying both primary muons and electrons and its further ability to control backgrounds from secondary electrons or background muons from pion decays that fake primary leptons. Even so, it might even be helpful if the electron identification capabilities of such a detector were further bolstered by incorporating transition radiation detectors directly downstream from the tracking detectors.

4.3.4. Estimated uncertainties

Table 5 displays a comparison between the uncertainties in the νN DIS measurements of $\sin^2\theta_W$ from today's most precise measurement [71] and rough estimates of the corresponding uncertainties from a νMC measurement, which will now be discussed in turn.

Table 5
Estimates of $\sin^2\theta_W$ uncertainties in a νMC analysis, compared to those for the NuTeV preliminary result [71] (see the text for details on how the estimated uncertainties for νMCs were arrived at)

Source of uncertainty	NuTeV	νMC
Data statistics	0.00135	< 0.00010
Total exp. syst.	0.00063	Negligible (?)
ν_e flux modeling	0.00039	Irrelevant
Transverse vertex position	0.00030	Negligible
Event energy measurements	0.00018	Irrelevant
Event length	0.00027	Irrelevant
Primary Lepton ID	N.A.	< 0.00020(?)
Total physics model	0.00064	< 0.00050
Charm production, strange sea	0.00047	< 0.00030
Charm sea ($\pm 100\%$)	0.00010	Negligible
$\sigma^{\bar{\nu}}/\sigma^{\nu}$	0.00022	Negligible
Rad. correction	0.00011	< 0.00010
Non-isoscalar target	0.00005	< 0.00005
Higher twist	0.00014	< 0.00014
Longitudinal cross section	0.00032	Negligible
Total uncertainty	0.00162	< 0.00050
Equivalent ΔM_W	80 MeV/c^2	< 25 MeV/c^2

The statistical uncertainty from the roughly one million events at the NuTeV experiment was the largest uncertainty in $\sin^2\theta_W$ analysis. Table 2 suggests νMC event statistics of 10^9 events or more, corresponding to a reduction in statistical uncertainty by at least a factor of 30 and pushing the absolute statistical uncertainty in $\sin^2\theta_W$ to below 0.0001.

Turning now to experimental uncertainties, the NuTeV uncertainty of 0.0004 due to ν_e flux was relevant only for calorimetric neutrino targets and will no longer exist for the tracking target/detectors discussed for νMCs that will be capable of distinguishing, on an event-by-event basis, between NC interactions and the CC interactions of ν_e's. Uncertainties from energy scale and event length in the NuTeV analysis will also be irrelevant for νMC detectors because they were associated with NuTeV's statistical event-length method of separating NC from CC events.

The improved νMC method of identifying primary leptons on an event-by-event basis will instead have to contend with uncertainties in the identification efficiencies for the primary leptons that distinguish CC from NC events. Every misidentification moves that event between the numerator and denominator of the experimental ratios of Eqs. (79) and (80), so it is clear that the fractional uncertainty in the level of misidentifications must be reduced to well below the 10^{-3} magnitude desired for the fractional uncertainty in $\sin^2\theta_W$. Some confidence that this might be achievable comes from the very high lepton identification efficiencies for the detector scenario discussed above.

Both the rejection of backgrounds and the positive identification of the primary lepton are generally more difficult for low-energy leptons, so the $\sin^2\theta_W$ measurement would benefit from using cuts on the minimum lepton energy. The value of this energy cut must be balanced against

increasing theoretical uncertainties as progressively more of the event sample is cut away. In any case, estimation of the identification efficiency for primary leptons may well be the largest experimental uncertainty in a measurement dominated by theoretical uncertainties.

An improved understanding of several potential theoretical uncertainties will be required to attain a $\sin^2\theta_W$ measurement that could be meaningfully interpreted as equivalent to a sub-25 MeV W mass uncertainty. In particular, calculations and/or measurements to minimize the charm production uncertainty, higher-twist effects, radiative corrections and uncertainties in the longitudinal structure function R_L will need to be dealt with.

In this respect, it is helpful that several of the theoretical uncertainties can be calibrated using the same νMC event sample as used for the $\sin^2\theta_W$ analysis. Hence, the enormous increase in statistical power of νMCs over today's neutrino experiments should also help to minimize some of the systematic uncertainties in Table 5.

Good examples of theoretical uncertainties that are amenable to experimental calibration are the large uncertainty due to charm mass effects and the related uncertainties in estimating the charm and strange seas of the nucleons. A next-to-leading-order (NLO) fit to the charm mass from CCFR [17] obtained $m_c = 1.71 \pm 0.19 \pm 0.02\ \mathrm{GeV}/c^2$, corresponding to a charm production uncertainty in the CCFR $\sin^2\theta_W$ measurement of $\delta\sin^2\theta_W = 0.003$. Since the statistics at a νMC might be three or more orders of magnitude larger than in the CCFR experiment, Table 5 somewhat arbitrarily chooses an improvement by a factor of 10 on the CCFR uncertainty. This is less improvement than the factor of 30 or more that would be predicted from straightforward statistical scaling but a careful analysis would be required to establish the actual level at which residual theoretical uncertainties set in that cannot be calibrated away using the experimental data.

Strange quark mass effects in $\nu_\ell\bar{u} \to \ell^-\bar{s}$ and $\nu_\ell s \to \nu_\ell s$ provide a much smaller theoretical effect that fell below the uncertainty threshold for the NuTeV analysis but whose corrections and uncertainties would need to be checked for a νMC analysis. Although presumably a very small correction, its effects are difficult to reliably establish because lattice gauge calculations predict that m_s has an awkward value: $m_s \simeq 300\ \mathrm{MeV} \simeq \Lambda_{\mathrm{QCD}}$.

Higher-twist effects are assessed as one of the larger theoretical uncertainties in today's measurements. However, a recent study [36] indicates that most of the higher-twist effects might be able to be reinterpreted as higher-order QCD corrections that can be determined from the structure functions measured in the νMC data sample. For the theoretical precision required at a νMC measurement, it may be necessary to evaluate and correct for the residual small effects from "radiative higher-twist processes" such as $\nu_\ell n \to \gamma\ell^- p$. The radiative photon present in CC events generates a CC/NC asymmetry and can boost the apparent Q^2 of events to high-enough values to evade cuts designed to suppress higher-twist corrections.

As was already mentioned in Section 2, cancellations of theoretical uncertainties by applying isospin invariance relations are very important for reducing the uncertainties in $\sin^2\theta_W$ and in other analyses in νN DIS experiments and this is the motivation for using neutrino targets that are approximately isoscalar. This theoretical handle was useful for both the CCFR and NuTeV analyses, using a neutrino target detector with a neutron excess of $(N-Z)/(N+Z) = 0.0567 \pm 0.0005$. Isospin invariance relations should be even more applicable for, e.g., a CCD target at a νMC since the silicon substrate of CCDs has a neutron excess of only 0.3% and even the residual target components will have small non-isoscalarities: aluminum conductor has a neutron excess of 3.6% and the dominant carbon component of the support structure has an excess of less than 0.1%.

Indeed, the νMC neutrino target might be sufficiently isoscalar that uncertainties due to the neutron excess might fall below those due to nucleon isospin-violating effects [73] arising from electromagnetic and quark-mass contributions that break the generally assumed isospin invariance relations between the up and down quarks in protons and neutrons: $u_p(x,Q^2)=d_n(x,Q^2)$ and $u_n(x,Q^2)=d_p(x,Q^2)$. Such effects will be present even in a deuterium target [9] or other pure isoscalar targets.

The theoretical uncertainty due to electroweak radiative corrections in the NuTeV experiment, $\delta \sin^2\theta_W = 0.00051$, deserves further theoretical attention for a νMC since it does not appear to be amenable to data-based reductions from the improved statistics and experimental conditions at a νMC and so it might well dominate the total uncertainty at a νMC if the theoretical calculations are not improved upon, as will now be discussed.

The current state of electroweak radiative corrections suffers from the fact that only one attempt at a complete calculation exists, by Bardin and Dokuchaeva [74], which, curiously, is unpublished. This calculation includes electroweak effects to one loop, is lengthy and complicated, and it would benefit from independent confirmation. Further, it has several theoretical shortcomings, as follows. The Bardin–Dokuchaeva result depends explicitly on quark masses, which introduces a spurious model dependence. Similar calculations of EW radiative corrections in W mass production in $\bar{p}p$ annihilation show that quark mass effects can be absorbed into parton distributions and fragmentation functions [75]. The calculation is only approximately valid to leading log in QCD. In particular, it neglects scaling violation effects in important diagrams involving muon bremsstrahlung. It also neglects contributions from longitudinal partons and effects from the target mass. Further, it does not incorporate heavy quark effects in CC and NC charm production and, finally, it is not differential in the final state radiated photon momentum vector.

A νMC measurement of $\sin^2\theta_W$ would benefit greatly from a new EW radiative correction program with the aim of reducing the residual error on the effective W mass to ± 1 MeV. To reach this level, it may be necessary to re-sum large lepton logs, to include order $\alpha\alpha_S$ contributions, and to apply EM radiative corrections to input parton distribution function sets. Such a program should also provide the capability for the explicit generation of $\gamma\mu q$ final states.

4.3.5. *Comparisons of expected precisions from* $\sin^2\theta_W$ *measurements in different experimental processes*

To summarize the content of Table 5, the uncertainty on a νMC DIS measurement of $\sin^2\theta_W$ might well be equivalent to on the order of a 25 MeV uncertainty on the W mass and could perhaps improve on this if the theoretical uncertainties due to radiative corrections can be controlled.

In order to put this in the context of collider measurements at the energy frontier, Fig. 14 adds the inferred W mass information from a νMC determination of $\sin^2\theta_W$ to a plot showing the expected status of collider W and top quark mass measurements by the year 2010. Although the level of the bands and the actual slope of the curves might change depending on other parameters in the measurements, this figure gives a good idea of the level of accuracy one might expect.

The most precise measurement of M_W by the year 2010 is expected to come from direct measurements at TeV33. The contour represents the 68% confidence level from the TeV33 expectations of $\delta M_W = 20$–30 MeV/c^2 and $\delta M_t = 1$–2 GeV/c^2, with $\int \mathscr{L}\,dt = 10$ fb^{-1} and using the traditional M_T method [76]. As can be seen in Fig. 14, since the errors from both the direct measurements and the νMC are going to be extremely small, and the νMC measurement provides the Standard Model-based band in M_W–M_T plane, the measurements would be complementary to each other in

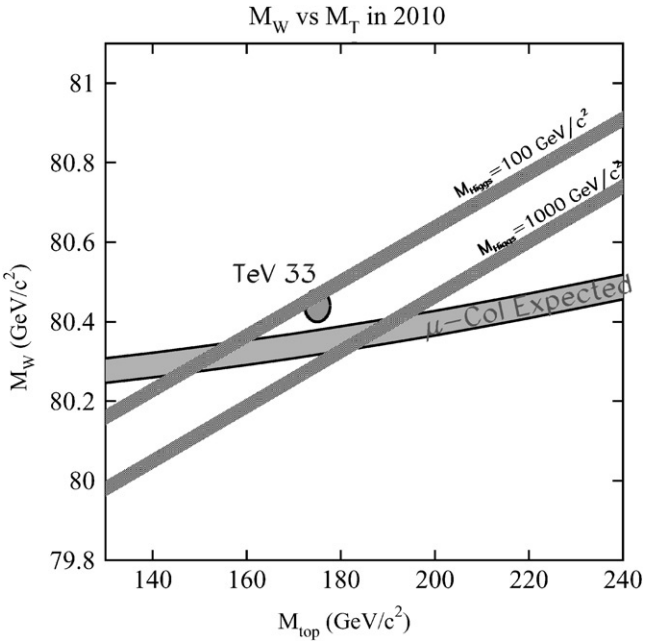

Fig. 14. Expected future restrictions in the size of the allowed regions in a plot of W mass versus top quark mass, following experiments at TeV 33 and at a νMC, as illustrated by the thicknesses of the bands and ellipse. The exact positions of the shaded regions are for illustrative purposes only.

testing the Standard Model by providing an independent prediction of the Standard Model Higgs mass to better than $\sim$20%.

4.4. *Summary on* $\sin^2\theta_W$ *measurements at* ν*MCs*

This section has demonstrated that precision tests of the electroweak section of the Standard Model can be expected to play an important role in the physics program of νMCs. Two possible tests were discussed, one each from neutrino–nucleon scattering and neutrino–electron scattering.

The former process will allow tests of unparalleled statistical accuracy but will likely suffer from substantial QCD uncertainties and, perhaps, also from experimental systematic uncertainties. By contrast, neutrino–electron scattering may be a statistical challenge even at a νMC, but it offers the possibility of a very clean measurement if experimental systematics associated with normalization and backgrounds can be well enough controlled by an appropriate design of the detector and analysis.

5. Rare and exotic processes

Despite the impressive direct and indirect searches for new physics available at the higher center of mass energies at the Tevatron, LEP, HERA and LHC colliders, some searches remain unique to neutrino experiments and these could be improved quite significantly with the much higher event

statistics and improved experimental conditions promised at νMCs. This section presents several examples of such processes, emphasizing the complementarity of these studies to already existing programs.

Additionally, two rare processes, $\bar{\nu}_e e^-$ annihilation and W/Z-γ scattering, present novel tests of low-energy features of the Standard Model.

5.1. New physics sensitivity

5.1.1. Flavor changing neutral currents

Besides testing current predictions of the Standard Model, a νMC offers opportunities to search for new phenomena in yet unexplored physical regions. An example is neutral current production of a *single* heavy quark:

$$\nu_\mu N \to \nu_\mu c X_{C=0},\ \nu_\mu N \to \nu_\mu \bar{c} X_{C=0}\ ,$$
$$\nu_\mu N \to \nu_\mu b X_{B=0},\ \nu_\mu N \to \nu_\mu \bar{b} X_{B=0}\ , \tag{83}$$

which would signal the presence of flavor changing neutral current (FCNC) processes. These reactions can provide important constraints on new physics as they occur in the Standard Model only at the one-loop level while new physics effects can occur at both the tree level and one-loop level. Examples of the former include new intermediate bosons with FCNC quark couplings while examples of the latter include a wide class of new physics models such as supersymmetry and technicolor. Some of these models are already constrained from other measurements [84]. Unfortunately, gains in sensitivity to this type of new physics increase only slowly with event statistics. For instance, in the models with new tree-level FCNC interactions, such as string-inspired models with neutral Z' bosons, the FCNC rate due to Z' exchange is proportional to $1/M_{Z'}^4$ and so sensitivity to $M_{Z'}$ only improves at best as the fourth root of rate increases.

The FCNC vertices $\nu\nu sb$ that contribute to Eq. (83) will be extensively studied in exclusive and inclusive B decays at the B factories as well as at CERN [83]. ALEPH has obtained the best bound so far: $BR(B \to \nu\bar{\nu}X) \leqslant 7.7 \times 10^{-4}$. Within the Standard Model one predicts a value of $\sim 4 \times 10^{-5}$. In contrast, studies of the $\nu\nu db$ vertex will be extremely challenging even at future B factories. Processes that involve neutrinos, such as $B \to X_s \nu\bar{\nu}$ and $\nu_\mu N \to \nu_\mu b X_{B=0}$, have the considerable advantage over the corresponding FCNC processes involving charged leptons in that their rates are mostly determined by short-distance physics, which ensures the robustness of the theoretical predictions.

Single b quark production is enhanced in the Standard Model through the GIM mechanism acting with high mass intermediate top quark states:

$$\sigma(\nu N \to \nu b X_{B=0}) \propto G_F^4 (m_t^4/M_W^4) \ln(m_t^4/M_W^4)(m_t^2/M_W^2)[|V_{td}|^2 D + |V_{ts}|^2 S]\eta(m_b^2/2ME) \tag{84}$$

(with next-to-leading order QCD corrections available [84]) where D and S represent the down and strange quark contributions from the nucleon, respectively, $\eta(m_b^2/2ME)$ represents a kinematic threshold suppression from the heavy b quark mass, and the contributions from D and S are likely to be similar. Even so, Eq. (84) predicts the FCNC with a $\nu\nu db$ vertex to occur only at the level of 10^{-8} of the event sample even for νMCs at high-enough energies for the B threshold effects to become small. Most likely, therefore, the Standard Model backgrounds will instead come from other

processes that have been experimentally misidentified and goal of the analyses will be to search for new physics effects that enhance the FCNC event sample to considerably above the predicted background level.

For single charm quark production, the irreducible Standard Model backgrounds will almost certainly be negligible since, besides the CKM factors, the production amplitude is suppressed in the Standard Model by $m_b^4 m_t^4$ relative to single b production, although with the caveat that the prediction is more sensitive to long-distance QCD effects that are not currently calculable from first principles. Again, experimentally misidentified events will dominate the backgrounds.

A high-performance detector with excellent vertex tagging, lepton identification and reconstruction of event kinematics will be required to cope with large background levels involving both CC- and NC-allowed production of charm or beauty. The allowed CC channels,

$$\nu_\mu N \to \mu^- c X \ , \tag{85}$$

$$\bar{\nu}_e N \to e^+ b X \ , \tag{86}$$

will be most dangerous as $y \to 1$ and so the very low-energy final state muon or electron can escape detection. This background could be suppressed to some extent by imposing a cut on the minimum allowed transverse momentum, p_t, in the event, which can be large for the signal NC events when the neutrino has a large p_t but should be zero within the detector resolution for charged current events. Neutral current production of heavy quark pairs

$$\nu_\mu N \to \nu_\mu c \bar{c} X \ , \tag{87}$$

$$\nu_\mu N \to \nu_\mu b \bar{b} X \ , \tag{88}$$

forms the other background when one or other of the heavy quark decays is not picked up by the vertex detector because it occurs too quickly or goes into an unfavorable final state. This background, in particular, makes setting any stringent limits from FCNC production of charm difficult at νMCs, even with an excellent vertexing geometry such as that shown in Fig. 3.

The situation is more promising with B decays since almost every B decay gives two chances for detection: at the primary B decay vertex and at the decay of the daughter charm hadron. Also, charged current b production may be accompanied by a $\bar{c}$, and this information can be used as well.

Even for FCNC B production at a νMC, the only interesting limit may well be for the subset of FCNC B production that occurs off a valence d quark, i.e., involving the FCNC vertices $\nu\nu db$. This restriction provides two important additional experimental handles: (1) kinematically, almost all of the NC background events will be at relatively low Bjorken x while the PDF for d valence quarks extends to high Bjorken x, and (2) d valence quarks will produce B^- mesons approximately half the time but never a B^+, while the B's forming the NC background are sign symmetric.

Further discussion on the experimental and theoretical issues for $\nu\nu db$ FCNC searches at νMCs is given elsewhere [14].

5.1.2. Generic four-fermion operators

Neutrino–nucleon processes at low-momentum transfer are sensitive to generic four-fermion contact terms produced by the high-energy neutral current interactions. Other, flavor changing, couplings are well constrained by the limits on processes like $\pi \to e\nu$. These four-fermion interactions

can be generated in a variety of new physics scenarios. Examples include, but are not limited to, supersymmetric theories with $\mathscr{R}$-parity non-conservation, new vector bosons Z' which appear in many superstring-motivated models, models with TeV-scale gravity and quark compositeness models. For instance, the low-energy remnant of a generic high-energy electron–quark neutral current interaction can be represented by non-zero coupling constants, η, in the Lagrangian:

$$\mathscr{L}_{\mathrm{NC}} = \sum_q [\eta^{eq}_{\mathrm{LL}}(\overline{e_{\mathrm{L}}}\gamma_\mu e_{\mathrm{L}})(\overline{q_{\mathrm{L}}}\gamma^\mu q_{\mathrm{L}}) + \eta^{eq}_{\mathrm{RR}}(\overline{e_{\mathrm{R}}}\gamma_\mu e_{\mathrm{R}})(\overline{q_{\mathrm{R}}}\gamma^\mu q_{\mathrm{R}}) + \eta^{eq}_{\mathrm{LR}}(\overline{e_{\mathrm{L}}}\gamma_\mu e_{\mathrm{L}})(\overline{q_{\mathrm{R}}}\gamma^\mu q_{\mathrm{R}}) + \eta^{eq}_{\mathrm{RL}}(\overline{e_{\mathrm{R}}}\gamma_\mu e_{\mathrm{R}})(\overline{q_{\mathrm{L}}}\gamma^\mu q_{\mathrm{L}})] \ . \tag{89}$$

A similar equation can be written for direct neutrino–quark interactions. One can use SU(2) symmetry to relate ν and e couplings:

$$\begin{aligned} \eta^{\nu u}_{\mathrm{LL}} &= \eta^{ed}_{\mathrm{LL}} \ , \\ \eta^{\nu d}_{\mathrm{LL}} &= \eta^{eu}_{\mathrm{LL}} \ , \\ \eta^{\nu u}_{\mathrm{LR}} &= \eta^{eu}_{\mathrm{LR}} \ , \\ \eta^{\nu d}_{\mathrm{LR}} &= \eta^{ed}_{\mathrm{LR}} \ , \end{aligned} \tag{90}$$

so that νN interactions can be used to constrain the η's in the Lagrangian of Eq. (89).

A particular example of a high-energy model that leads to a low-energy Lagrangian of this type is provided by R-parity-violating ($\mathscr{R}$) SUSY, with the Lagrangian:

$$\mathscr{L}_{\mathscr{R}} = \lambda'_{ijk}(\tilde{e}^i_{\mathrm{L}}\overline{d^k_{\mathrm{R}}}u^j_{\mathrm{L}} + \tilde{u}^j_{\mathrm{L}}\overline{d^k_{\mathrm{R}}}e^i_{\mathrm{L}} + \tilde{d}^{k*}_{\mathrm{R}}\overline{e^{ic}_{\mathrm{L}}}u^j_{\mathrm{L}} - \tilde{\nu}^i_{\mathrm{L}}\overline{d^k_{\mathrm{R}}}d^j_{\mathrm{L}} - \tilde{d}^j_{\mathrm{L}}\overline{d^k_{\mathrm{R}}}\nu^i_{\mathrm{L}} - \tilde{d}^{k*}_{\mathrm{R}}\overline{\nu^{ic}_{\mathrm{L}}}d^j_{\mathrm{L}}) + \mathrm{h.c.} \tag{91}$$

At low values of transferred momenta, this Lagrangian can be approximated in terms of local four-fermion interactions:

$$\begin{aligned} \mathscr{L}_{ed} &= \frac{(\lambda'_{1j1})^2}{m^2_{\tilde{u}^j_{\mathrm{L}}}}\overline{e_{\mathrm{L}}}d_{\mathrm{R}}\overline{d_{\mathrm{R}}}e_{\mathrm{L}} + \frac{(\lambda'_{1j1})^2}{m^2_{\tilde{d}^j_{\mathrm{L}}}}\overline{\nu_{\mathrm{L}}}d_{\mathrm{R}}\overline{d_{\mathrm{R}}}\nu_{\mathrm{L}} \\ &= \left(-\frac{(\lambda'_{1j1})^2}{2m^2_{\tilde{u}^j_{\mathrm{L}}}}\overline{e_{\mathrm{L}}}\gamma^\mu e_{\mathrm{L}} - \frac{(\lambda'_{1j1}2}{2m^2_{\tilde{d}^j_{\mathrm{L}}}}\overline{\nu_{\mathrm{L}}}\gamma^\mu \nu_{\mathrm{L}}\right)\overline{d_{\mathrm{R}}}\gamma_\mu d_{\mathrm{R}} \ . \end{aligned} \tag{92}$$

Assuming that the squarks of first two generations are degenerate and imposing SU(2) symmetry constraints gives

$$\eta^{ed}_{\mathrm{LR}} = -\frac{(\lambda'_{1j1})^2}{2m^2_{\tilde{u}^j_{\mathrm{L}}}} = -\frac{(\lambda'_{1j1})^2}{2m^2_{\tilde{d}^j_{\mathrm{L}}}} = \eta^{\nu d}_{\mathrm{LR}} \ . \tag{93}$$

Indeed, the best constraint on this coupling, $\eta^{ed}_{\mathrm{LR}} < 0.07^{+0.24}_{-0.24}$, already comes from the analysis of neutrino–nucleon scattering experiments [85]. Data from νMCs should complement new constraints on the new physics contributions that will become available from new Tevatron, LHC and DESY analyses.

5.1.3. Heavy neutral lepton mixing

Another opportunity for νMCs to significantly improve on already existing bounds on new physics from neutrino experiments is provided by the ability to search for the existence of neutral heavy leptons [86]. In several models [87,88], neutral heavy leptons are considered heavy isosinglets that interact and decay by mixing with their lighter neutrino counterparts. The high-intensity neutrino beams created by νMCs provide an ideal setting to search for neutral heavy leptons with a mass below 100 MeV.

It is postulated that neutral heavy leptons, L_0, could be produced from muon decays when one of the neutrinos from the decay mixes with its heavy, iso-singlet partner. The expression for the number of neutral heavy leptons produced in a muon beam is

$$N_{L_0} = N_\nu \,\mathrm{Br}\left(\frac{\mu \to L_0 \nu e}{\mu \to \nu\nu e}\right) \epsilon e^{-L/\gamma c\tau} \mathrm{Br}\left(\frac{L_0 \to \text{detectable}}{L_0 \to \text{total}}\right) (1 - e^{-\delta l/\gamma c\tau}) \,. \tag{94}$$

Here N_ν is the number of neutrinos produced from muon decays, $\mathrm{Br}(\mu \to L_0 \nu e/\mu \to \mu\nu e)$ is the branching ratio of muons decaying into neutral heavy leptons versus ordinary muon decays, L is the distance from the beam line to the detector, δl is the length of the detector, ϵ is the combined detector efficiency and geometric efficiency, τ is the L_0 lifetime, and $\mathrm{Br}(L_0 \to \text{detectable}/L_0 \to \text{total})$ is the branching ratio for the neutral heavy lepton decaying via a detectable channel (mainly, $L_0 \to \nu ee$).

Note here that the muon has two possible ways of producing L_0's:

$$\mu^- \to L_0 + \bar{\nu}_e + e^- \tag{95}$$

$$\mu^- \to \nu_\mu + \bar{L}_0 + e^- \,. \tag{96}$$

The branching ratio for each of these reactions is given by

$$\mathrm{Br}(\mu \to L_0 \bar{\nu}_e e/\mu \to \nu_\mu \nu_e e) = |U_{\mu L}|^2 (1 - 8x_m^2 + 8x_m^6 - x_m^8 + 12x_m^4 \ln x_m^2) \,, \tag{97}$$

$$\mathrm{Br}(\mu \to \nu_\mu \bar{L}_0 e/\mu \to \nu_\mu \nu_e e) = |U_{eL}|^2 (1 - 8x_m^2 + 8x_m^6 - x_m^8 + 12x_m^4 \ln x_m^2) \,. \tag{98}$$

Here x_m is defined as m_{L_0}/m_μ and $|U_{(\mu,e)L}|^2$ is defined as the coupling constant between the specific type of neutrino and the neutral heavy lepton.

Once produced, a neutral heavy lepton of such low mass will either decay via three neutrinos ($L_0 \to \nu\nu\nu$), or through the channels:

$$L_0 \to \nu_\mu + e^+ + e^- \,, \tag{99}$$

$$L_0 \to \nu_e + e^+ + e^- \,. \tag{100}$$

The first decay mode involves only the neutral current, whereas the second contains a mixture of both neutral and charged current interactions. The branching ratios for decay processes (99) and (100) have been calculated [89]. Note that the number of L_0's detectable at the νMC depends roughly on U^4.

Using the above model with some additional assumptions, one can estimate the number of neutral heavy leptons produced at the νMC that then decay to two electrons and a neutrino and are detected in an experiment. The plots in Fig. 15 show limits for the coupling constants at a νMC as a function of the L_0 mass and for a number of different muon energies and detector distances. All the plots assume a pure, unpolarized muon beam containing 10^{20} muons/yr with straight sections such that

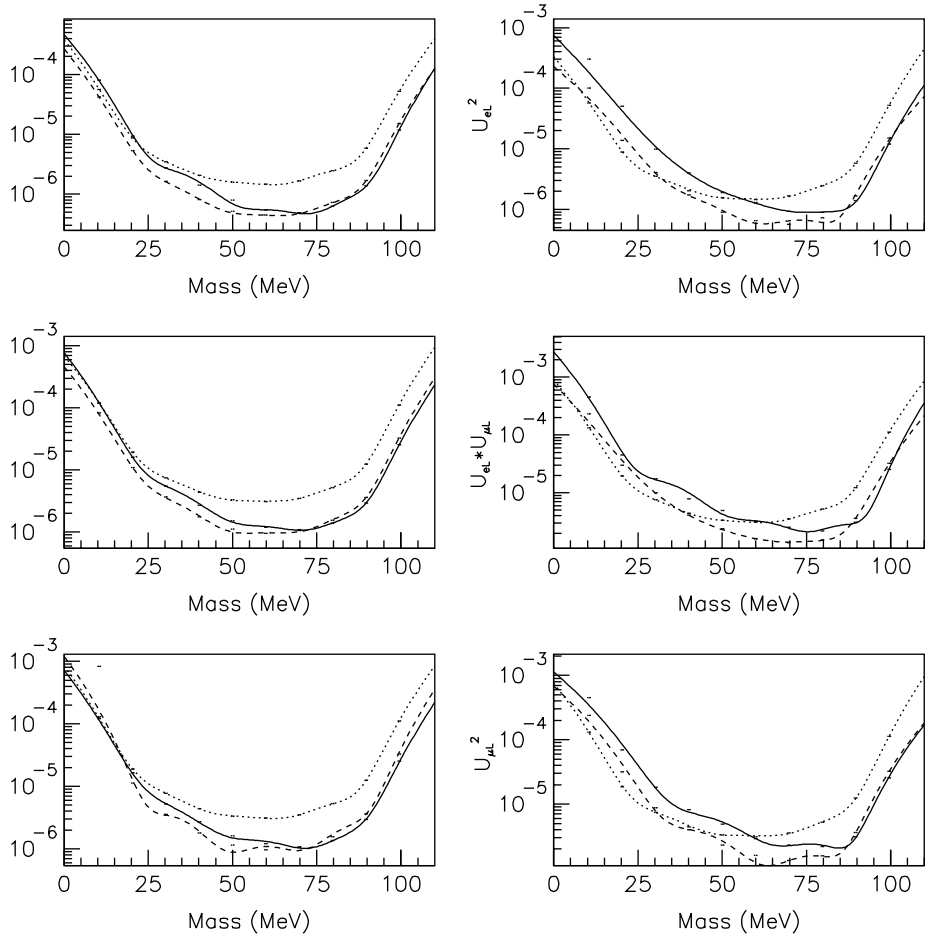

Fig. 15. Plots for limits on the (from top to bottom) coupling values $|U_{eL}|^2$, $|U_{\mu L}U_{eL}|$ and $|U_{\mu L}|^2$ as a function of L_0 mass for one year of running under the assumptions given in the text. The solid, dashed and dotted lines represent νMC energies of 10, 20 and 250 GeV, respectively. The plots on the left show limits for $L = 12$ m, and the plots on the right show limits for $L = 1$ km.

25% of the muons will decay to neutrinos pointing toward the detector. The detector parameters are based on the detector for the NuTeV L_0 searches [90–92]: 3 m in diameter and 30 m in length and with enough resolution to detect the e^+e^- vertex from the L_0 decay. Finally, it is assumed that backgrounds are negligible.

It is seen from Fig. 15 that one achieves the best limits from using relatively low-energy muon beams. This is a significant improvement over previous neutral heavy lepton searches, where limits fail to reach below 6.0×10^{-6} in the low-mass region.

The νMC may prove to be an ideal location to continue the search for neutral heavy leptons. The high-intensity neutrino beam allows for a neutral heavy lepton search to be sensitive to coupling constants in the low-mass region. In addition, such a neutral heavy lepton program could easily interface with an already existing detector utilizing the neutrino beam. It is also clear that a neutral

Table 6
Threshold neutrino energies for various hadronic final states

Final state	E_ν (GeV)
$\bar{\nu}_\mu\mu^-$	11
$\gamma\pi^-$	19
$\pi^0\pi^-$	76
$(\pi\pi\pi)^-$	172
γK^-	240
$(K\pi)^-$	358
$(K\pi\pi)^-$	446

heavy lepton search would receive the most benefit at lower muon energies, and thus would yield best results at lower energy νMCs.

5.2. Studies of low-energy QCD

5.2.1. $\bar{\nu}_e e^-$ annihilation

Section 4.2 shows that neutrino–electron elastic and quasi-elastic scattering can be used to extract the electroweak parameter $\sin^2\theta_W$ from purely leptonic interactions. This section instead discusses the neutrino–electron annihilation processes of Eq. (67),

$$\bar{\nu}_e e^- \to \bar{\nu}_\mu\mu^-, \bar{\nu}_\tau\tau^-, \bar{u}d\ldots\ . \tag{101}$$

Electron antineutrino–electron annihilation is expected to show considerable complexity once the center of mass energy exceeds the threshold for annihilation into hadronic final states. The process can be compared to $e^+e^- \to$hadrons but with the ρ, ω, ϕ and other low-lying vector resonances replaced by π^-, ρ^- and a_1^-. The axial component of the weak current produces coupling to axial vector resonances and, at low energy, to the pion. These latter couplings are absent in electron–positron annihilation and thus the weak annihilation of the electron offers a novel complement to electron–positron physics. Direct measurements of $\bar{\nu}_e e^-$ annihilation would complement the detailed studies of hadronic tau decays that currently provide some of the most powerful tests of QCD at low-momentum transfer.

These measurements bridge two asymptotic limits of QCD: the perturbative regime operative at high Q^2 and the chiral limit ($m_u = m_d = m_s = 0$) that is approached at low $\sqrt{s}$, and would provide some important information about the QCD spectral functions used in reducing the theoretical hadronic uncertainties in studies of CP violation in kaon decays, particularly in the interpretation of ϵ'/ϵ measurements [77,78]. Unfortunately, since the $\tau^-\nu_\tau$ threshold occurs at $E_\nu = 3.1$ TeV, there is a long way to go in neutrino energy in order to completely overlap the $\sqrt{s}$ region probed by tau decays.

Table 6 summarizes neutrino energy thresholds for s-channel final states. The thresholds for all channels are quite high. Nevertheless, one can see that a 50 GeV muon storage ring could provide access to the lowest lying final states and explore the interesting region near $\sqrt{s} = m_\pi$ to provide a clean test of PCAC, and a 250 GeV muon beam would extend the reach up to the threshold for kaon production.

5.2.2. W^*/Z^*-photon scattering

Just as intense neutrino beams open up the possibility of directly exploring weak annihilation of leptons in analogy to e^+e^- annihilation, so too does one acquire access to the analog of two-photon physics: the scattering of virtual W or Z beams from quasi-real photons in the Coulomb field of the nucleus. The general reaction is of the form

$$\nu_\ell A \to f_\ell F \bar{f} A \ ,$$

where $F, \bar{f}$ are fermions, and $f_\ell = \nu_\ell$ or ℓ^-. For $F\bar{f} = \nu_\ell \ell^+$ both CC and NC diagrams contribute. Otherwise, $f_\ell = \ell^-$ proceeds through $W\gamma$ scattering and $f_\ell = \nu_\ell$ through $Z\gamma$ scattering.

The creation of lepton pairs in the Coulomb field of the nucleus is sensitive to W–Z interference and provides a direct test of the Standard Model. Previous experimental observations are ambiguous [79,80,53]. The purely coherent part of the cross section for $\nu_{\ell_1} A \to \ell_1^- \nu_{\ell_2} \ell_2^+$ at asymptotically large energies is [81,82]

$$\sigma_{\ell_1\ell_2}(E \to \infty) = \frac{4Z^2\alpha^2 G_F^2}{9\pi^3} E K_{\ell_1\ell_2}(E,A)(1-\chi) \ ,$$

$$K_{\ell_1\ell_2}(E,A) = \frac{5\pi\beta(A)}{32}\left(\log\frac{2E\beta(A)}{\rho_{\ell_1\ell_2}} + \frac{1}{3}\log\frac{2E\beta(A)}{\rho_{\ell_1\ell_2}} - R_{\ell_1\ell_2}\right) \ . \tag{102}$$

$K_{\ell_1\ell_2}(E,A)$ is a reaction and nucleus-dependent form factor with $\beta(A) \simeq A^{-1/3}\ \mathrm{fm}^{-1} = 6A^{-1/3}\ \mathrm{GeV}$ set by the nuclear size, and $\rho_{\ell_1\ell_2}, \rho_{\ell_1\ell_2}, R_{\ell_1\ell_2}$ are simple functions of either $\beta(A)$ or final state fermion masses. The factor $Z^2\alpha^2$ reflects the coherent electromagnetic nature of the process and the scale of the cross section is set by $G_F^2\beta_I E$. Since the effective center-of-mass energy is $\sqrt{s} \simeq \sqrt{2\beta_I E}$ and $\beta_I \gg m_e$, all possible leptonic final states are accessible (including those with $\tau^\pm$) to a neutrino beam derived from a 250 GeV muon beam.

The factor χ incorporates effects of neutral currents, including interference in the $\ell^+\ell^-$ final states. A nice electroweak test is to measure χ through the ratios

$$\frac{\sigma_{\mu\mu}(\nu_\mu A \to \mu^-\mu^+\nu_\mu A)}{\sigma_{\mu e}(\nu_\mu A \to \mu^- e^+ \nu_e A)} = (1-\chi)\frac{K_{\mu\mu}(E,A)}{K_{\mu e}(E,A)} \ ,$$

where $K_{\mu\mu}(E,A)/K_{\mu e}(E,A)$ will depend only weakly on nuclear form factor and energy.

Hadronic resonances are also possible. We expect similar states to those produced in $\gamma\gamma$ collisions, namely $0^{-+}, 0^{++}, 2^{++}, \ldots$ with $I = 0$ and 1. Some Cabibbo-allowed examples include

$$\begin{aligned}
&\nu_e A \to e^- \pi^+ A \ , \\
&\nu_e A \to \nu_e \pi^0 A, \nu_e \eta A, \nu_e \eta' A \ , \\
&\nu_e A \to e^- a_1^+ A \ , \\
&\nu_e A \to \nu_e f_0 A, \nu_e a_1^0 A \ , \\
&\nu_e A \to e^- D_s^+ A \ .
\end{aligned} \tag{103}$$

Unfortunately, some of these hadronic resonances do not provide a unique experimental signature. Single pion production, for example, can occur through the diffractive process $\nu_e A \to e^-\pi^+ A$ mediated by a collision of the pion component of the virtual W boson with a pomeron from the nucleus or nucleon.

Experimental backgrounds that have to be controlled for these studies include coherent meson production mediated by W/Z-pomeron scattering. Especially tricky are the diffractive D_s^*/D_s channels where the D_s undergoes two-body τ decay:

$$\nu_\ell A \to \ell^- D_s^{+*}/D_s^+ A \to \ell^-(\gamma)\tau^+\nu_\tau \to \ell^-(\gamma)\ell'^+\nu_\tau\bar{\nu}_\tau\nu_{\ell'} \ . \tag{104}$$

Also of concern are backgrounds from inclusive charged current charm production, $\nu_\mu N \to \mu^- cX$, where the charm quark fragments into a charmed hadron which takes nearly all of the event's hadronic energy and then decays semileptonically into a final state where leptons carry nearly all the energy.

5.3. Conclusions on rare and exotic processes at νMCs

Rare processes that could be studied at a νMC would probe, both directly and indirectly, an energy range from fractions of a GeV to above the TeV scale. This would provide important information complementary to the existing results in some areas (e.g., in low-energy QCD studies, FCNC, contact interactions) and could substantially improve current bounds on the parameters of some new physics models (e.g., heavy neutral lepton searches).

6. Charm decay physics

6.1. Introduction

A νMC will constitute a rather impressive charm factory. Figs. 4 and 5 show that one can expect between 2×10^8 and 2×10^9 well-reconstructed charm events in a total event sample of 10^{10} events, depending on the νMC energy. Several species of charmed hadrons should be produced, with measured [93] relative production fractions for the more common charmed hadrons of

$$D^0 : D^+ : D_s^+ : \Lambda_c^+ = 0.60 : 0.20 : 0.10 : 0.10 \ . \tag{105}$$

Also, the Σ_c^{++} and Σ_c^+ are expected [94] to have comparable production cross sections to Λ_c^+. The charmed-strange baryons Ξ_c^+ and Ξ_c^0 should be produced at levels down by a factor of a few and Ω_c should be still less common.

The ratios of Eq. (105) are relatively independent of the neutrino energy for energies above 10 GeV and are for production from neutrinos; the corresponding antiparticles containing anti-charm will be produced from antineutrinos in similar ratios, although with differences in the absolute cross sections and kinematic distributions. The large asymmetry between D^0 and D^+ production is due to the prevalence of D^* production with its preference for decays into D^0.

As well as providing good all-around event reconstruction, νMCs will have two other distinct and important experimental advantages over all other types of charm facilities. Firstly, reconstruction of the charm decay vertex should be superior to that at any collider experiment, particularly for the reconstruction of the challenging 1-prong charm decays, as illustrated by Fig. 3. Secondly, a uniquely pure and efficient tag of whether the production flavor is charm or anti-charm is provided by the 100% correlated sign of the primary lepton from the interaction

$$\nu_\ell q \to \ell^- c, \qquad \bar{\nu}_\ell \bar{q} \to \ell^+ \bar{c} \ . \tag{106}$$

This section discusses several areas for charm decay physics at νMCs where these experimental capabilities should be important. The theoretical interest of each measurement will be discussed, and brief summaries of the expected experimental techniques and sensitivities at νMCs will be included. Expected relative strengths and weaknesses of νMCs compared to other future charm facilities will also be touched on. However, detailed numerical predictions for measurement precisions await more extensive feasibility studies than have been performed for this report.

There are also possibilities for B decay physics using the neutrinos from multi-TeV muon colliders [14,9], where $b\bar{b}$ production in neutral current interactions should be at the level of 10^{-3} of the total cross section. Associated production of $b\bar{c}$ and $c\bar{b}$ can also be studied, however the relevant production cross sections are suppressed by approximately two orders of magnitude compared to the $b\bar{b}$ production cross section.

6.2. Theoretical motivation for charm physics

It is clear that, from the point of view of Standard Model electroweak physics, charm decays represent a decidedly dull affair. First, the relevant CKM parameters are reasonably well known, for the smallness of $|V_{cb}|$ and $|V_{ub}|$ constrains V_{cs} and V_{cd} very tightly through three-family unitarity (see Section 3). Second, D^0–$\bar{D}^0$ oscillations proceed slowly. Third, CP asymmetries are small due to the fact that both decaying and final state particles contain quarks of only the first two generations. Finally, rare charm decay rates are tiny and, again, are dominated by long-distance effects.

These apparent vices can, however, be turned into virtues. Since the weak dynamics apparently hold no secrets, one can employ charm decays as a laboratory to study QCD in the interface of perturbative and non-perturbative dynamics. Also, precisely because the Standard Model promises us no drama in charm decays, one can conduct searches for D^0–$\bar{D}^0$ oscillations, CP violation and rare charm decays as probes for new physics with almost no background from the Standard Model.

6.3. Probing strong interactions through charm decays

Improved measurements of charm decays are needed for phenomenological and theoretical reasons even in the *absence* of new physics, for the following reasons:

- to improve the data base needed for analyzing B decays one needs more precise measurements of the *absolute* branching ratios of charm hadrons;
- measurements of the leptonic decay rates $D_{(s)} \to \ell\nu$ are required for determining the meson decay constants; these decay constants give us quantitative insight into the dynamics of heavy–light bound state systems and can be used for tuning the lattice QCD methods and a more reliable evaluation of B^0–$\bar{B}^0$ oscillations;
- more precise studies of *inclusive* semileptonic D, D_s, Λ_c, etc., decays would provide us with valuable novel insights into the inner workings of QCD and at the same time sharpen our tools for a quantitative treatment of B decays.

6.3.1. Absolute charm branching ratios

As the discussion about the charm content in the final state of B decays illustrates, a significant bottleneck in the detailed analysis of beauty decays of the $b \to c$ type is currently caused by the

uncertainties in the absolute branching ratios of charm hadron decays to specified final states, in particular of D_s, Λ_c and Ξ_c. A νMC should be well suited to obtaining these branching ratios, as we now discuss. This information will be useful even if it is obtained only after the next generation of B experiments have accumulated their samples.

As what is typically the less difficult part of the measurements, the expected excellent particle identification and event reconstruction at νMCs should give good capabilities for determining relative branching ratios for each hadron. The more difficult task of obtaining the production normalization factors to convert these to absolute branching ratios should then be achieved by fitting the experimental decay length distributions in a procedure that was studied for the COSMOS (E803) neutrino experiment at Fermilab.

The COSMOS technique [95] envisions fitting normalization factors to the several known decay exponentials—one for each charmed hadron species—in the observed neutral and charged distributions for the variable $x = d/p$, with d the charmed hadron distance to the decay vertex and p its reconstructed momentum. It is helpful that the exponential decay constants in this variable are well separated for both the charged and neutral hadron distributions:

$$\begin{aligned} x(D^+) &= 170\ \mu\text{m}/(\text{GeV}/c)\ , \\ x(D_s^+) &= 71\ \mu\text{m}/(\text{GeV}/c)\ , \\ x(\Xi_c^+) &= 43\ \mu\text{m}/(\text{GeV}/c)\ , \\ x(\Lambda_c^+) &= 27\ \mu\text{m}/(\text{GeV}/c) \end{aligned} \tag{107}$$

and

$$\begin{aligned} x(D^0) &= 67\ \mu\text{m}/(\text{GeV}/c)\ , \\ x(\Xi_c^0) &= 12\ \mu\text{m}/(\text{GeV}/c)\ , \\ x(\Omega_c^0) &= 7\ \mu\text{m}/(\text{GeV}/c)\ . \end{aligned} \tag{108}$$

Auxiliary information for the fit will be available from particle identification in the detector. In particular, the presence of a proton in the final state will reliably indicate the decay of a baryon rather than a meson.

To test the method for the COSMOS environment, exponential fits were performed [95] for simulated decay length distributions from approximately 14 000 reconstructed D^+, D_s^+ and Λ_c^+ charm decays. The fitted statistical uncertainties for the three species were 3.4%, 12% and 5.4%, respectively. These simulations show that statistical uncertainties would be negligible for such a fit at a νMC, which would have several orders of magnitude more events. The uncertainties in the charm production rates would instead be dominated by uncertainties in modeling the level of vertexing inefficiencies. Hopefully, these uncertainties could also be made small due to the favorable vertexing geometry shown in Fig. 3 and to the considerable potential for using the data itself to estimate the inefficiencies.

Another area where νMCs can be expected to make significant or even unique contributions is in the analysis of final states that contain *more than one* neutral hadron, e.g.,

$$D^0 \to \pi^+\pi^-\pi^0\pi^0, \quad D^+ \to \pi^+\pi^0\pi^0, \quad D_s^+ \to \pi^+\pi^0\eta\ldots\ . \tag{109}$$

Even all neutral final states like

$$D^0 \to 2\pi^0, 3\pi^0 \tag{110}$$

might become observable.

Such neutral-rich channels are rather elusive for the usual e^+e^- annihilation and photoproduction experiments. A νMC could access these modes through the expected sample of 10^{6-7} NC-produced $c\bar{c}$ events. Vertex tagging one of the charmed hadrons would allow a search for such decay modes in the other. Filling in these 'white spots' in the map of charm decays would close or at least narrow the gap between exclusive and inclusive decays and thus can provide us with important lessons on how quark–hadron duality is realized in subclasses of total decays. For example: a quark-based description leads to the prediction that the (Cabibbo-suppressed) inclusive rates driven by $c \to s\bar{s}u$ and $c \to d\bar{d}u$ should practically coincide since $m_d,\ m_s \ll m_c$. Yet exclusive channels like $D^0 \to K^+K^-$ and $D^0 \to \pi^+\pi^-$ do not at all follow this expectation! Duality suggests that a (near) equality will emerge for $\Gamma(D \to K\bar{K} + \pi's)$ versus $\Gamma(D \to \pi's)$. Testing this expectation requires the measurement of final states with neutrals.

Experimental studies of multi-body decays with more than one neutral meson in the final state (in particular, Dalitz plot analyses) also allow us to have different handles on the studies of direct CP violation in D decays in and beyond the Standard Model [96] as well as on the dynamics of hadronic resonances governing these transitions (see, e.g., the E791 analysis [97,98]).

6.3.2. $D_s, D^+ \to \mu^+\nu, \tau^+\nu$

The primary goal behind measuring leptonic decays, $D_s \to \ell^+\nu$, or the Cabibbo-suppressed versions, $D^+ \to \ell^+\nu$, with $\ell = \mu, \tau$, is the desire to extract the decay constants f_{D_s} and f_D. These quantities are important probes of heavy meson wave functions. In addition, these decay constants have been extracted from Monte-Carlo simulations of QCD on the lattice with estimated uncertainties of about 20% on their absolute values and about 10% on their ratio. Improvements are expected for future lattice calculations. For the proper evaluation of these calculations, one wants to calibrate them against experimental results of similar accuracy.

Currently, the branching ratios for $D_s \to \ell\nu$ transitions have been measured by the CLEO collaboration with large uncertainties, $\mathrm{Br}(D_s \to \mu\nu) = 4.0^{+2.2}_{-2.0} \times 10^{-3}$ and $\mathrm{Br}(D_s \to \tau\nu) = (7 \pm 4) \times 10^{-2}$. No measurement is currently available for other D mesons although there is an upper bound: $\mathrm{Br}(D^+ \to \mu\nu) < 7.2 \times 10^{-2}$. This can be explained by the $\lambda = 0.2$ CKM suppression factor for the D^+ leptonic decays relative to those of the D_s.

Once the absolute values of f_D or f_{D_s} are known experimentally with about 10% accuracy or better, then one will be able to feel more confident about extrapolating to the decay constants in the B system, f_B and f_{B_s}, which are crucial quantities for a quantitative understanding of B^0–$\bar{B}^0$ oscillations and the extraction of V_{td} from them.

Observing and measuring these transitions has always represented a highly non-trivial experimental challenge (and much more so for $D^+ \to \ell^+\nu$), so the potentially exceptional performance for observing 1-prong D decays at νMCs could allow them to make a significant contribution here even down the line. As a secondary goal one might even perform a detailed comparison of the rates for $D \to \mu\nu$ and $D \to \tau\nu$ as a probe for new physics in the form of a non-minimal Higgs sector, for charged Higgs exchanges would affect the latter much more than the former.

6.3.3. Inclusive charm hadron decays

Heavy quark expansions (HQE) allow the treatment of inclusive heavy flavor decays, including their non-perturbative aspects [99–103]. In addition to total decay widths, other central quantities are inclusive semileptonic branching ratios and decay spectra for the different meson and baryon species. These techniques provide the basis for some of the most reliable methods for extracting $|V_{cb}|$ and $|V_{ub}|$ in B decays. Obviously, one wants to cross-check these methods in a system where the CKM parameters are known, namely the charm system, by testing how precisely $|V_{cs}|$ and $|V_{cd}|$ can be extracted from semileptonic charm decays. In addition, one can extract the size of the matrix elements of four-fermion operators that are of direct relevance in *beauty* decays and at the same time provide important calibration points for lattice simulations of QCD.

No data of sufficient detail are available. The B factories (CLEO, BaBar and Belle) will significantly improve the situation, but might not achieve the desired experimental accuracy. Furthermore, it turns out that comparing neutrino with charged lepton spectra in semileptonic decays provides us with particularly probing insights.

One has to keep the following in mind. Since the expansion parameter is μ_{had}/m_c with $\mu_{had} \sim 0.7$–1 GeV, one has to allow for uncalculated higher-order contributions to modify the results significantly in charm decays. To have a handle on this complication, one needs to be able to perform detailed comparisons of the lepton spectra separately in D^0, D^+, D_s and Λ_c decays, which should be possible at νMCs.

FOCUS and SELEX data will presumably yield precise lifetimes for $\Xi_c^{0,+}$ baryons, but quite possibly not for Ω_c. The latter is presumably the shortest lived hadron in the single charm sector, with $\tau(\Omega_c) < 10^{-13}$ s; due to its different spin structure its lifetime is affected by different matrix elements than for the other baryons. It is also quite unclear whether next-generation experiments like LHC-B and BTeV can measure such a short lifetime with good accuracy. A νMC thus could make a relevant measurement that would serve as an a posteriori calibration of some theoretical tools. Furthermore, a whole new spectroscopy could be entered into, namely that of baryons carrying two units of charm: $[ccq]$.

In principle, radiative inclusive (and exclusive) decays can also be studied. The predicted branching ratio for the short-distance contribution is tiny, $\mathrm{Br}(c \to u\gamma) = (4.2\text{–}7.9) \times 10^{-12}$ [104], although two-loop QCD corrections could bring it up to 5×10^{-8} [105]. This could have made it a sensitive probe of new physics as these processes occur in the Standard Model only at one loop. Unfortunately, the problem is that the long-distance effects can actually completely dominate this decay, enhancing it up to $\sim 10^{-5}$, and these enhancements cannot be estimated model-independently.

6.4. Searches for new physics in charm decays

6.4.1. D^0–$\bar{D}^0$ oscillations

The phenomenon of meson–antimeson mixing has been studied both experimentally and theoretically for a long time as it provides an extremely sensitive test of the Standard Model as well as its various possible extensions. This is especially true for D^0–$\bar{D}^0$ mixing, as was already indicated.

To study such oscillations one must tag separately the flavor of the produced meson and of the decaying meson. The charge of the primary lepton from a CC interaction uniquely tags the production sign of the charm quark at an νMC. This should easily be the cleanest and most efficient tag. It can

be checked against a more conventional alternative method involving production of the charged D^* mesons and studies of the decay chain $D^{*\pm} \to D^0(\bar{D}^0)\pi^\pm$ [106,107], where anti-correlation studies of the charge of the π and the decay products of D would reveal whether mixing took place.

For charmed mesons with tagged production flavor, D^0–$\bar{D}^0$ oscillations are most cleanly probed through "wrong-sign" semileptonic decays with the branching ratios

$$r_D = \frac{\Gamma(D^0 \to \ell^- X)}{\Gamma(D^0 \to \ell^+ X)} \simeq \frac{1}{2}(x_D^2 + y_D^2), \qquad x_D = \frac{\Delta m_D}{\Gamma_D}, \quad y_D = \frac{\Delta \Gamma_D}{2\Gamma_D} \tag{111}$$

for $\Delta m_D = m_{D^0} - m_{\bar{D}^0}, \Gamma_D$ the D width and $\Delta\Gamma_D$ the difference in the D^0 and $\bar{D}^0$ mass widths.

In principle, one can determine the flavor of the final state through charged kaons; mis-tags that happen due to doubly Cabibbo suppressed decays can be eliminated using a time-dependent analysis, as discussed below.

The most recent experimental limits, which are from fixed target experiments at FNAL and from CLEO at CESR and combine tagging through "wrong" sign leptons and kaons, read

$$r_D \leqslant 5 \times 10^{-4}, \quad 95\%\ \text{CL};\ \text{CLEO [108]}\ , \tag{112}$$

$$-0.04 \leqslant y_D \leqslant 0.06, \quad 90\%\ \text{CL};\ \text{E791 [109]}\ , \tag{113}$$

$$-0.058 \leqslant y'_D \leqslant 0.01, \quad 95\%\ \text{CL};\ \text{CLEO [108]}\ , \tag{114}$$

where

$$y'_D \equiv y_D \cos\delta_{K\pi} - x_D \sin\delta_{K\pi}\ , \tag{115}$$

with $\delta_{K\pi}$ denoting the strong phase shift between $D^0 \to K^+\pi^-$ and $\bar{D}^0 \to K^+\pi^-$ (see [110] for the recent analysis), and

$$y_{\rm CP} = 0.0342 \pm 0.0139 \pm 0.0074; \quad \text{FOCUS [111]}\ , \tag{116}$$

where $y_{\rm CP} = y_D$ in the Standard Model. Since possible new physics effects or hadronic uncertainties will affect these experiments differently, a careful analysis to extract the true values of Δm_D and $\Delta\Gamma_D$ from the data should be performed [112]. The B factories at Cornell, SLAC and KEK will refine the search for D^0–$\bar{D}^0$ oscillations to an expected sensitivity of $r_D \sim$ few $\times 10^{-4}$ [113].

While the Standard Model undoubtedly predicts slow D^0–$\bar{D}^0$ oscillations—$x_D, y_D \ll 1$—there is considerable uncertainty in the numerical predictions. A *conservative* Standard Model bound is given by [114,115]

$$r_D|_{\rm SM} < 10^{-4} \simeq y_D, \quad x_D|_{SM} \leqslant 10^{-2}\ . \tag{117}$$

Bolder predictions have been made that x_D and y_D cannot exceed 10^{-3} [114,115] and therefore $r_D \leqslant 10^{-6}$ within the Standard Model. On the other hand, new physics could enhance x_D up to, and actually even above, the present bound,

$$x_D|_{\rm NP} \sim 0.1\ , \tag{118}$$

without violating any other limit and while leaving y_D unaffected. Examples of such new physics processes include various supersymmetric models [116] (including SUSY models with quark–squark alignment that actually require Δm_D close to the current experimental bound) [117], models with

singlet up quarks [118], various leptoquark models [119] and multiscalar models with [120], and without [121], natural flavor conservation. Any experimental effort to lower the current limit on Δm_D is essential in determining the available parameter space for many possible extensions of the Standard Model!

The cleanest way to probe for D^0–$\bar{D}^0$ oscillations is to analyze the time evolution of transitions into "wrong-sign" leptons:

$$\Gamma(D^0(t) \to \ell^+ X) \propto e^{-t/\tau_D} x_D^2 \left(\frac{t}{\tau_D}\right)^2 . \tag{119}$$

Here we have invoked the $\Delta Q = -\Delta C$ rule of the Standard Model which makes oscillations the only source for wrong-sign leptons.

Since one is embarking on a search for new physics, one should generalize Eq. (19) to allow for a violation of the $\Delta Q = -\Delta C$ rule, giving

$$\Gamma(D^0(t) \to \ell^+ X) \propto e^{-t/\tau_D} \times \left[\left(1 + \frac{1}{2}\Delta\Gamma_D t\right)|\hat{\rho}_{\text{wrong}}|^2 + \frac{1}{4}(\Delta m_D t)^2 - \frac{1}{2}\Delta\Gamma_D t \,\text{Re}\,\frac{p}{q}\,\hat{\rho}_{\text{wrong}} + \Delta m_D t \,\text{Im}\,\frac{p}{q}\,\hat{\rho}_{\text{wrong}}\right] , \tag{120}$$

where

$$\hat{\rho}_{\text{wrong}} \equiv \frac{T(D^0 \to \ell^- X)}{T(D^0 \to \ell^+ X)} \tag{121}$$

denotes the ratio of $\Delta C = \Delta Q$ to $\Delta C = -\Delta Q$ amplitudes,

$$|D_{1,2}\rangle = p|D^0\rangle \pm q|\bar{D}^0\rangle \tag{122}$$

relates mass and flavor eigenstates, and the oscillating functions multiplying the usual e^{-t/τ_D} term have been expanded in powers of the proper time t since $x_D, y_D \ll 1$. The $\Delta C = \Delta Q$ term has no t dependence beyond that of e^{-t/τ_D}, the pure oscillation term has a t^2 dependence, while the interference between the two generates a term linear in t.

The violation of the $\Delta Q = -\Delta C$ rule arises even within the Standard Model for the decays $D^0 \to K^+\pi^-$ due to doubly Cabibbo-suppressed transitions (DCST) producing the direct decay $D^0 \to K^+\pi^-$, with a branching ratio $\text{Br}(D^0 \to K^+\pi^-) = (2.8 \pm 0.9) \pm 10^{-4}$ [110,122], and thus mimicking the signal for $D\bar{D}$ mixing. The equation corresponding to Eq. (120) is

$$\Gamma(D^0(t) \to K^+\pi^-) \propto e^{-\Gamma_{D^0} t} \tan^4\theta_C |\hat{\rho}_{K\pi}|^2 \times \left[1 + \frac{1}{2}\Delta\Gamma_D t + \frac{(\Delta m_D t)^2}{4\tan^4\theta_C|\hat{\rho}_{K\pi}|^2} - \frac{\Delta\Gamma_D t}{2\tan^2\theta_C|\hat{\rho}_{K\pi}|}\,\text{Re}\left(\frac{p}{q}\frac{\hat{\rho}_{K\pi}}{|\hat{\rho}_{K\pi}|}\right) + \frac{\Delta m_D t}{\tan^2\theta_C|\hat{\rho}_{K\pi}|}\,\text{Im}\left(\frac{p}{q}\frac{\hat{\rho}_{K\pi}}{|\hat{\rho}_{K\pi}|}\right)\right] , \tag{123}$$

where

$$\tan^2\theta_C\hat{\rho}_{K\pi} \equiv \frac{T(D^0 \to K^+\pi^-)}{T(D^0 \to K^-\pi^+)} \tag{124}$$

is the fraction of wrong-sign decays.

One can also search for lifetime differences in certain well-chosen D^0 decay channels in order to probe the contributions to oscillations from the y_D term of Eq. (111). With CP invariance holding (at least) to a good approximation, CP eigenstates can be treated as mass eigenstates. While $D^0 \to K^+K^-, \pi^+\pi^-$ will then exhibit $\Gamma_+, D^0 \to K_S\phi, K_S\omega, K_S\rho, K_S\eta$, etc. will be controlled by Γ_-, where Γ_+ [Γ_-] denotes the width for the CP even [odd] state and

$$\Delta\Gamma = \Gamma_+ - \Gamma_- \ . \tag{125}$$

Furthermore, the width for $D^0 \to K^-\pi^+$ is approximately given by $(\Gamma_+ + \Gamma_-)/2$ [111,112].

6.4.2. CP violation in D decays

There is a wide field of potential CP violation in D decays that can be discussed in close qualitative analogy to B decays.

CP asymmetries that necessarily involve D^0–$\bar{D}^0$ oscillations can arise in final states that are CP eigenstates, like K^+K^- or $\pi^+\pi^-$:

$$\begin{aligned}\Gamma(D^0(t) \to K^+K^-) &\propto e^{-\Gamma_D t}\left(1 + \sin\Delta m_D t\,\mathrm{Im}\frac{q}{p}\,\bar{\rho}_{K^+K^-}\right)\\ &\simeq e^{-\Gamma_D t}\left(1 + \frac{\Delta m_D t}{\Gamma_D}\frac{t}{\tau_D}\,\mathrm{Im}\,\frac{q}{p}\bar{\rho}_{K^+K^-}\right)\ .\end{aligned} \tag{126}$$

With $x_D|_{\mathrm{SM}} \leqslant 10^{-2}$ and $\mathrm{Im}(q/p)\bar{\rho}_{K^+K^-}|_{\mathrm{KM}} \sim \mathcal{O}(10^{-3})$, one arrives at an asymmetry of only around 10^{-5}, which would likely be too small to measure even at a νMC. Yet with new physics one conceivably has $x_D|_{\mathrm{NP}} \leqslant 0.1$ and $\mathrm{Im}(q/p)\bar{\rho}_{K^+K^-}|_{\mathrm{NP}} \sim \mathcal{O}(10^{-1})$, leading to an asymmetry that could be as large as of order 1%.

Likewise, one can search for CP violation by comparing the proper time distribution of Eq. (123) for the doubly Cabibbo-suppressed transitions $D^0 \to K^+\pi^-$ with that for $\bar{D}^0$ decays:

$$\begin{aligned}\Gamma(\bar{D}^0(t) \to K^-\pi^+) &\propto e^{-\Gamma_{D^0}t}\tan^4\theta_C|\hat{\bar{\rho}}_{K\pi}|^2\\ &\times\left[1 + \frac{1}{2}\Delta\Gamma_D t + \frac{(\Delta m_D t)^2}{4\tan^4\theta_C|\hat{\bar{\rho}}_{K\pi}|^2} - \frac{\Delta\Gamma_D t}{2\tan^2\theta_C|\hat{\bar{\rho}}_{K\pi}|}\,\mathrm{Re}\left(\frac{q}{p}\frac{\hat{\bar{\rho}}_{K\pi}}{|\hat{\bar{\rho}}_{K\pi}|}\right)\right.\\ &\left.+\frac{\Delta m_D t}{\tan^2\theta_C|\hat{\bar{\rho}}_{K\pi}|}\,\mathrm{Im}\left(\frac{q}{p}\frac{\hat{\bar{\rho}}_{K\pi}}{|\hat{\bar{\rho}}_{K\pi}|}\right)\right]\ ,\end{aligned} \tag{127}$$

where

$$\tan^2\theta_C\hat{\bar{\rho}}_{K\pi} \equiv \frac{T(\bar{D}^0 \to K^-\pi^+)}{T(\bar{D}^0 \to K^+\pi^-)}\ . \tag{128}$$

In such new physics scenarios one would expect a considerably enhanced asymmetry—perhaps as large as $1\%/\tan^2\theta_C \sim 20\%$—but at the cost of smaller statistics. Hoping for an asymmetry of several percent is more realistic, though. Effects of that size would unequivocally signal the intervention of new physics! One should note that these rough estimates are based on $x_D \simeq 10^{-2}$ which would correspond to $r_D \simeq 10^{-4}$. This implies that, even if oscillations have not been found on the $r_D = 10^{-4}$ level in semileptonic D^0 decays, a CP asymmetry of several percent (or conceivably 10%) could still be encountered in $D^0 \to K^+\pi^-$!

Direct CP violation can occur as well. There are actually two types of effects: differences between partial rates for CP conjugate transitions

$$A_{\rm CP} = \frac{\Gamma(D \to f) - \Gamma(\bar{D} \to \bar{f})}{\Gamma(D \to f) + \Gamma(\bar{D} \to \bar{f})} \tag{129}$$

and asymmetries in final state distributions such as, e.g., Dalitz plot populations.

Strong final state interactions play an important part in both cases: in the former they must induce the phase shifts that are essential to make a difference observable; in the latter they can very significantly affect the observable asymmetry. The existence of resonances in the neighborhood of the charmed meson mass is proof that hadron dynamics is active in this energy region and will affect the weak decays of charmed particles.

The good news is that whenever there are CP violating weak phases one can count on final state interactions to make them observable. The bad news is that interpreting a signal as evidence for new physics will pose a highly non-trivial theoretical challenge.

The Standard Model with the CKM *ansatz* can induce direct CP asymmetries only in Cabibbo-suppressed channels. Model-dependent estimates usually predict direct CP asymmetries to be of the order of 10^{-3} but, exceptionally, they could reach the 10^{-2} level [123]. A measurement of the branching ratios for all related channels—in particular also those with neutral hadrons in the final state, as sketched above—would enable us to constrain the strong phase shifts quite significantly. A *v*MC will have a significant advantage in this respect!

6.4.3. *T* odd correlations in Λ_c decays

One special feature of *v*MCs is represented by the production of Λ_c in CC and NC reactions:

$$\nu N \to \nu \Lambda_c X \quad \text{or} \quad \mu \Lambda_c X \ . \tag{130}$$

This allows novel studies of various Λ_c decay form factors with a Q^2 range extending to well above $m^2_{\Lambda_c}$. Yet even more intriguing and promising would be a detailed analysis of the final state in its semileptonic decays:

$$\Lambda_c^+ \to \ell^+ \nu_\ell \Lambda \ . \tag{131}$$

With the parent c quark being left-handed one expects the Λ_c to emerge in a highly polarized state. The usual valence quark description actually suggests that the Λ_c polarization is completely carried by its c quark, i.e., a left-handed c quark fragments into a left-handed Λ_c. Yet even with unpolarized Λ_c one can form an experimentally observable T odd correlation

$$C_{T+-} \equiv \langle \vec{\sigma}_\Lambda \cdot (\vec{p}_\Lambda \times \vec{p}_\ell) \rangle \tag{132}$$

connecting the spin and momentum of the daughter hyperon with the lepton momentum.

In a general experimental process, observing a non-vanishing value for a T odd correlation does not automatically establish that T (and CP) invariance is violated since in general final state interactions could fake such an effect. However, this problem does not occur for Eq. (131) since it cannot be affected by either strong or electromagnetic final state interactions! This is analogous to the well-known situation in $K^+ \to \mu^+ \nu\pi^0$ (versus $K_L \to \mu^+ \nu\pi^-$). Like there, the CKM *ansatz* cannot generate an observable effect here, yet certain new physics scenarios can. An effect of order 10^{-2} is not inconceivable, particularly if the channel $\Lambda_c \to \tau\nu\Lambda$ could be studied [124].

6.5. Summary on charm decay physics at νMCs

The research program at a νMC is likely to improve our knowledge and understanding of charm decays quite significantly even ten years from now:

- It would fill out many white spots on our map of D, Λ_c, Ξ_c and Ω_c decays by measuring many new relative and absolute branching ratios, including final states with more than one neutral particle.
- It would allow the measurement of $D^+, D_s^+ \to \mu\nu$, $\tau\nu$ in a very clean environment.
- It could probe for D^0–$\bar{D}^0$ oscillations and for CP asymmetries involving them with superbly clean systematics. It would significantly improve on the sensitivity that can be obtained at B factories for such phenomena.
- It would enable us to search for direct CP asymmetries in many different channels and at the same time provide us with information that could help us in properly interpreting a signal.

7. Neutrino oscillation experiments with a muon storage ring/neutrino factory

7.1. Status of neutrino oscillations at the time of νMCs

In a modern theoretical context, one generally expects non-zero neutrino masses and associated lepton mixing [9]. Experimentally, there has been accumulating evidence for such masses and mixing. All solar neutrino experiments (Homestake, Kamiokande, SuperKamiokande, SAGE and GALLEX) show a significant deficit in the neutrino fluxes coming from the Sun [125]. This deficit can be explained by oscillations of the ν_e's into one or more other weak eigenstates, with $\Delta m^2_{\rm sol}$ of the order 10^{-5} eV$^2/c^4$ for solutions involving the Mikheev–Smirnov–Wolfenstein (MSW) resonant matter oscillations [126,127] or of the order of 10^{-10} eV$^2/c^4$ for vacuum oscillations. Accounting for the data with vacuum oscillations (VO) requires almost maximal mixing. The MSW solutions include one for small mixing angles (SMA) and one with essentially maximal mixing (LMA).

Another piece of evidence for neutrino oscillations is the atmospheric neutrino anomaly, observed by Kamiokande [128], IMB [129], SuperKamiokande [130] with the highest statistics, and by Soudan [131] and MACRO [132]. This data can be fit by the inference of $\nu_\mu \to \nu_x$ oscillations with $\Delta m^2_{\rm atm} \sim 3.5 \times 10^{-3}$ eV$^2/c^4$ [130] and maximal mixing $\sin^2 2\theta_{\rm atm} = 1$. The identification $\nu_x = \nu_\tau$ is preferred over $\nu_x = \nu_{\rm sterile}$ at about the 2.5σ level [133], and the identification $\nu_x = \nu_e$ is excluded by both the SuperKamiokande data and the Chooz experiment [134,135].

In addition, the LSND experiment [136] has reported observing $\bar{\nu}_\mu \to \bar{\nu}_e$ and $\nu_\mu \to \nu_e$ oscillations with $\Delta m^2_{\rm LSND} \sim 0.1$–$1$ eV$^2/c^4$ and a range of possible mixing angles, depending on $\Delta m^2_{\rm LSND}$. This

result is not confirmed, but also not completely ruled out, by a similar experiment, KARMEN [137]. Inclusion of the signal reported by LSND with the other two pieces of evidence would imply three distinct mass differences and hence four neutrinos. Some proposals for the form of the mixing matrix invoke only three generations of neutrinos to account for all signatures, while others invoke a fourth sterile neutrino.

A number of fits have been made to the existing neutrino data. The fit by the SuperKamiokande collaboration to its data yields a minimum in the χ^2 at $\sin^2(2\theta_{\rm atm}) = 1$, with an allowed region of $0.8 \lesssim \sin^2(2\theta_{\rm atm}) \lesssim 1$. In terms of the basic angles in the lepton mixing matrix, this implies that θ_{23} is close to $\pi/4$ and allows a small, non-zero θ_{13}, consistent with the bound from CHOOZ. As will be discussed below, a major physics capability of the muon storage ring/neutrino factory is the ability to measure θ_{13}.

There are currently intense efforts to confirm and extend the evidence for neutrino oscillations in all of the various sectors—solar, atmospheric and accelerator. Some of these experiments are running; in addition to SuperKamiokande and Soudan-2, these include the Sudbury Neutrino Observatory, SNO, and the K2K long-baseline experiment between KEK and Kamioka. Others are in development and testing phases, such as BOONE, MINOS, the CERN-Gran Sasso program, KAMLAND and Borexino [138]. Among the long-baseline neutrino oscillation experiments, the approximate distances are $L \simeq$ 250 km for K2K, 730 km for both MINOS, from Fermilab to Soudan and the proposed CERN-Gran Sasso experiments. The sensitivity of these experiments is projected to reach down roughly to the level $\Delta m^2 \sim 10^{-3}\ \mathrm{eV}^2/c^4$. Experiments that are planned as part of this program include ICANOE [139] and OPERA [140]. Although they are expected to begin operation after MINOS, they will involve somewhat different detector designs and plan to focus on establishing τ appearance. This, then, is the program of research for the next several years.

7.2. *Oscillation experiments at* νMCs

Although a neutrino factory based on a muon storage ring will turn on several years after this near-term period in which K2K, MINOS and the CERN-Gran Sasso experiments will run, it would still be expected to play a valuable role. A conventional beam from, say, π^+/K^+ decays, is primarily ν_μ with some small but imprecisely characterized admixture of $\bar{\nu}_\mu, \nu_e$ and $\bar{\nu}_e$. In contrast, muon storage rings will produce well understood and completely pure 2-component beams with large components of electron neutrinos: μ^- beams would yield 50% ν_μ and 50% $\bar{\nu}_e$, and, correspondingly, μ^+ beams would provide 50% $\bar{\nu}_\mu$ and 50% ν_e. Furthermore, these could be produced with extremely high intensities, of order 10^{20}–10^{21} neutrinos/yr.

Given the form of the oscillation probabilities, a neutrino beam for an oscillation experiment would optimally be made from the lower end of the spectrum of energies considered in this report. Because of the lower requirements on beam focusing and acceleration, making a muon storage ring for the purposes of an oscillation experiment has been proposed as a first step towards developing a muon collider. Energies being considered range from 20 to 50 GeV, and the geometry of the final muon ring is very different from a traditional collider ring, in that the straight section that points to a neutrino experiment comprises between 25% and 40% of the "circumference" of the ring.

The types of neutrino oscillations that can be searched for with the neutrino factory based on a muon storage ring, along with the final state charged lepton species for neutrino–nucleon DIS that

tags the interacting neutrino flavor, are listed below for the case of the $\nu_\mu\bar{\nu}_e$ beam from μ^-, decaying as $\mu^- \to \nu_\mu e^- \bar{\nu}_e$:

(1) $\nu_\mu \to \nu_\mu, \nu_\mu \to \mu^-$ (survival);
(2) $\nu_\mu \to \nu_e, \nu_e \to e^-$ (appearance);
(3) $\nu_\mu \to \nu_\tau, \nu_\tau \to \tau^-,\ \tau^- \to (e^-, \mu^-), \ldots$ (appearance*);
(4) $\bar{\nu}_e \to \bar{\nu}_e, \bar{\nu}_e \to e^+$ (survival);
(5) $\bar{\nu}_e \to \bar{\nu}_\mu, \bar{\nu}_\mu \to \mu^+$ (appearance);
(6) $\bar{\nu}_e \to \bar{\nu}_\tau, \bar{\nu}_\tau \to \tau^+;\ \tau^+ \to (e^+, \mu^+), \ldots$ (appearance*);

where the asterisks denote that the tau appearance signatures may be somewhat indirect in involving detection of the leptonic daughters of tau decays rather than the decay vertices of the taus themselves.

It is clear from the list of processes above that, since the beam contains both neutrinos and antineutrinos, the only way to distinguish parent neutrinos from antineutrinos is to measure the charge sign of the final state lepton. The $\nu_\mu \to \nu_e$ oscillation will produce a wrong-sign e^- as will the $\nu_\mu \to \nu_\tau$ oscillation followed by τ decay to e^-. The easiest wrong-sign lepton signatures to detect arise from the oscillations $\bar{\nu}_e \to \bar{\nu}_\mu$, giving a μ^+, and from $\bar{\nu}_e \to \bar{\nu}_\tau$, giving a τ^+ which will decay part of the time to μ^+. If one is searching for τ final states, muon storage ring energies above 30 GeV should be used to minimize the threshold kinematic suppression.

The discussion in Section 1.2.2 that is associated with Eq. (9) predicts roughly how the sensitivity of an oscillation experiment would scale with the beam energy, E, and baseline length, L, with the event rate going as

$$\frac{\mathrm{d}N}{\mathrm{d}t} \sim \frac{E^3}{L^2}\ . \tag{133}$$

To set the scale, consider an experiment that sees 2×10^{20} 30 GeV muon decays in a straight section pointed at a detector 2800 km away. In the absence of oscillations, the $\nu_\mu(\bar{\nu}_e)$ charged current rate would be 52 500 (22 600) events per 10 kt [7]. Fig. 16 shows the relative ν_e and $\bar{\nu}_\mu$ statistics for two configurations: one is a 20 GeV μ^+ ring with a detector at 2800 km, the other is a 50 GeV μ^+ ring with a detector at 9100 km, which is close to the distance from either Fermilab or CERN to Kamiokande.

Now recall the general formula for the probability of a two-species neutrino oscillation in vacuum, say of $\nu_e \to \nu_\mu$:

$$\begin{aligned} P(\nu_e \to \nu_\mu) &= 4|U_{13}|^2|U_{23}|^2 \sin^2\left(\frac{\Delta m^2_{\mathrm{atm}} L}{4E}\right) \\ &= \sin^2(2\theta_{13})\sin^2(\theta_{23})\sin^2\left(\frac{\Delta m^2_{\mathrm{atm}} L}{4E}\right)\ . \end{aligned} \tag{134}$$

Where the $\sin^2$ term is small, it can be expanded to give a factor of $(L/E)^2$ that cancels the L dependence in Eq. (133) and reduces the E dependence to a linear factor. Underlying these considerations of optimal energy is the fact that, even if one designs an experiment for τ appearance, the overall event rate of detected τ's may be rather small for beam energies low enough that kinematic suppression is important.

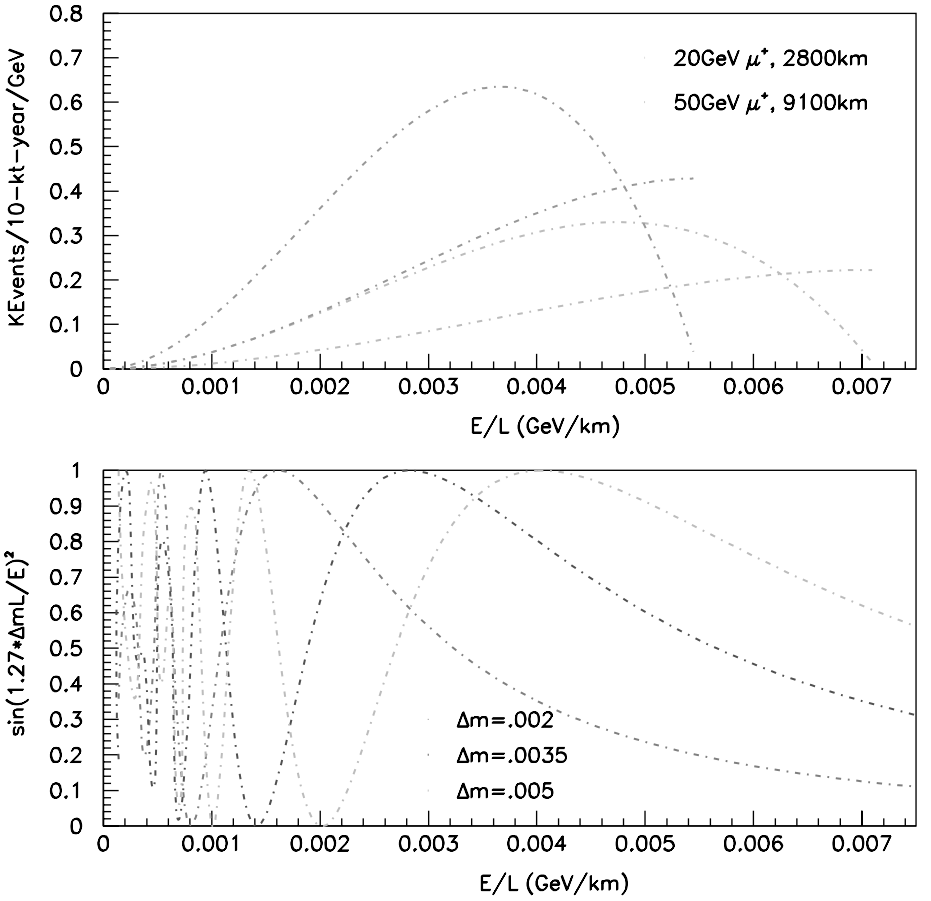

Fig. 16. The upper plot shows ν_e and $\bar{\nu}_\mu$ event rates per GeV as a function of E/L for two different experiments. The lower plot shows the L/E dependence of the oscillation probability, assuming the largest δm^2 is $2 \times 10^{-3}, 3.5 \times 10^{-3}$ or 5×10^{-3} eV$^2/c^4$.

It is quite likely that, by the time a neutrino factory turns on, Δm^2_{atm} and $\sin^2(2\theta_{23})$ will be known at the 10–30% level. Although a neutrino factory could undoubtedly improve the precision on those two parameters, the novel physics that can be addressed is a determination of θ_{13}, and the sign of Δm^2_{atm}. By using matter effects, and a comparison of ν_a versus $\bar{\nu}_a$ oscillations (by switching the muon storage ring from μ^- to μ^+), the sign of Δm^2_{atm}, can be determined.

7.3. Matter effects

With the advent of the muon storage ring, the distances at which one can place the detectors will become large enough so that, for the first time, matter effects can be exploited in accelerator-based oscillation experiments. Simply put, matter effects are the matter-induced oscillations which

neutrinos undergo along their flight path through the Earth from the source to the detector. Given the typical density of the Earth, matter effects are important for the neutrino energy range $E \sim O(10)\,\mathrm{GeV}$ and $\Delta m^2_{\mathrm{atm}} \sim 10^{-3}\,\mathrm{eV}^2/c^4$ values that are relevant for νMC long-baseline experiments.

Follow-up studies to initial discussion [126] of matter-induced resonant neutrino oscillations include an early study of these effects that assumed three neutrino generations [141] and a discussion of the sensitivity of an atmospheric neutrino experiment to small Δm^2 due to the long baselines and the necessity of taking into account matter effects was discussed [142]. Many analyses were performed in the 1980s of the effects of resonant neutrino oscillations [127] on the solar neutrino flux, and matter effects in the Earth [143,144], and of matter effect on atmospheric neutrinos [145]. Work continues [146,147] on matter effects relevant to atmospheric neutrinos. Early studies of matter effects on long-baseline neutrino oscillation experiments [148] have been extended to cover neutrino factories [7,149–151].

In recent papers by one of the authors (RS) and I. Mocioiu, calculations were presented of the matter effect for parameters relevant to the possible long-baseline neutrino experiments envisioned for the muon storage ring/neutrino factory [152,153]. In particular, these authors compared the results obtained with constant matter density along the neutrino path versus results obtained by incorporating the actual density profiles. They studied the dependence of the oscillation signal on both $E/\Delta m^2_{\mathrm{atm}}$ and on the angles in the leptonic mixing matrix, and commented on the influence of $\Delta m^2_{\mathrm{sol}}$ and CP violation on the oscillations. Additional recent studies are listed in Refs. [154,155].

7.4. Detector considerations

In order to measure oscillation parameters that describe the transitions above, one would ideally want a detector that could identify the existence and flavor of any outgoing lepton from the neutrino interaction, as well as the hadronic and leptonic energy in the event. When measuring very small oscillation probabilities, however, backgrounds must be taken into account. Naively one would think that simply detecting a muon of opposite charge to that in the storage ring is a signal for the electron neutrino oscillating. However, pions and kaons are produced copiously in neutral and charged current neutrino interactions, and if one decays to a muon before it interacts in the detector this can constitute a significant background. At higher energies charmed mesons are also produced which decay immediately to muons 10% of the time. Ultimately, detectors will need to be designed that have sufficient resolution on both the energies and the angles of the final state lepton and hadronic shower to be able to remove these backgrounds.

Although detectors exist that could identify all of the final state leptons and their charges, the challenge is to make them on the several kiloton scale. If the largest Δm^2 is in the LSND region, there will undoubtedly be more work done to optimize relatively low-mass detectors that emphasize tau appearance. However, the only detectors which have thus far been proposed on the 10–40 kt scale are for detecting wrong-sign muon events. The two detector technologies that have been considered in detail for oscillation experiments for a muon storage ring will now be discussed in turn: one is a magnetized sampling calorimeter such as the one used by MINOS [156] and the other is a liquid argon time projection chamber (TPC) combined with a muon spectrometer such as the one proposed by the ICANOE [157] collaboration for the CERN to Gran Sasso neutrino beam.

7.4.1. Magnetized sampling calorimeters

Magnetized sampling calorimeters consist simply of alternating layers of magnetized steel and readout, where the readout traditionally consists of scintillator and/or drift chambers.

The charged particle efficiency of the readout planes can be close to 100%, so the performance of the sampling calorimeter depends primarily on the sampling frequency of the detector. A steel/scintillator sandwich with sampling every 5 cm of steel would have a fractional hadron energy (H) resolution of approximately [156]

$$H \equiv \frac{\sigma_E}{E_{had}} \simeq \frac{0.76}{\sqrt{E_{had}\ (\mathrm{GeV})}}\ . \tag{135}$$

With fine enough transverse segmentation, the hadron angular resolution is dominated by the hadron energy resolution. The muon energy and angular resolution are expected to be much better than for the hadronic shower.

Although separating ν_e charged current events from neutral current events is difficult and determining the charge of the outgoing electron impossible in this detector, a muon in the final state can be easily and efficiently detected, and its charge, momentum and initial outgoing angle can be determined once the muon traverses enough steel to be spatially separated from the hadronic shower. Kinematic cuts can be made on the muon momentum and its component transverse to the hadronic shower to reduce the background from charm production. With signal efficiencies from 25% to 30%, the backgrounds can be reduced to a level of 10^{-5}–10^{-6}, depending on the neutrino energy. At higher energies the backgrounds are larger but the faster improvement in the background rejection actually causes a reduction in the background contributions to the analysis [158].

7.4.2. Liquid argon TPCs

The ICANOE-type detector would consist of a large volume of liquid argon instrumented with time projection chambers (TPCs), followed by a much thinner volume of magnetized steel where a muon's charge sign and momentum can be determined. The TPC would have very small wire spacing (3 mm) and would act much like an electronic bubble chamber. Electron neutrino charged current interactions could be distinguished from neutral current interactions, although the electron charge could not be measured. By breaking up the event samples into four distinct classes—right-sign muons, wrong-sign muons, electron-like events and neutral current events—one could fit all four distributions simultaneously to determine oscillation parameters. ν_τ's might also be identified on a statistical basis by looking at the acoplanarity distribution in the event sample.

The energy and angular resolutions for all the final states would be extremely good, e.g.,

$$\frac{\sigma_H}{E_H} \simeq \frac{0.20}{\sqrt{E_{had}\ (\mathrm{GeV})}} \tag{136}$$

for the hadronic energy and 150 mrad for hadron shower angles. However, the ability of this detector to see wrong-sign muons would depend primarily on the segmentation between the liquid argon and the magnetized spectrometer and on the thickness of the spectrometer itself. The thinner one makes the spectrometer, the more likely one is to have backgrounds from charge misidentification. The thicker the spectrometer, the less room there is for the liquid argon in a given volume. The thinner

the liquid argon, the higher the acceptance for low-energy muons (since muons lose approximately 210 MeV/m in liquid argon [159]), but the less target volume one has overall. Clearly optimization of this geometry is needed, and will depend somewhat on the energy of the muon storage ring.

7.4.3. Muon detector conclusions

Although the two types of detectors have different strengths, detailed studies [160,149,150, 153,161,3,4] have shown that either would be adequate to make precise measurements of $|\delta m^2|$, sign (δm^2) and $\sin^2\theta_{23}$, and to extend the sensitivity of $\sin^2\theta_{13}$ by 1–2 orders of magnitude in the scenario where the largest Δm^2 is described by the atmospheric neutrino anomaly.

7.4.4. Tau and electron detectors

Alternative technologies must be employed to achieve electron or tau identification event by event, or electron or tau charge sign measurements. If LSND is confirmed and the largest Δm^2 would suggest baselines on the order of tens of km, then a much higher premium will be placed on designing detectors that can do tau and electron charge determination, and they will not have to be as massive. At these short baselines, detectors on the 1 kt scale could be quite adequate to make precision measurements on $\nu_e \to \nu_\tau$ and $\nu_\mu \to \nu_\tau$. Even if LSND is not confirmed, efforts to make massive tau and electron charge identification detectors should not be abandoned since these two channels still comprise a large part of the mixing matrix and should be researched to confirm our understanding of neutrino mixing.

One category of new detectors uses thin ($\sim$100 μm) sheets of emulsion combined with low-density ($\sim$300 μm) spacers, and thin sheets of metal to give the detector mass. With emulsion one can measure the kink that occurs when a tau decays by comparing the slope of a track before and after the spacer. Such a geometry, with lead as the mass, is described in Ref. [162]. This would be very useful for identifying taus and electrons. However, for charge identification one needs to introduce a magnetic field. This could be done using an extremely large external magnet, such as the one used in ATLAS, and thin steel plates, or by using a coil and magnetized steel to make the mass [163]. Since the overhead for analysis of each event is high in this sort of detector, one would place it in a region where the tau appearance probability is maximized.

7.5. Conclusions on neutrino oscillation studies at νMCs

In conclusion, neutrino masses and mixing are generic theoretical expectations. The seesaw mechanism naturally yields light neutrinos, although its detailed predictions are model dependent and may require a lower mass scale than the GUT mass scale. Current atmospheric neutrino data are consistent with maximal mixing in the relevant channel, which at present is favored to be $\nu_\mu \to \nu_\tau$. Even after the near-term program of experiments by K2K, MINOS, the CERN-Gran Sasso experiments and mini-BOONE, a high-intensity neutrino factory generating 10^{20}–10^{21} neutrinos/yr will add greatly to our knowledge of the neutrino masses and mixing matrix. Ideally, the muon storage ring should be coupled with two long-baseline neutrino oscillation experiments, located at different baselines, that can take advantage of matter effects to amplify certain transitions and with a massive detector that will identify μ's and τ's with charge discrimination. In particular, it should be able to measure $\Delta m^2_{\rm atm}$ and $\sin^2(2\theta_{23})$ to the level of several percent and also give important information about the sign of $\Delta m^2_{\rm atm}$ and about $\sin^2(2\theta_{13})$.

8. Summary

Beams from νMCs have the potential to provide vast improvements over today's conventional neutrino beams from π/K decays. They are much more intense, have a much smaller transverse extent and produce precisely predictable beam spectra.

Oscillation experiments may extend even to intercontinental baselines, while unprecedented event statistics approaching of order of 10^9–10^{10} precisely constructed DIS events will open new regimes of neutrino interaction physics. The extraordinary rates will enable use of active vertexing targets surrounded by a high-resolution spectrometer and calorimeter. The first polarized targets for neutrino scattering can be substituted for special studies.

Highlights of a νMC physics program include:

- substantially extending the reach of accelerator-based experiments to study neutrino oscillations;
- measurements of the CKM quark mixing matrix elements $|V_{cd}|, |V_{ub}|, |V_{cs}|$ and $|V_{cb}|$ in inclusive high-Q^2 scattering, with few percent accuracies achievable for the first two;
- a realistic opportunity to determine the detailed quark-by-quark structure of the nucleon;
- mapping out the quark-by-quark spin structure with polarized targets, and, perhaps, determining the gluon contribution to the nucleon's spin;
- some of the most precise measurements and tests of perturbative QCD;
- tests of the electroweak theory through measurements of $\sin^2\theta_W$ with fractional uncertainties approaching 10^{-4};
- a new realm to search for exotic physics processes;
- a charm factory with unique and novel capabilities;
- a new laboratory for the study of nuclear physics with neutrino beams.

The potential experimental capabilities of νMCs reach so far beyond present neutrino programs that physics surprises not touched upon in this report can be expected. To see, we must build the machines.

Acknowledgements

We thank Janet Conrad, Keith Ellis, Michelangelo Mangano, Michael Shaevitz and Don Summers for helpful information and comments. This work was performed under US Department of Energy Contract Numbers DE-AC02-98CH10886, DE-AC02-76CH03000, DE-FG02-91ER40684, DE-FG02-91ER40685 and DE-FG03-99ER41093, under US National Science Foundation Contract Numbers PHY 96-05080, NSF 97-22101, PHY 98-13383 and PHY 00-87419 and under the auspices of the Illinois Board of Higher Education.

References

[1] The Muon Collider Collaboration, Status of muon collider research and development and future plans, Phys. Rev. ST Accel. Beams, 3 August 1999.

[2] The Muon Collider Collaboration, $\mu^+\mu^-$ collider: a feasibility study, BNL-52503, Fermilab-Conf-96/092, LBNL-38946, July 1996.
[3] C. Albright et al., Physics at a neutrino factory, FERMILAB-FN-692, May 9, 2000. Available at http://www.fnal.gov/projects/muon_collider/nu/study/study.html.
[4] S. Ozaki, R. Palmer, M. Zisman, J. Gallardo (Eds.), Feasibility Study-II of a Muon-Based Neutrino Source, BNL-52623, June 2001. Available at http://www.cap.bnl.gov/mumu/studyii/FS2-report.html.
[5] B.J. King, Assessment of the prospects for muon colliders, paper submitted in partial fulfillment of requirements for Ph.D., Columbia University, New York, 1994, available from http://xxx.lanl.gov/as physics/9907027.
[6] B.J. King, Neutrino physics at a muon collider, Proceedings of the Workshop on Physics at the First Muon Collider and Front End of a Muon Collider, Fermilab, November 6–9, 1997, hep-ex/9907033.
[7] S. Geer, Phys. Rev. D 57 (1998) 6989 [hep-ph/9712290].
[8] T. Bolton, Heavy quark production in deep inelastic neutrino scattering, preprint KSU-HEP-00-003, Kansas State University.
[9] I. Bigi et al., BNL-67404, May 2000.
[10] N. Holtkamp, D. Finley (Eds.), A Feasibility Study of a Neutrino Source Based on a Muon Storage Ring, Fermilab-Pub-00/108-E, March 2000. Available at http://www.fnal.gov/projects/muon_collider/nu/study/report/machine_report/.
[11] R. Raja, A. Tollestrup, Phys. Rev. D 58 (1998) 013005 [hep-ex/9801004].
[12] J.M. Conrad, M.H. Shaevitz, T. Bolton, Rev. Mod. Phys. 70 (1998) 1341.
[13] C. Johnstone, private communication.
[14] B.J. King, Mighty MURINEs: Neutrino physics at very high energy muon colliders, Proceedings of the HEMC'99 Workshop—Studies on Colliders and Collider Physics at the Highest Energies: Muon Colliders at 10 TeV to 100 TeV, Montauk, NY, September 27–October 1, 1999, hep-ex/0005007.
[15] Particle Data Group, D.E. Groom, et al., Eur. Phys. J. C 15 (2000) 1, http://pdg.lbl.gov.
[16] H. Plothow-Besch, Comput. Phys. Commun. 75 (1993) 396.
[17] A.O. Bazarko, et al. (CCFR Collaboration), Z. Phys. C 65 (1995) 189.
[18] M. Goncharov, et al. (NuTeV Collaboration), Precise measurement of dimuon production cross-sections in muon neutrino Fe and muon antineutrino Fe deep inelastic scattering at the Tevatron, e-print number hep-ex/0102049; Phys. Rev. D 64 (2001) 112006.
[19] E. Eskut, et al. (CHORUS Collaboration), Phys. Lett. B 503 (2001) 1.
[20] A. Alton, et al. (NuTeV Collaboration), Observation of neutral current charm production in ν_μFe scattering at the Tevatron, hep-ex/0008068; Phys. Rev. D (2001) 012002; Int. J. Mod. Phys. A 16S1B (2001) 764–766.
[21] A.A. Petrov, T. Torma, Phys. Rev. D 60 (1999) 093009 [hep-ph/9906254].
[22] G. Altarelli, G. Parisi, Nucl. Phys. B 126 (1977) 298.
[23] Yu.L. Dokshitser, D.I. Diakonov, S.I. Troian, Phys. Lett. B 78 (1978) 290.
[24] Yu.L. Dokshitser, et al., Phys. Rep. 58 (1980) 269.
[25] V.N. Gribov, L.N. Lipatov, Sov. J. Nucl. Phys. 15 (1972) 438.
[26] D.J. Gross, C.H. Llewellyn Smith, Nucl. Phys. B 14 (1969) 337.
[27] J. Chyla, A. L. Kataev, Phys. Lett. B 297 (1992) 385.
[28] S.A. Larin, J.A. Vermaseren, Phys. Lett. B 259 (1991) 345.
[29] V.M. Braun, A.V. Kolesnichenko, Nucl. Phys. B 283 (1987) 723.
[30] G.G. Ross, R.G. Roberts, Phys. Lett. B 322 (1994) 425 [hep-ph/9312237].
[31] S.L. Adler, Phys. Rev. 143 (1966) 1144.
[32] W.G. Seligman, et al. (CCFR Collaboration), Phys. Rev. Lett. 79 (1997) 1213.
[33] J.H. Kim, et al. (CCFR/NuTeV Collaboration) Phys. Rev. Lett. 81 (1998) 3595.
[34] H. Georgi, H.D. Politzer, Phys. Rev. D 14 (1976) 1829.
[35] M.A. Aivazis, J.C. Collins, F.I. Olness, W. Tung, Phys. Rev. D 50 (1994) 3102 [hep-ph/9312319].
[36] U.K. Yang, A. Bodek, Phys. Rev. Lett. 82 (1999) 2467 [hep-ph/9809480].
[37] H.L. Lai, et al. (CTEQ Collaboration) Eur. Phys. J. C 12 (2000) 375 [hep-ph/9903282].
[38] M. Virchaux, A. Milsztajn, Phys. Lett. B 274 (1992) 221.
[39] H. Deden, et al. (Gargamelle Neutrino Collaboration) Nucl. Phys. B 85 (1975) 269.
[40] X. Guo, J. Qiu, hep-ph/9810548.

[41] An ICE target will be used in the laser electron gamma-ray source (LEGS) experiment at Brookhaven National Laboratory, http://www.legs.bnl.gov.
[42] D.A. Harris, K.S. McFarland, A small target neutrino deep-inelastic scattering experiment at the first muon collider, Proceedings of the Workshop on Physics at the First Muon Collider and Front End of a Muon Collider, Fermilab, November 6–9, 1997, hep-ex/9804010.
[43] M.R. Adams, et al. (E665 Collaboration) Nucl. Instrum. Methods A 291 (1990) 533.
[44] C. Boros, J.T. Londergan, A.W. Thomas, Phys. Rev. D 59 (1999) 074021 [hep-ph/9810220].
[45] S.A. Kulagin, hep-ph/9812532.
[46] K.J. Eskola, V.J. Kolhinen, P.V. Ruuskanen, C.A. Salgado, Nucl. Phys. A 661 (1999) 645 [hep-ph/9906484].
[47] A. Benvenuti, et al., Z. Phys. C 63 (1994) 29.
[49] M. Vakili et al. (CCFR Collaboration), Phys. Rev. D 61 (2000) 052003.
[50] A concise review with a critical overview of the literature is given in: I. Bigi, M. Shifman, N. Uraltsev, Ann. Rev. Nucl. Part. Sci. 47 (1997) 591 [hep-ph/9703290], with references to earlier work.
[51] J. Goldman, A next-to-leading-order QCD analysis of charged current event rates in νN deep inelastic scattering at the Tevatron, Ph.D. Thesis, Kansas State University, 2000, unpublished.
[52] P. Annis, et al. (CHORUS collaboration) Phys. Lett. B 435 (1998) 458.
[53] T. Adams, et al. (NuTeV Collaboration) Phys. Rev. D 6 (2000) 092001.
[54] F.J. Hasert, et al. (Gargamelle Neutrino Collaboration) Phys. Lett. B 46 (1973) 138.
[55] H. Abramowicz, et al., Phys. Rev. Lett. 57 (1986) 298;
D. Bogert, et al., Phys. Rev. Lett. 55 (1985) 1969;
M. Jonker, et al. (CHARM Collaboration) Phys. Lett. B 99 (1981) 265.
[56] LEP Electroweak Working Group Summaries, see, e.g., CERN-EP-2000-016.
[58] H.S. Chen, G.J. Zhou, Phys. Lett. B 331 (1994) 441.
[59] D. Amidei, R. Brock, et al., Report of the TeV2000 Study Group, Fermilab-PUB/96-082.
[60] S.C. Bennett, C.E. Wieman, Phys. Rev. Lett. 82 (1999) 2484.
[61] K.S. Kumar, E.W. Hughes, R. Holmes, P.A. Souder, Mod. Phys. Lett. A 10 (1995) 2979.
[62] A. Czarnecki, W.J. Marciano, Int. J. Mod. Phys. A 15 (2000) 2365 [hep-ph/0003049];
A. Czarnecki, W.J. Marciano, Phys. Rev. D 53 (1996) 1066 [hep-ph/9507420].
[63] S. Sarantakos, A. Sirlin, W.J. Marciano, Nucl. Phys. B 217 (1983) 84.
[64] P. Villain, et al., Phys. Lett. B 335 (1994) 246;
P. Villain, et al., Phys. Lett. B 302 (1993) 351;
P. Villain, et al., Phys. Lett. B 281 (1992) 159.
[65] W. Willis, P. Rehak, private communications.
[66] E. Aprile, K.L. Giboni, C. Rubbia, Nucl. Instrum. Methods A 253 (1987) 273.
[67] C. Arroyo, B.J. King, et al., Phys. Rev. Lett. 72 (1994) 3452.
[68] K.S. McFarland, et al., CCFR, Eur. Phys. J. C 1 (1998) 509.
[69] C.H. Llewellyn Smith, Nucl. Phys. B 228 (1983) 205.
[70] E.A. Paschos, L. Wolfenstein, Phys. Rev. D 7 (1973) 91.
[71] G.P. Zeller, et al. (NuTeV Collaboration), Phys. Rev. Lett. 88 (2002) 091802 [hep-ex/0110059].
[73] E. Sather, Phys. Lett. B 274 (1992) 433.
[74] D. Yu. Bardin, V.A. Dokuchaeva, JINR E2-86-260, 1986.
[75] U. Baur, Electroweak radiative corrections to W boson production at the Tevatron, SUNY-Buffalo preprint UB-HET-98-02, September 1998 (e-Print Archive: hep-ph/9809327).
[76] U. Baur, M. Demarteau, Precision electroweak physics at future collider experiments, Fermilab-Conf-96/423, 1996.
[77] J.F. Donoghue, E. Golowich, Phys. Rev. D 49 (1994) 1513 [hep-ph/9307262].
[78] J.F. Donoghue, E. Golowich, Phys. Lett. B 478 (2000) 172 [hep-ph/9911309].
[79] D. Geiregat, et al. (CHARM-II Collaboration) Phys. Lett. B 245 (1990) 271.
[80] S.R. Mishra, et al. (CCFR Collaboration) Phys. Rev. Lett. 66 (1991) 3117.
[81] W. Czyz, G.C. Sheppey, J.D. Walecka, Nuovo Cimento 34 (1964) 404.
[82] R. Belusevic, J. Smith, Phys. Rev. D 37 (1988) 2419.
[83] Y. Grossman, Z. Ligeti, E. Nardi, Nucl. Phys. B 465 (1996) 369 [hep-ph/9510378].
[84] A.J. Buras, R. Fleischer, hep-ph/9704376.

[85] D. Zeppenfeld, K. Cheung, hep-ph/9810277.
[86] M. Gronau, C.N. Leung, J.L. Rosner, Phys. Rev. D 29 (1984) 2539.
[87] R.N. Mohapatra, G. Senjanovic, Phys. Rev. D 23 (1981) 165.
[88] D. Wyler, L. Wolfenstein, Nucl. Phys. B 218 (1983) 205.
[89] L.M. Johnson, D.W. McKay, T. Bolton, Phys. Rev. D 56 (1997) 2970 [hep-ph/9703333].
[90] A. Vaitaitis, et al. (NuTeV Collaboration) Phys. Rev. Lett. 83 (1999) 4943.
[91] J.A. Formaggio, et al. (NuTeV Collaboration) Phys. Rev. Lett. 84 (2000) 4043.
[92] T. Adams et al. (NuTeV Collaboration), hep-ex/0104037.
[93] N. Ushida, et al. (E531 Collaboration) Phys. Lett. B 206 (1988) 375.
[94] R.E. Shrock, B.W. Lee, Phys. Rev. D 13 (1976) 2539.
[95] Tim Bolton, E803 Physics, KSU HEP 95-02, unpublished notes.
[96] X.H. Guo, A.W. Thomas, Phys. Rev. D 61 (2000) 116009 [hep-ph/9907370].
[97] E.M. Aitala, et al. (E791 Collaboration) Phys. Lett. B 462 (1999) 401 [hep-ex/9906045];
A second E791 rare charm decay paper has recently been accepted by PRL and is available at Los Alamos as hep-ex 0011077.*
[98] E.M. Aitala, et al. (E791 Collaboration), D0 – > V l+ l- and h h l l, hep-ex/0011077.
[99] M.A. Shifman, M.B. Voloshin, Sov. J. Nucl. Phys. 41 (1985) 120.
[100] J. Chay, H. Georgi, B. Grinstein, Phys. Lett. B 247 (1990) 399.
[101] I.I. Bigi, N.G. Uraltsev, A.I. Vainshtein, Phys. Lett. B 293 (1992) 430 [hep-ph/9207214].
[102] B. Blok, L. Koyrakh, M. Shifman, A.I. Vainshtein, Phys. Rev. D 49 (1994) 3356 [hep-ph/9307247].
[103] A.F. Falk, M. Luke, M.J. Savage, Phys. Rev. D 53 (1996) 6316 [hep-ph/9511454].
[104] G. Burdman, E. Golowich, J.L. Hewett, S. Pakvasa, Phys. Rev. D 52 (1995) 6383 [hep-ph/9502329].
[105] C. Greub, T. Hurth, M. Misiak, D. Wyler, Phys. Lett. B 382 (1996) 415 [hep-ph/9603417].
[106] J. Anjos, et al., Phys. Rev. Lett. 60 (1988) 1239.
[107] E791 Collaboration, Phys. Rev. Lett. 77 (1996) 2384;
E791 Collaboration, Phys. Rev. D 57 (1998) 13.
[108] R. Godang, et al. (CLEO Collaboration) Phys. Rev. Lett. 84 (2000) 5038 [hep-ex/0001060].
[109] H. Park, hep-ex/0005044.
[110] A.F. Falk, Y. Nir, A.A. Petrov, Strong phases and D0 anti-D0 mixing parameters JHEP 9912 (1999) 019 [hep-ph/9911369].
[111] J.M. Link, et al. (FOCUS Collaboration) Phys. Lett. B 485 (2000) 62 [hep-ex/0004034].
[112] S. Bergmann, Y. Grossman, Z. Ligeti, Y. Nir, A.A. Petrov, Phys. Lett. B 486 (2000) 418 [hep-ph/0005181].
[113] For a comprehensive review of B physics at the $\Upsilon(4S)$, see P.F. Harrison, H.R. Quinn (BABAR Collaboration), The BaBar physics book: Physics at an asymmetric B factory, SLAC-R-0504, 1998.
[114] I. Bigi, N.G. Uraltsev, Nucl. Phys. B 592 (2000) 92 [hep-ph/0005089].
[115] E. Golowich, A.A. Petrov, Phys. Lett. B 427 (1998) 172 [hep-ph/9802291];
For a review, see G. Burdman, in: Workshop on the Tau/Charm Factory, Argonne National Lab, 1995, AIP Conference Proceedings No. 349, p. 409, or A.A. Petrov, hep-ph/0009160.
[116] J. Ellis, D.V. Nanopoulos, Phys. Lett. B 110 (1982) 44;
F. Gabbiani, E. Gabrielli, A. Masiero, L. Silvestrini, Nucl. Phys. B 477 (1996) 321 [hep-ph/9604387].
[117] Y. Nir, N. Seiberg, Phys. Lett. B 309 (1993) 337;
M. Leurer, Y. Nir, N. Seiberg, Nucl. Phys. B 420 (1994) 468.
[118] G.C. Branco, et al., Phys. Rev. D 52 (1995) 4217.
[119] S. Davisdon, et al., Z. Phys. C 61 (1994) 613.
[120] L.F. Abbot, et al., Phys. Rev. D 21 (1980) 1393;
Y. Grossman, Nucl. Phys. B 426 (1994) 355.
[121] S. Pakvasa, H. Sugawara, Phys. Lett. B 73 (1978) 61;
T.P. Chen, M. Sher, Phys. Rev. D 35 (1987) 3484;
L. Hall, S. Weinberg, Phys. Rev. D 48 (1993) R979;
D. Atwood, et al., Phys. Rev. D 55 (1997) 3156.
[122] I.I. Bigi, in: S.C. Loken (Ed.), Proceedings of the XIII International Confernce on High Energy Physics, World Scientific, Singapore, 1986, p. 857;
G. Blaylock, A. Seiden, Y. Nir, Phys. Lett. B 355 (1995) 555.

[123] F. Buccella, M. Lusignoli, A. Pugliese, Phys. Lett. B 379 (1996) 249 [hep-ph/9601343].
[124] A. Ali et al., B Quark Physics with 2×10^9 Z Bosons, LC-TH-2001-018; DESY-00-183; TTP-00-28; UND-HEP-00-BIG-12; 2nd ECFA/DESY Study 1998–2001, 1583–1593 [hep-ph/0012218].
[125] Fits and references to the Homestake, Kamiokande, GALLEX, SAGE, and Super Kamiokande data include N. Hata, P. Langacker, Phys. Rev. D 56 (1997) 6107;
J. Bahcall, P. Krastev, A. Smirnov, Phys. Rev. D 58 (1998) 096016;
J. Bahcall, P. Krastev, Phys. Lett. B 436 (1998) 243;
J. Bahcall, P. Krastev, A. Smirnov, Phys. Rev. D 60 (1999) 093001, http://www.sns.ias.edu/∼jnb/;
M. Gonzalez-Garcia, P. de Holanda, C. Pena-Garay, J.W.F. Valle, Nucl. Phys. B 573 (2000) 3–26 [hep-ph/9906469];
Recent Super Kamiokande data are reported in Super Kamiokande Collaboration, Y. Fukuda, et al., Phys. Rev. Lett. 82 (1999) 1810, 243.
[126] L. Wolfenstein, Phys. Rev. D 17 (1978) 2369.
[127] S.P. Mikheyev, A. Smirnov, Yad. Fiz. 42 (1985) 1441 [Sov. J. Nucl. Phys. 42 (1986) 913];
S.P. Mikheyev, A. Smirnov, Nuovo Cimento C 9 (1986) 17.
[128] Kamiokande Collaboration, K.S. Hirata, Phys. Lett. B 205 (1988) 416;
Kamiokande Collaboration, K.S. Hirata, Phys. Lett. B 280 (1992) 146;
Y. Fukuda, et al., Phys. Lett. B 335 (237) 1994;
S. Hatakeyama, et al., Phys. Rev. Lett. 81 (1998) 2016.
[129] IMB Collaboration, D. Casper, et al., Phys. Rev. Lett. 66 (1991) 2561;
R. Becker-Szendy, et al., Phys. Rev. D 46 (1992) 3720;
R. Becker-Szendy, et al., Phys. Rev. Lett. 69 (1992) 1010.
[130] Super-Kamiokande Collaboration, Y. Fukuda, et al., Phys. Lett. B 433 (1998) 9;
Super-Kamiokande Collaboration, Y. Fukuda, et al., Phys. Rev. Lett. 81 (1998) 1562;
Super-Kamiokande Collaboration, Y. Fukuda, et al., Phys. Rev. Lett. 82 (1999) 2644;
Super-Kamiokande Collaboration, Y. Fukuda, et al., Phys. Lett. B 467 (1999) 185
[131] Soudan Collaboration, W. Allison, et al., Phys. Lett. B 391 (1997) 491;
Soudan-2 Collaboration, Phys. Lett. B 449 (1999) 137;
A. Mann, in: Proceedings of the 1999 Photon–Lepton Symposium, hep-ex/9912007.
[132] MACRO Collaboration, M. Ambrosio, et al., Phys. Lett. B 434 (1998) 451 [hep-ex/0001044].
[133] J. Learned, in: Proceedings of the Workshop on the Next Generation Nucleon Decay and Neutrino Detector NNN99, Stony Brook, September 1999.
[134] M. Apollonio, et al., Phys. Lett. B 420 (1998) 397;
M. Apollonio, et al., Phys. Lett. B 466 (1999) 415.
[135] For recent experimental reviews, see, e.g., L. DiLella, hep-ex/9912010; H. Robertson, hep-ex/0001034, and talks at the Workshop on the Next Generation Nucleon Decay and Neutrino Detector NNN99, Stony Brook, September 1999, http://superk.physics.sunysb.edu/NNN99/scientific_program/.
[136] LSND Collaboration, C. Athanassopoulous, et al., Phys. Rev. Lett. 77 (1996) 3082;
LSND Collaboration, C. Athanassopoulous, et al., Phys. Rev. Lett. 81 (1998) 1774.
[137] KARMEN Collaboration, K. Eitel, B. Zeitnitz, in: Proceedings of Neutrino-98, Nucl. Phys. Proc. Suppl. 77 (1999) 212.
[138] References and websites for these experiments and future projects can be found, e.g., at http://www.hep.anl.gov/ndk/hypertext/nu_industry.html.
[139] ICANOE Collaboration, F. Cavanna, et al., LNGS-P21-99-ADD-1,2, November 1999;
A. Rubbia, hep-ex/0001052.
[140] OPERA Collaboration, CERN-SPSC-97-24, hep-ex/9812015.
[141] V. Barger, K. Whisnant, S. Pakvasa, R.J.N. Phillips, Phys. Rev. D 22 (1980) 2718;
V. Barger, K. Whisnant, R.J.N. Phillips, Rev. Rev. Lett. 45 (1980) 2084.
[142] D. Ayres, T. Gaisser, A.K. Mann, R. Shrock, in: Proceedings of the 1982 DPF Summer Study on Elementary Particles and Future Facilities, Snowmass, p. 590;
D. Ayres, B. Cortez, T. Gaisser, A.K. Mann, R. Shrock, L. Sulak, Phys. Rev. D 29 (1984) 902.
[143] P. Krastev, S. Petcov, Phys. Lett. B 205 (1988) 8.
[144] A.J. Baltz, J. Weneser, Phys. Rev. D 37 (1988) 3364.

[145] C.W. Kim, A. Pevsner, Neutrinos in Physics and Astrophysics, Harwood, Langhorne, 1993.
[146] S. Petcov, Phys. Lett. B 434 (1998) 321;
M. Chizhov, M. Maris, S. Petcov, hep-ph/9810501;
M. Chizhov, S. Petcov, hep-ph/9903424;
M.Chizhov, S. Petcov, Phys. Rev. Lett. 83 (1999) 1096.
[147] E. Akhmedov, A. Dighe, P. Lipari, A. Smirnov, Nucl. Phys. B 542 (1999) 3;
E. Akhmedov, Nucl. Phys. B 538 (1999) 25 [hep-ph/0001264].
[148] P. Krastev, Nuovo Cimento A 103 (1990) 361;
R.H. Bernstein, S.J. Parke, Phys. Rev. D 44 (1991) 2069.
[149] De Rujula, M.B. Gavela, P. Hernandez, Nucl. Phys. B 547 (1999) 21.
[150] M. Campanelli, A. Bueno, A. Rubbia, hep-ph/9905240.
[151] D. Dooling, C. Giunti, K. Kang, C.W. Kim, Phys. Rev. D 61 (2000) 073011 [hep-ph/9908513].
[152] I. Mocioiu, R. Shrock, in: Proceedings of the Workshop on the Next Generation Nucleon Decay and Neutrino Detector NNN99, Stony Brook, September 1999, hep-ph/9910554.
[153] I. Mocioiu, R. Shrock, Phys. Rev. D 62 (2000) 053017 [hep-ph/0002149].
[154] S.M. Bilenky, C. Giunti, W. Grimus, Phys. Rev. D 58 (1998) 033001;
K. Dick, M. Freund, M. Lindner, A. Romanino, Nucl. Phys. B 562 (1999) 29;
M. Tanimoto, Phys. Lett. B 462 (1999) 115;
A. Donini, M.B. Gavela, P. Hernandez, S. Rigolin, Nucl. Phys. B 574 (2000) 23 [hep-ph/9909254];
M. Koike, J. Sato, Phys. Rev. D 61 (2000) 073012 [hep-ph/9909469];
P.F. Harrison, W.G. Scott, Phys. Lett. B 476 (2000) 349 [hep-ph/9912435].
[155] M. Freund, M. Lindner, S.T. Petcov, A. Romanino, Nucl. Phys. B 578 (2000) 27 [hep-ph/9912457].
[156] The MINOS experiment, http://www-numi.fnal.gov:8875.
[157] The ICANOE experiment, http://pcnometh4.cern.ch.
[158] A. Villanueva, et al., Nufact'99 Workshop, Lyon, July 5–9, 1999.
[159] Doke et al., Nucl. Instrum. Methods A 237 (1985) 475.
[160] V. Barger, S. Geer, K. Whisnant, Phys. Rev. D 61 (2000) 053004.
[161] A. Cervera, A. Donini, M.B. Gavela, J.J. Gomez Cadenas, P. Hernandez, O. Mena, S. Rigolin, Nucl. Phys. B 579 (2000) 17 [hep-ph/0002108].
[162] P. Strolin, Nufact'99 Workshop, Lyon, July 5–9, 1999.
[163] D.A. Harris, A. Para, Nucl. Instrum. Methods A 451 (2000) 173 [hep-ex/0001035].